

UCGE Reports  
Number 20202

Department of Geomatics Engineering

**Mitigation of Narrow Band Interference on  
Software Receivers based on Spectrum Analysis**

(URL: <http://www.geomatics.ucalgary.ca/links/GradTheses.html>)

by

**Zhi Jiang**

**October 2004**



UNIVERSITY OF  
CALGARY

THE UNIVERSITY OF CALGARY

Mitigation of Narrow Band Interference on Software Receivers  
based on Spectrum Analysis

by

Zhi Jiang

A THESIS  
SUBMITTED TO THE FACULTY OF GRADUATE STUDIES  
IN PARTIAL FULFILMENT OF THE REQUIREMENTS FOR THE  
DEGREE OF MASTER OF SCIENCE

DEPARTMENT OF GEOMATICS ENGINEERING

CALGARY, ALBERTA

October, 2004

© Zhi Jiang 2004

# Abstract

This thesis describes an extensive investigation into the development of a narrow-band radio frequency interference (RFI) mitigation algorithm and performance testing using a software Global Positioning System (GPS) receiver. Traditionally, most RFI mitigation methods have been implemented and tested using conventional hardware receivers. With the rapid development of computer technologies, the signal processing computational load is becoming less of a concern, and thus it becomes feasible to develop and test new interference mitigation methods based on software receivers together with modern digital signal processing techniques.

In this research, a narrow-band RFI mitigation algorithm based on spectrum analysis is discussed in the acquisition, tracking and position domains. A series of hardware simulation tests is conducted to assess the performance of this algorithm. For high level interference, a fixed detection threshold as previously suggested in the literature is not sufficient. An adaptive detection threshold that is a function of the standard deviation of the normalized spectrum and the correlator power output is proposed in this research. Soft thresholding in bit synchronization and improved acquisition based on earlier information are used under high dynamic conditions and a high level interference environment. The factors that are crucial for weak signal detection (namely coherent integration time, tracking

loop bandwidth and integration time in the loop filter) are evaluated to assess the effectiveness of this algorithm. Some interference suppression strategies for spread spectrum systems, namely windowing and overlap processing, are also investigated. The result shows that the frequency excision algorithm is effective to mitigate a certain power level of narrow-band RFI, including CW, AM and FM. Windowing and overlapped processing have shown to be good strategies to improve the performance of this algorithm by increasing anti-jamming capability by 2 dB.

# Acknowledgements

I would like to express my sincere appreciation to my supervisor, Dr. Gérard Lachapelle, for his continued guidance, encouragement and financial support throughout my graduate studies. Beyond sharing his knowledge, lessons I have learned from his positive attitude, spirit of cooperation and understanding will benefit me throughout my life.

I would also like to thank other professors, students, and staff of the Department of Geomatics Engineering. Specifically, thank Dr. Changlin Ma for many of his ideas that have been implemented in this work. I would also like to express gratitude to Sameet M. Deshpande for his valuable comments and proofreading of my thesis. Dr. Mark Petovello, Bo Zheng, Haitao Zhang, Lei Dong and Ping Lian are also thanked for their kind help during my research.

A special recognition and thanks is given to my wife, Yan, for always believing in me and supporting me. Thank you for your patience, love and understanding. To my son, Chaofan, thank you for bringing me so much joy and making my life colourful. I am also indebted to my parents and parents-in-law for their untiring support.

# Table of Contents

Approval Page .....	ii
Abstract.....	iii
Acknowledgements.....	v
Table of Contents .....	vi
List of Tables .....	ix
List of Figures .....	x
List of Abbreviations .....	xiii
1 Introduction .....	1
1.1 Background.....	2
1.1.1 Software receiver versus hardware receiver.....	2
1.1.2 Interference overview .....	3
1.2 Literature review .....	5
1.3 Research objectives.....	8
1.4 Thesis outline.....	9
2 Theory of FFT-based Narrow-band Interference Excision and Introduction to Receiver Technology .....	10
2.1 Narrow-band versus wide-band interference.....	10
2.2 Fast Fourier Transform.....	12
2.3 Algorithm for FFT-based narrow-band interference mitigation.....	15
2.4 Introduction to GPS receiver technology .....	20
2.4.1 GPS signal acquisition overview .....	20
2.4.2 GPS signal tracking overview.....	24
2.4.3 Raw measurement derivation.....	28
2.4.4 Loop filter determination.....	30
3 Test Setup and Methodology .....	35
3.1 RF GPS signal with interference generation .....	35
3.1.1 GSS STR6560 multi-channel GPS/SBAS simulator.....	35

3.1.2	Interference generation combined with GPS signal .....	36
3.2	Intermediate frequency signal generation, sampling and.....	39
	quantization .....	39
3.3	Metrics definition .....	40
3.4	Software approach of FFT-based mitigation algorithm.....	43
3.4.1	Interference detection .....	44
3.4.2	Interference mitigation .....	46
4	Mitigation Analysis in Acquisition .....	52
4.1	CW Interference frequency determination .....	52
4.2	Impact of CW interference on correlation function .....	55
4.2.1	CW frequency effect on correlation function .....	55
4.2.2	CW power effect on correlation function .....	56
4.3	Mitigation result using a 4.75 MHz sampling rate .....	58
4.4	Mitigation result using a 7 MHz sampling rate .....	64
4.5	Nyquist's law and analysis of sampling rate on acquisition.....	66
4.5.1	Nyquist's law .....	66
4.5.2	Analysis of sampling rate on acquisition .....	68
4.6	Influence of coherent integration time on interference mitigation.....	69
4.7	Conclusion .....	72
5	Mitigation Analysis in Tracking and Position .....	73
5.1	CW interference mitigation results in tracking.....	73
5.1.1	IP component mitigation results.....	73
5.1.2	Doppler mitigation results .....	76
5.1.3	Estimated $C/N_0$ .....	80
5.2	CW Interference mitigation results in position domain .....	83
5.2.1	Bench marks for performance analysis in position domain.....	83
5.2.2	Warm and cold start.....	85
5.2.3	CW interference mitigation in the position domain.....	86
5.2.4	Stochastic repeatability test .....	90
5.3	AM interference mitigation results in the position domain .....	94
5.4	FM interference mitigation results in the position domain .....	100
6	Kinematic Tests.....	109
6.1	Test setup.....	109
6.2	Results and analysis .....	109

7	Application of Data Window in FFT-based Mitigation Algorithm	123
7.1	The advantage of using a data window	123
7.2	Window selection	125
7.2.1	Blackman-Harris window	126
7.2.2	Hamming window	128
7.2.3	Gaussian window	129
7.3	Implementation of overlapped processing	131
7.4	Results and analysis	133
8	Conclusions and Recommendations for Future Work	142
8.1	Conclusions	142
8.2	Recommendations for future work	145
	References	147

# List of Tables

Table 1.1: Types and sources of jamming interference .....	4
Table 2.1: Loop Filter Characteristics .....	32
Table 3.1: Decision statistic results summary .....	46
Table 4.1: Worst C/A line for each of the 37 codes .....	54
Table 4.2: Peak value versus noise floor and SNR .....	63
Table 5.1: Frequency limits versus centre frequency.....	102
Table 5.2: Comparison of FM frequency on GPS position.....	103
Table 6.1: Impact of integration time in loop filters on position errors .....	110

# List of Figures

Figure 2.1: GPS signal acquisition .....	21
Figure 2.2: GPS receiver signal tracking loop .....	25
Figure 2.3: Software Receiver Delay lock loop.....	27
Figure 2.4: Pseudorange construction [after Ward 1996] .....	29
Figure 2.5: Second order loop filter .....	33
Figure 2.6: Digital representation of Laplace transform.....	34
Figure 3.1: System hardware configuration.....	38
Figure 3.2: Hardware front-end “GPS Signal Tap”.....	40
Figure 3.3: Sky view at the beginning of the simulation.....	43
Figure 3.4: 1 ms FFT without CW interference.....	48
Figure 3.5: 1 ms FFT with CW interference ( $J/S = 30$ dB).....	48
Figure 3.6: Flowchart of frequency excision algorithm .....	51
Figure 4.1: Spectrum of Gold code [from Heppe, 2002] .....	52
Figure 4.2: Correlations for different spectral lines .....	55
Figure 4.3: Correlation for CW interference of different power levels .....	57
Figure 4.4: Acquisition results without mitigation .....	58
Figure 4.5: PDF of noise and signal used in computation of noise power [after Kaplan, 1996]: .....	60
Figure 4.6: Acquisition results with mitigation at a 4.75 MHz sampling rate .	62
Figure 4.7: Acquisition results with mitigation at a 7 MHz sampling rate .....	65

Figure 4.8: Spectrum aliasing .....	67
Figure 4.9: Impact of coherent time on mitigation results .....	71
Figure 5.1: IP component comparison.....	74
Figure 5.2: Comparison of Doppler with 4.75 MHz sampling rate .....	76
Figure 5.3: Comparison of Doppler with 7 MHz sampling rate .....	76
Figure 5.4: Doppler error comparison (5 seconds of data).....	78
Figure 5.5: Doppler error comparison (30 seconds of data) .....	79
Figure 5.6: C/N <sub>0</sub> comparison .....	82
Figure 5.7: Position errors under noise only conditions.....	83
Figure 5.8: Position error comparison of 6 tests under noise only conditions .....	84
Figure 5.9: Comparison of mitigation results with CW interference .....	87
Figure 5.10: Comparison of the effect of the sampling rate on position.....	89
Figure 5.11: Comparison of coherent integration time on position.....	91
Figure 5.12: Rate of successful position fixing .....	93
Figure 5.13: Impact of modulating signal frequency of AM interference on mitigation results .....	96
Figure 5.14: Influence of modulation depth of AM interference on mitigation results.....	98
Figure 5.15: Mitigation results comparison with AM interference.....	99
Figure 5.16: Influence of frequency deviation of FM interference on position .....	104
Figure 5.17: Mitigation results with FM interference .....	106

Figure 6.1: Pseudorange errors compared with true value.....	111
Figure 6.2: A histogram showing successful bit synchronization .....	114
Figure 6.3: Bit synchronization result for PRN 20.....	116
Figure 6.4: Histogram of bit synchronization in warm start.....	117
Figure 6.5: Histogram of bit synchronization using the improved procedure .....	119
Figure 6.6: Pseudorange error using improved bit synchronization procedure .....	120
Figure 6.7: Stochastic repeatability test results under kinematic mode .....	121
Figure 7.1: Plot of 4-term Blackman-Harris window .....	127
Figure 7.2: Plot of Hamming window.....	128
Figure 7.3: Plot of Gaussian window .....	129
Figure 7.4: Block diagram of 50 percent overlap processing.....	132
Figure 7.5: Enlarged spectra of windowed and non-windowed data .....	134
Figure 7.6: Effect of windowing on GPS position estimation. ....	136
Figure 7.7: Pseudorange error comparison between “with window” and “without window” .....	138
Figure 7.8: Position errors of stochastic repeatability test with windowing .	139
Figure 7.9: Success rate of stochastic repeatability test with windowing....	140

# List of Abbreviations

AC	Alternating-current
ADC	Analog-to-Digital Converter
ATF	Adaptive transversal filter
AGC	Automatic Gain Control
AM	Amplitude Modulation
ASIC	Application Specific Integrated Circuit
ATF	Adaptive Transversal Filter
AWGN	Additive White Gaussian Noise
BPSK	Binary Phase Shift Keying
C <sup>3</sup> NAV <sup>2</sup> ™	Combined Code and Carrier for Navigation with GPS and GLONASS
C/A	Coarse-Acquisition
C/No	Carrier-to-Noise
CDMA	Code Division Multiple Access
COTS	Commercial-Off-The-Shelf
CRPA	Controlled Reception Pattern Antenna
CW	Continuous Wave
dB	DeciBel
dBm	DeciBel per milliwatt
dBW	DeciBel per Watt

DFT	Discrete Fourier transform
DLL	Delay Lock Loop
DS	Direct Sequence
DSP	Digital Signal Processors
FA	False Alarm
FB	Filter Bank
FCC	Federal Communications Commissions
FFT	Fast Fourier Transform
FLL	Frequency Lock Loop
FM	Frequency Modulation
GNSS	Global Navigation Satellite System
GPIB	General Purpose Interface Bus
GPS	Global Positioning System
GUI	Graphical User Interface
I	In-phase
ICU	Interference Combiner Unit
IF	Intermediate Frequency
IFFT	Inverse FFT
IMU	Inertial Measurement Units
IP	In-phase prompt
J/S	Jammer-to-Signal
LOS	Line-Of-Sight
LNA	Low Noise Amplifier

LS	least square
MD	Missed Detection
NAVSTAR	NAVigation Satellite Timing And Ranging
NCO	Numeric Controlled Oscillator
ND	Normal Detection
NO	normal Operation
PC	Personal Computer
PDF	Probability Density Function
PLAN	Position, Location, and Navigation
PLL	Phase Lock Loop
PN	Pseudo Noise
PRN	Pseudo Random Noise
Q	Quadrature
RF	Radio Frequency
RFI	RF Interference
RMS	Root Mean Square
SA	Selective Availability
SNR	Signal-to-Noise Ratio
SS	Spread Spectrum
SSG	Satellite Signal Generators
SV	Space Vehicle

# CHAPTER 1

## Introduction

Despite the fact that its principal objective was to offer the United States military accurate estimates of position, velocity, and time, GPS has created a whole new industry that crucially depends upon adequate signal reception. However, Radio Frequency (RF) interference, whether intentional or unintentional, has been a major threat to the GPS community since the advent of the system. In-band interference (where the frequency falls on the pass-band of the filter in the GPS receiver's preamplifier) can severely disrupt receiver operation, such threats being more serious because of the widespread use of RF equipment. Most commercial GPS receivers have little, if any, protection from external RF interference [Ward, 2002]. The reasons are due to many distinct considerations. The additive cost to the receiver is a major concern; thus, there is a need to develop an RFI mitigation algorithm with quantifiable improvements in accuracy and reliability, and without additional hardware requirements. Software receivers together with modern digital signal processing techniques provide a reliable and versatile tool for RFI mitigation research.

## 1.1 Background

### 1.1.1 Software receiver versus hardware receiver

In a conventional receiver, the front-end, which down-converts the RF signals to a low intermediate frequency (IF) and digitizes it into discrete signals; and the lower level signal processing, which includes correlation and accumulation are performed in a dedicated hardware component: the Application Specific Integrated Circuit (ASIC) which is very fast but extremely difficult to modify for experimental purposes. Upper level signal processing, which includes receiver processing and navigation processing, is performed in a programmable microprocessor. The architecture of a software receiver departs from that of conventional hardware GPS receivers. All of the processing is done in software residing on a programmable microprocessor which is less efficient, but easily re-configurable. The advantages of using software receivers over comparable hardware components lie in the following aspects [Tsui, 2000]:

- Eliminate additional components used in frequency translation: local oscillators, mixers, filters, which contribute potential nonlinear effects and temperature and age-based performance variations.
- Utilizing block processing rather than epoch to epoch, the signal can be analyzed in different domains, so that a wider range of properties of the signal can be used than a traditional receiver.

- Easy to implement the latest signal processing techniques without the need for hardware development.
- Easier and cost-effective to expand analysis to include new signals (GPS L5, Galileo signals, etc.).

The main challenge to a software receiver is the programmable processing power. According to Moore's Law, every 18 months, processing power doubles while cost holds constant. In many software applications, Moore's insight proved to be prescient, and it promises to remain true for the foreseeable future. With an exponential increase in computer processing power, the computational load is becoming less of a concern for signal processing, and thus it becomes feasible to develop and test software receiver-based interference mitigation techniques.

### **1.1.2 Interference overview**

Although the GPS frequency bands are protected by international and U.S. Federal Communication Commission (FCC) frequency assignments, there possibility exists spurious unintentional interference and even intentional interference [Kaplan, 1996]. The signal power attenuation due to the long travel path from distant satellites makes GPS vulnerable to interference. Table 1.1 summaries the different types and sources of jamming interference.

Table 1.1: Types and sources of jamming interference

Types of Interference	Typical Sources
Wide-band-Gaussian	Intentional noise jammers
Wide-band phase/frequency modulation	Television transmitter's harmonics of near-band microwave link transmitters overcoming front-end filter of the GPS receiver
Wide-band-spread spectrum	Intentional spread spectrum jammers or near-field of pseudolites
Wide-band-pulse	Radar transmissions
Narrow-band phase/frequency modulation	AM station transmitter's harmonics or CB transmitter's harmonics
Narrow-band-swept continuous wave	Intentional CW jammers or FM stations transmitter's harmonics
Narrow-band-continuous wave	Intentional CW jammers or near-band unmodulated transmitter's carriers

[Kaplan, 1996]

The major types of interference can be classified as Additive White Gaussian Noise (AWGN), narrow-band, and pulsed [Ward, 2002].

AWGN is the best model for thermal noise as well as thermal noise added by lossy components in the front-end. Broadband interference can also be modeled as AWGN. The impacts of AWGN on GPS include increasing the noise floor and reducing the Signal to Noise Ratio (SNR); AWGN also causes cycle slips, jitter in tracking loops, and bit errors [Ward, 2002]. Narrow-band interference may arise from spurious signals generated in nearby electrical equipment, or certain types of jamming. If narrow-band interference is centred close to the carrier frequency (e.g. L1), it can effectively avoid the selection filter and lead to a Phase Lock Loop (PLL)

lock on this interfering signal instead of the GPS ranging signals, even after spreading by the Pseudo-random Noise (PN) correlator. Pulsed interference is typically associated with radars, certain navigation equipment or some communications equipment; the effect of such strong, short pulses is a linear reduction in effective SNR. Only narrow-band interference will be discussed in this thesis.

## **1.2 Literature review**

GPS signals are vulnerable to the RFI originating in unrelated sources even with spread spectrum technology. Taking advantage of the GPS signal processing gain by itself is not always sufficient to overcome such interference. For example, a narrow-band interferer with a power level 14 dB greater than the desired signal will disrupt GPS receiver operation [Ward, 1996]. Additional remedies must be sought against this problem.

A large number of mitigation techniques have been developed to improve the performance of GPS receivers. These techniques can be classified into four main categories.

### **1. Front-end filtering technique [Kaplan, 1996]**

The goal of this technique is to minimize the pass-band of the filter, with sharp and deep stop-band rejection. It utilizes a narrow-band antenna and a passive low insertion loss band-pass filter. It is used when the source of powerful,

near-band interference is known and expected, such as unintentional interference due to the proximity of a RF source.

2. Code/carrier loop techniques including aiding [Kaplan, 1996]

Jamming performance is improved by narrowing the pre-detection bandwidth of the receiver as well as the code and carrier tracking loop filter bandwidths. Reducing these bandwidths also reduces the line-of-sight dynamics that each channel can tolerate. This can be mitigated somewhat by increasing the loop filter order for an unaided receiver. But in the presence of accurate external aiding, it can effectively remove dynamic stress on tracking loops. Examples of navigation sensors which have been integrated with GPS include Inertial Measurement Units (IMU), Doppler radar and air speed/baro altimeter/magnetic compass sensors.

3. Temporal filtering technique [Parkinson and Spilker, 1996]

This technique is effective only for narrow-band jammers. If there is no RFI, then the thermal noise spectrum will be fairly uniform in the frequency domain. If there is a significant level of narrow-band interference in the signal it will be manifested by an anomaly which is above the thermal noise level. The digital signal processing technique can effectively filter out the narrow-band anomaly and reduce the narrow-band interference down to the thermal noise level. The temporal filtering process is accomplished by performing digital signal

processing of the digitized IF signal using real time filtering techniques. The filter can be formed in the time domain using an Adaptive Transversal Filter (ATF), or in the frequency domain using a Fast Fourier Transform (FFT).

#### 4. Antenna design enhancements [Parkinson and Spilker, 1996]

The main idea of this technique is to increase the antenna gain toward satellites and decrease gain toward jammers. One type is called a beam-steered array which points a narrow beam of antenna gain toward each satellite being tracked. The other type is called a controlled reception pattern antenna (CRPA), which contains multiple antenna elements physically arranged into an array that can steer gain nulls toward jammers.

The temporal filtering technique using FFT, combined with an adaptive code-tracking loop technique will be discussed in detail in this thesis. The principle of this technique, also referred to as the frequency excision algorithm, is based on spectrum analysis. If a frequency anomaly is found in the spectrum, this component will be excised from the corresponding frequency bin [Cutright et al., 2003].

RFI mitigation using spectrum analysis is not a new technique: much research has been done, dating back to the early 1980s, e.g. Li and Milstein (1982), Dipietro (1989), Young and Lehnert (1994), Wang and Amin (1998). These

investigations have focused on spread spectrum communications systems. Only in recent years has such a frequency domain analysis-based interference mitigation method been applied to GPS by some researchers, namely Peterson et al. (1996), Badke and Spanias (2002) and Cutright et al. (2003). Most of these methods were implemented and tested using conventional hardware receivers. However, many implementation issues, such as the determination of the detection threshold for different kinds of interference and different interference levels, the impact of narrow-band interference, the effectiveness of the mitigation algorithm in a software receiver for signal acquisition and tracking, and position fixing, have not been fully addressed. Thus, further research into this algorithm, aided by the flexibility that a software GPS receiver provides could enhance the application of the frequency excision algorithm in the field of GPS.

### **1.3 Research objectives**

A software GPS receiver developed by the Positioning, Location, and Navigation (PLAN) research group in University of Calgary provides an excellent platform for interference study (Ma et al., 2004). Selection of this software receiver platform provides researchers and developers with more evaluation and testing flexibility than a comparable hardware platform. New algorithms can be implemented and receiver parameters can be modified without the cost and delay associated with hardware development.

The first objective of this thesis is to develop an algorithm to mitigate narrow-band

interference that can be embedded into a software Coarse/Acquisition (C/A)-code GPS receiver to improve anti-jamming performance in terms of accuracy, reliability and sensitivity.

The second objective is to verify the effectiveness of this algorithm. The verification will be conducted in a software receiver, and the effectiveness of this algorithm for signal acquisition, tracking, and position-fixing will be studied. The maximum tolerance of this algorithm to CW, AM and FM interference and the effects of the sampling rate on this algorithm will also be investigated.

## **1.4 Thesis outline**

Chapter 1 provides the necessary background information and establishes the intent and focus of the thesis. Chapter 2 describes the principle of the FFT-based narrow-band interference mitigation method. Chapter 3 describes the test set up, the definition of the metrics, and software approaches used in evaluating mitigation algorithms. Chapter 4 presents the results in the acquisition domain. Chapter 5 presents the test results in tracking and position domain. Chapter 6 presents the results of kinematic testing. Chapter 7 discusses strategies for improving the mitigation performance through the use of data windows. Finally, the conclusions and recommendations for future research are presented in Chapter 8.

## CHAPTER 2

# Theory of FFT-based Narrow-band Interference Excision and Introduction to Receiver Technology

The Global Positioning System uses a direct sequence spread spectrum (DS-SS) signal which incorporates some degree of jamming protection in the signal structure itself. However, a weak GPS signal - normally in the range of -160 to -156 dBW for the C/A-code - which is well below the background RF noise level sensed by an antenna makes it easy for the interference signal to overcome the inherent jamming protection of the DS-SS signal. Interference signals are spread in the frequency domain by the GPS signal de-spreading process. These spectrally dispersed interference signals make it difficult for the GPS receiver to track the peak of the correlation function. Thus, a frequency-domain interference excision algorithm is a good approach to mitigate this susceptibility. This algorithm is, however, effective only against narrow-band interference.

### 2.1 Narrow-band versus wide-band interference

Narrow-band interference usually occupies more than 100 KHz of bandwidth and

less than the entire available spectrum for C/A-code, a bandwidth of 2.046 MHz [Rash, 1997]. However, qualification of narrow-band signals will also depend on the bandwidth of the desired signal. For example, a 5 MHz interfering signal can be regarded as wide if the receiver utilizes a wide correlator design with a 4 MHz pre-correlation filter; similarly, the same interfering signal can be regarded as narrow with narrow correlator designs, which have bandwidths of up to 20 MHz. Unintentional narrow-band interference most often arises from spurious signals generated by inadequately shielded electrical equipment. Some narrow-band radio links adjacent to GPS frequencies are also known to cause local interference problems [MacGougan, 2003].

Wide-band interference occurs across the entire GPS C/A-code spectrum, covering bandwidths of 2.046 MHz or more. Wide-band interference is also dependent upon the bandwidth of the original signal. The lower limit of what is considered wide-band, therefore depends on assignments in the receiver's pre-correlation filters. The impact of wide-band interference that is of interest in this research is the increase in the effective noise floor in a GPS receiver. Furthermore, when the Jammer-to-Signal ratio (J/S) exceeds the processing gain of the spreading code, the correlation function is destroyed, making it impossible to measure the pseudorange.

Wide-band interference in the GPS spectrum originates typically, for example, in

television transmitters' harmonics, or when near-band microwave link transmitters overcome the front-end filter of the GPS receiver [Kaplan, 1996].

## 2.2 Fast Fourier Transform

To perform frequency analysis on a discrete-time GPS signal, the time domain sequence must be converted to an equivalent frequency-domain representation. Such a frequency-domain representation leads to the Discrete Fourier Transform (DFT), which is a powerful computational tool for performing frequency analysis of discrete-time signals.

The Fourier transform separates a waveform or function into sinusoids of different frequencies which sum to the original waveform. It identifies or distinguishes the constituent frequency sinusoids and their respective amplitudes.

The Fourier transform of an aperiodic signal with finite duration  $x(t)$  is defined as

$X(F)$ :

$$X(F) = \int_{-\infty}^{\infty} x(t)e^{-j2\pi Ft} dt \quad (2.1)$$

The following set of conditions that guarantee the existence of the Fourier transform are known as the Dirichlet conditions [Proakis, 1996a]:

1. the signal  $x(t)$  has a finite number of finite discontinuities;
2. the signal  $x(t)$  has a finite number of maxima and minima; and
3. the signal  $x(t)$  is absolutely integrable; that is,

$$\int_{-\infty}^{\infty} |x(t)| dt < \infty \quad (2.2)$$

In any case, if  $x(t)$  is an actual physical component, there always exists a Fourier transform.

For a finite duration sequence,  $x(n)$  of length  $L$ , the Fourier transform is as follows:

$$X(\omega) = \sum_{n=0}^{L-1} x(n) e^{-j\omega n} \quad 0 \leq \omega \leq 2\pi \quad (2.3)$$

When  $X(\omega)$  is sampled at equally spaced frequencies

$$\omega_k = 2\pi k / N, k = 0, 1, 2, \dots, N-1 \quad \text{where } N \geq L. \quad (2.4)$$

The resultant samples are

$$X(k) = \sum_{n=0}^{N-1} x(n) e^{-j2\pi kn / N} \quad k = 0, 1, 2, \dots, N-1 \quad (2.5)$$

This is a formula for transforming a sequence  $\{x(n)\}$  of length  $N \geq L$  into a sequence of frequency samples  $\{X(k)\}$  of length  $N$ . Since the frequency samples are obtained by evaluating the Fourier transform  $X(\omega)$  at a set of  $N$  equally spaced discrete frequencies,  $X(k)$  is called the DFT of  $x(n)$ .

Direct computation of the DFT is basically inefficient because it does not exploit the symmetry and periodicity properties of the phase factor,  $e^{-j2\pi / N}$

The FFT is a DFT algorithm developed by Tukey and Cooley (1965) which reduces the number of computations from something in the order of  $N^2$  to  $N \log_2 N$ , by exploiting the symmetry and periodicity properties of the phase factor.

In this algorithm, it re-expresses the DFT of an arbitrary composite size ( $n = n_1 n_2$ ) in terms of smaller DFTs of sizes  $n_1$  and  $n_2$ . It first computes  $n_1$  transforms of size  $n_2$ , and then computes  $n_2$  transforms of size  $n_1$ . The decomposition is applied recursively to both the  $n_1$  and  $n_2$  point DFTs. The general Cooley-Tukey factorization rewrites the indices  $j$  and  $k$  as  $j = n_2 j_1 + j_2$  and  $k = n_1 k_2 + k_1$ , respectively, where the indices  $j_a$  and  $k_a$  run from  $0..n_a-1$ . That is, it re-indexes the input ( $k$ ) and output ( $j$ ) as  $n_1$  by  $n_2$  two-dimensional arrays in column-major and row-major order, respectively. When this reindexing is substituted into the DFT formula for  $jk$ , the  $n_2 j_1 n_1 k_2$  cross term vanishes (Its exponential is unity).

### 2.3 Algorithm for FFT-based narrow-band interference mitigation

The interference immunity of a spread spectrum system corrupted by narrow band interference can be significantly enhanced by excising the interference prior to correlation of the received signal [Proakis, 1996b]. Several techniques exist for reducing this interference, including adaptive transversal filters (ATF) [Przyjemski, et al., 1993], FFTs, and filter banks (FB) [Rifkin and Vaccaro, 2000]. All these techniques attempt to filter out the interference before correlation. A steady-state  $2M+1$  tap linear phase ATF utilizes  $M$  taps on each side of the centre tap as a  $2M$  tap linear predictor of the value at the centre tap. This can be expressed in vector notation as:

$$r_n = x_{n-M} - w^T x_n \quad (2.6)$$

where  $w$  is the length  $2M$  vector of weights and  $x_n$  is the length  $2M$  vector of inputs existing at time  $n$ .

Therefore, a  $2M+1$  tap linear phase filter is realized with  $M$  complex multipliers,  $M$  complex adders, and an  $M+1$  complex adder tree utilizing  $\log_2^{(M+1)}$  complex adders. The computational complexity of this ATF based method determines if it can be implemented in ASIC, but is not efficient in a software receiver. The number of computations for FFT based methods is  $N \log_2^N$ . This method is used in this thesis, because it has the potential to be implemented in a real time software receiver. Filter bank represents an extension of the FFT based method

that attempts to further reduce the signal loss by extending the effective FFT length. The FB allows the spectrum estimation to occur more or less frequently and the filtering is performed over an arbitrary length. The testing of this method is left for future research.

The objective of the FFT-based narrow-band interference algorithm is to reduce the level of the interference; this is achieved at the expense of introducing some degree of distortion on the desired signal. The estimation and suppression of interference can be performed in the frequency domain by using DFT, which is efficiently implemented via an FFT algorithm. The received base band signal is processed in fixed-length blocks, transformed to the frequency domain with an FFT, filtered by using an appropriate weighting, and then transformed back into the time domain.

The received base band data stream has three components; namely, the signal samples  $s_k$ , the broadband noise samples  $\eta_k$ , and the narrow-band interference sample  $\theta_k$ . Each component is assumed to be uncorrelated with the other two and characterized by a zero mean. The individual component correlations [Dipietro, 1989] are given as:

$$E[s_k s_m^*] = \begin{cases} 0 & k \neq m \\ S & k = m \end{cases} \quad (2.7)$$

$$E[\eta_k \eta_m^*] = \begin{cases} 0 & k \neq m \\ \sigma^2 & k = m \end{cases} \quad (2.8)$$

$$E[\theta_k \theta_m^*] = r_{m-k} \quad (2.9)$$

where  $E[\ ]$  is the expectation operator and  $*$  denotes a complex conjugate. Hence, the signal and noise samples are each uncorrelated, while the narrow-band interferences are correlated.

The input sample stream is grouped into blocks of length  $N$  (the FFT length) for suppression processing. The vector  $X$  (length  $N$ ) is defined as the sum of the signal, noise and interference. Thus the  $N$  point filtered output vector  $\hat{X}(k)$  becomes

$$\hat{X}(k) = \sum_{n=0}^{N-1} \alpha_n x(n) e^{-j2\pi kn/N} \quad (2.10)$$

where  $\alpha_n$  is the frequency domain weighing function designed to suppress the interference effects.

The SNR at the output of the correlator is given by:

$$SNR = \frac{(E[s_k^H \hat{X}])^2}{Var(s_k^H \hat{X})} \quad [\text{Dipietro, 1989}] \quad (2.11)$$

where  $Var()$  is the variance operator and  $H$  denotes the conjugate transpose.

If the corresponding component in Equation 2.10 is replaced by the assumed statistical properties of the signal components and the characteristics of the DFT transformation matrix, this yields the SNR in the form:

$$SNR = \frac{(\sum_{k=1}^N \alpha_k)^2 S}{d1 + d2 + d3} \quad (2.12)$$

with

$$d1 = S \left( \sum_{k=1}^N \alpha_k^2 - \frac{(\sum_{k=1}^N \alpha_k^2)}{N} \right) \quad (2.13)$$

where  $d1$  is a “self noise” term which is analogous to that seen in linear prediction suppression processors [Proakis and Ketchum, 1982] - a term that vanishes in the case of no filtering.

$$d2 = \sigma^2 \sum_{k=1}^N \alpha_k^2 \quad (2.14)$$

where  $d2$  is the residual broadband noise.

$$d_3 = \frac{1}{N} \sum_{k=1}^N (\theta_k \alpha_k)^2 \quad (2.15)$$

where  $d_3$  is narrow-band interference power, and

$\theta_k$  is the  $k^{\text{th}}$  FFT bin component of the narrow-band interference signal.

If the value of  $\alpha_k$  is set at unity, this yields an expression of the pre-suppression SNR as:

$$SNR = \frac{NS}{\sigma^2 + \frac{1}{N} \sum_{k=1}^N (\theta_k)^2} \quad [\text{Dipietro, 1989}] \quad (2.16)$$

where  $N$  is the FFT length for suppression processing and  $S$  is equal to

$$E[s_k s_k^*].$$

Comparing the two equations, 2.11 and 2.15, the ratio of these two equations yields the improvement factor used to assess interference mitigation performance.

A thresholding algorithm is used to determine the weighting function. From either the model or real world data, the distribution of interferer powers suggests that only a small number of frequency domain cells contain nearly all of the interference power within the band [Dipietro, 1989]. Based on this conclusion, one possible strategy would be to set the weights on all cells with large interference values to zero, while leaving the others at unity. The computational challenge lies

in determining which cell constitutes a large interference. One way is to establish a threshold and any cell magnitude exceeding this level is declared as interference and removed by setting its corresponding weighting function to zero. The threshold may be established on the basis of knowledge of the interference distribution, or on the basis of heuristic experience, such as setting the threshold to excise a fixed percentage of the cells or total interference power. The other strategy would be to set any cell value exceeding the threshold to the background noise level, and thus whiten the interference spectrum. This approach will yield improved results, because the cell value containing interference will be reduced only to the background level, hence retaining most of the signal power. The drawback to this approach, however, is the requirement for the background noise level to be estimated, producing the unwanted consequence of increasing the computational burden.

## **2.4 Introduction to GPS receiver technology**

The FFT-based interference mitigation algorithm is developed in a software GPS receiver in this thesis. The impact of different receiver design parameters on the mitigation results will also be discussed. An overview to GPS receiver technology and criterion for choosing design parameters will be provided in this section.

### **2.4.1 GPS signal acquisition overview**

GPS signal acquisition is a two-dimensional search process, as illustrated in

Figure 2.1 below [Lin and Tsui, 2000]. The range dimension is associated with the replica code, while the Doppler dimension is associated with the replica carrier.

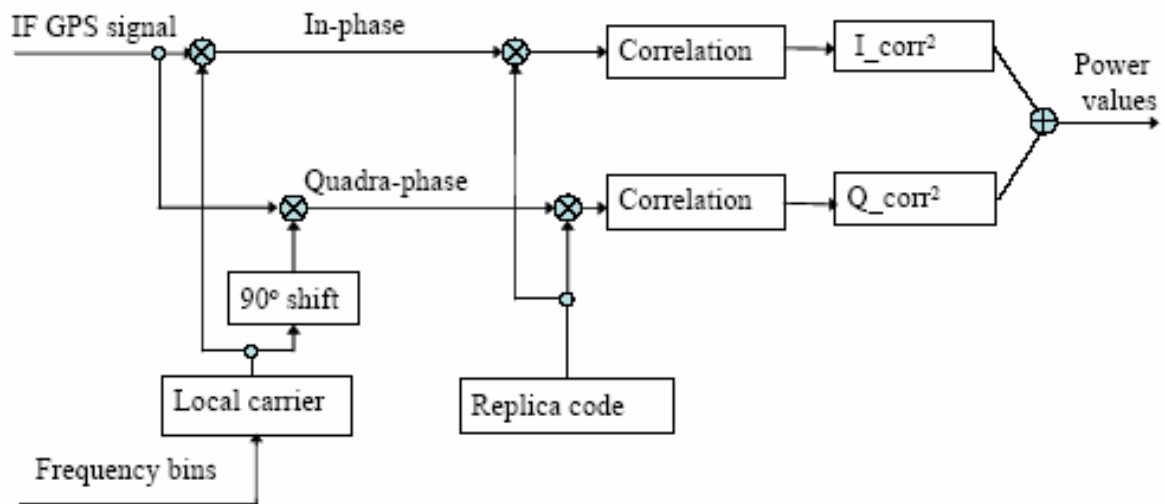


Figure 2.1: GPS signal acquisition

Pre-determination of the code phase is difficult because this is a function of the starting point and is dependent on the sampling rate. The code search space typically includes all possible code offset values. All 1023 C/A-code phases must therefore be searched. The combination of one code bin and one Doppler bin constitutes a searching cell. The Doppler change is a function of user dynamics and the stability of the receiver oscillator. If the Doppler uncertainty is unknown, the maximum user velocity plus maximum SV Doppler must be searched in both directions about zero Doppler. The Doppler searching space is usually from -5 kHz to 5 kHz [Ray, 2003]. The frequency resolution is determined by the coherent

integration time, which is also referred to as the dwell time. The rule-of-thumb Doppler bin is defined as follows to avoid significant signal attenuation due to frequency errors [Ward, 1996]:

$$\Delta f = 2 / (3T) \quad (2.17)$$

where  $T$  represents the coherent integration time.

The coherent integration time restricts the size of Doppler bins used in acquisition mode. Dwell times can vary from less than 1.0 ms for strong signals up to 20.0 ms for weak signals. It can be seen from Equation 2.16 that the corresponding Doppler bins are 667 Hz and 33 Hz. The poorer the expected  $C/N_0$  ratio, the longer the dwell time (and overall search time) must be in order to have reasonable success in signal acquisition [Kaplan, 1996]. Longer integration can provide improved frequency resolution and higher sensitivity, but this entails searching a larger number of bins and requires more time. Thus, there is a trade-off between the pre-detection integration time and acquisition speed.

Various acquisition methods incorporating search and detect strategies have been proposed in the literature [Krumvieda et al., 2001; Kaplan, 1996]. A cell-by-cell search method is usually used in conventional hardware receivers. In this method, the search region is divided into a number of cells of equal size. A local carrier is generated corresponding to a frequency bin and beat with the

incoming signal. A local code stream, corresponding to a code chip delay, is generated and then correlated with the incoming signal. The local code is shifted to correlate with the incoming signal until the peak is detected or all the cells are exhausted. The acquisition time is, therefore, the product of the dwell time and the number of search bins. Consequently, the acquisition time is very long, since the search is sequential in nature.

In a software GPS receiver, the computational burden can be reduced with the use of a block signal acquisition technique, namely a DFT-based circular convolution. This is achieved by the circular convolution giving the acquisition results of all possible code offsets at a specific carrier frequency in one DFT-based computation. The basic principle of this method lies in the fact that correlation in the time domain is equal to convolution in the frequency domain. The theory, proposed by Van Nee and Coenen [1991], involves the correlation between two periodic sequences,  $x(n)$  and  $h(n)$ :

$$z(n) = \sum_{m=0}^N x(m)h(n+m) \quad (2.18)$$

which is equivalent to

$$z(n) = IFFT(FFT(x(n)).FFT^*(h(n))) \quad (2.19)$$

where \* denotes the complex conjugate.

The correlation value at all possible code offsets can be calculated in one DFT operation which greatly reduces the computational burden. Even faster acquisition speed can be achieved if FFT is applied. This is the basis for choosing the FFT-based acquisition algorithm for investigation in this thesis.

#### **2.4.2 GPS signal tracking overview**

Acquisition produces a coarse estimate of the carrier Doppler and the code offset of incoming signals. The function of tracking is to track variations in the carrier Doppler and code offset due to line-of-sight dynamics between satellites and the receiver, together with bit and sub-frame synchronization to demodulate the navigation data to obtain ephemeris data. Figure 2.2 below illustrates the block diagram of the GPS receiver tracking loop.

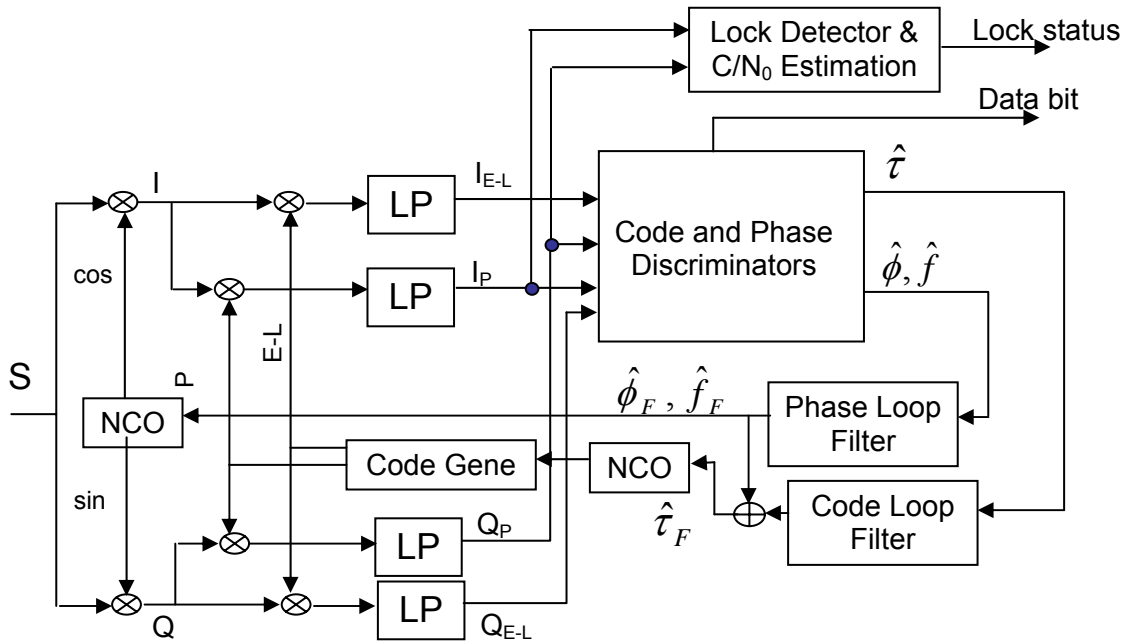


Figure 2.2: GPS receiver signal tracking loop

Both the carrier lock loop (frequency lock loop (FLL) or phase lock loop (PLL)) and delay lock loop (DLL) are required for signal tracking to match the carrier phase and code offset with the locally generated carrier and code. The carrier pre-detection integrators, the carrier loop discriminators and the carrier loop filters characterize the receiver carrier tracking loop. However, a paradox becomes apparent during determination of these three parameters. To maximize tolerance to dynamic stress, the pre-detection integration time should be short, the discriminator should be a FLL, and the carrier loop filter bandwidth should be wide. However, if interference exists or under weak signal conditions, the pre-detection integration time should be long and the carrier loop filter noise bandwidth should be narrow [Kaplan, 1996]. In order to obtain more accurate carrier Doppler phase

measurements, the discriminator should be PLL instead of FLL. In implementation, some compromises have to be made. The tracking loop will start with a short pre-detection integration time, using a FLL and a wide-band carrier loop filter. Then it switches to a Costas PLL with its pre-detection bandwidth and carrier tracking loop bandwidth set as narrow as the dynamics permit. It will revert to FLL operation during periods of high dynamic stress if necessary.

A DLL is used to track the C/A-code phase of incident signals. As in a regular phase lock loop, it consists of a code phase discriminator, a loop filter, and the C/A-code numerically-controlled oscillator (NCO). Figure 2.3 illustrates a typical DLL realized in the software receiver with a second order phase lock loop which tolerates constant acceleration [Ward, 1996 and Dong, 2003].

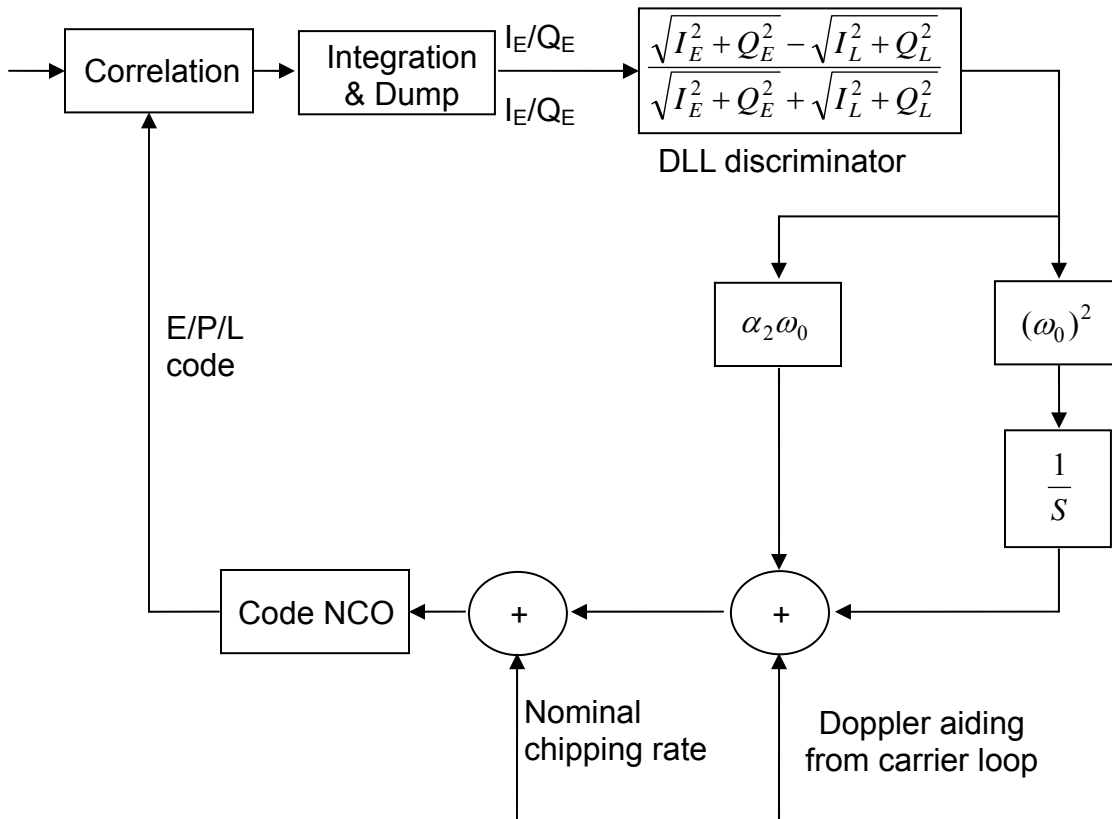


Figure 2.3: Software Receiver Delay lock loop

A normalized early-minus-late envelope DLL discriminator is used in the software receiver due to its wider tracking range than other types of discriminator. Its input-output relationship is linear between -0.5 chips to 0.5 chips, so no extra approximation will be introduced in the estimation of the code phase,  $\Delta\tau$ .

A second-order DLL loop which can track constant acceleration in an unbiased manner is used in the software receiver. The output of the loop filter is used to drive the code NCO and keep track of the code of the incoming signal to provide an accurate pseudorange measurement.

### 2.4.3 Raw measurement derivation

A pseudorange measurement can be calculated using the following equation:

$$\rho(t) = c[t_u(t) - t^{(s)}(t - \tau)] \quad [\text{Ward, 1996}] \quad (2.20)$$

where  $t^{(s)}(t - \tau) = Z$  count

- + Number of navigation bits
- + Number of C/A-codes
- + Number of whole C/A-code chips
- + Fraction of C/A-code chip

The pseudorange construction is simplified as shown in Figure 2.4

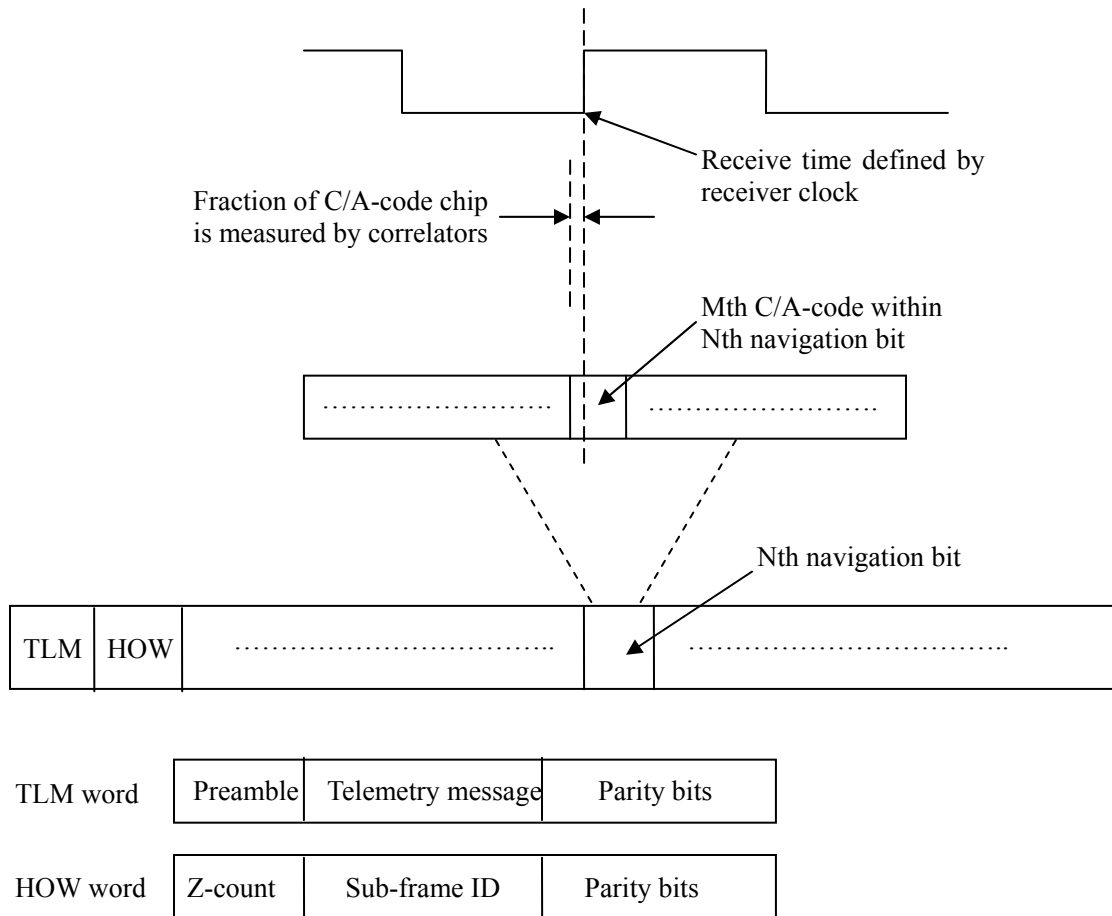


Figure 2.4: Pseudorange construction [after Ward 1996]

The arrival time  $t_u(t)$  kept by an inner clock is defined by a transition of the receiver clock. In general, these transitions occur at some time in the middle of a C/A-code chip, and so the larger task is to establish the transmission time, according to the satellite, of the received code feature identified by the receiver clock transition. Satellite time is kept by the Z-count which is also included in the navigation message. Since the Z-count establishes satellite time at the beginning

of each sub-frame, the transmission time is the Z-count plus the whole number of C/A-code chips since the beginning of the sub-frame. The elapsed time can be measured using the following components: the whole number of navigation bits, added to the whole number of C/A-codes since the beginning of the current navigation bits, added to the number of whole C/A-code chips since the beginning of the current code and added to the received fraction of the current chip. The last two are measured by the DLL and the rest are measured by counters in the bit synchronization and sub-frame synchronization modules.

The Doppler measure can be read directly from the carrier NCO while the carrier phase must be assisted by a carrier counter which is used to count the integer number of cycles that the incoming carrier has changed. The fractional portion is recorded with the carrier NCO; the summation of the integer and fractional parts gives the carrier phase measurement since locking of the loop.

After the pseudorange and carrier phase raw measurements have been derived, a least squares approach is employed to estimate the position solution and clock bias.

#### **2.4.4 Loop filter determination**

The objective of the loop filter is to reduce noise in order to produce an accurate estimate of the original signal at its output. The loop filter order and noise bandwidth determine the loop filter's response to signal dynamics. The loop filter's

output signal is effectively subtracted from the original signal to produce an error signal, which is fed back into the filter's input in a closed loop process.

The type of tracking loop chosen depends on the following design factors:

- Desired tracking performance
- Desired noise bandwidth (and resulting SNR), and
- Anticipated user dynamics

Table 2.1 summarizes the typical values and characteristics of first order, second order and third order tracking loops [Kaplan, 1996].

Table 2.1: Loop Filter Characteristics

Loop order	Noise bandwidth B <sub>n</sub> (Hz)	Typical filter values	Steady state error	characteristics
First	$\frac{\omega_0}{4}$	$\omega_0$ $B_n = 0.25\omega_0$	$\frac{(dR/dt)}{\omega_0}$	Sensitive to velocity stress. Used in aided code loops.  Unconditionally stable at all noise bandwidths
Second	$\frac{\omega_0(1+\alpha_2^2)}{4\alpha_2}$	$\omega_0^2$ $\alpha_2 = 1.414$ $B_n = 0.53\omega_0$	$\frac{(dR^2/dt^2)}{\omega_0^2}$	Sensitive to acceleration stress. Used in aided and unaided carrier loops. Unconditionally stable at all noise bandwidths
Third	$\frac{\omega_0(\alpha_3 b_3^2 + \alpha_3^2 - b_3)}{4(\alpha_3 b_3 - 1)}$	$\omega_0^3$ $\alpha_3 = 1.1$ $b_3 = 2.4$ $B_n = 0.784\omega_0$	$\frac{(dR^3/dt^3)}{\omega_0^3}$	Sensitive to jerk stress. Used in all unaided carrier loops. Remains stable at $B_n \leq 18$ Hz

Under kinematic test conditions, the acceleration was constant, and the second

order loop filter is sensitive enough to detect the acceleration stress. The second order loop filter is unconditionally stable at all noise bandwidths. By comparison, the third order loop filter is stable only when  $B_n \leq 18$  Hz [Kaplan, 1996], and the computational burden is high. The combination of robustness under kinematic stress and a manageable computational load support the choice of the second order loop filter for test purposes.

The block diagram of a second order loop filter is shown below [Kaplan, 1996]:

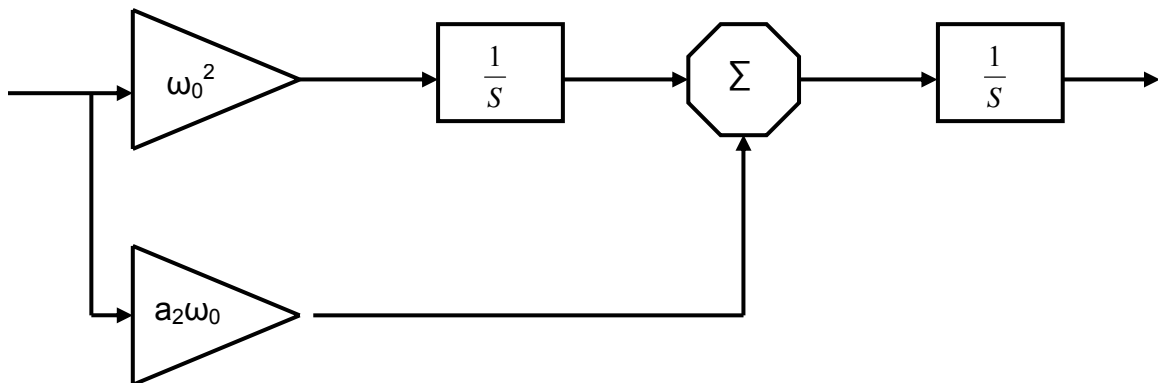


Figure 2.5: Second order loop filter

In Figure 2.5, analog integrators are represented by  $1/s$ , the Laplace transform of the time domain integration function. This transform can be implemented in digital form as shown in Figure 2.6.

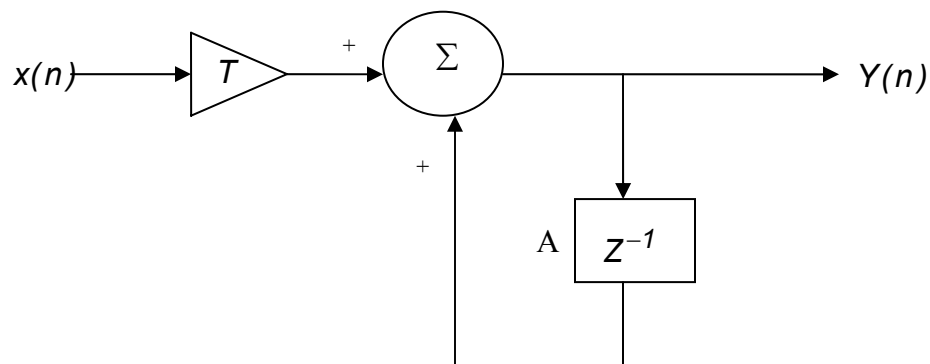


Figure 2.6: Digital representation of Laplace transform

The input  $x(n)$  which is quantized to a finite resolution produces a discrete integrated output,  $Y(n)$  as  $y(n) = T[x(n)] + A(n-1)$ , where  $n$  is the discrete sample sequence number.

The time interval between each sample  $T$  represents a unit delay  $Z^{-1}$  in the digital integrator. This provides a dynamic range capability. A comparatively long integration time produces a long response time and hence is not suitable for high dynamic conditions. If the signal is weak, for example, and interference occurs, a longer integration time is required. A balance must be made to achieve optimal sensitivity and accuracy.

## CHAPTER 3

### Test Setup and Methodology

In order to obtain repeatable and controllable GPS signals with narrow-band interference, a hardware GPS simulator and signal generator were used. These two signals were combined in an interference combiner unit. The output was fed to a *Signal Tap* which down-converts RF signals to IF signals and samples them. The resulting data was used in the software receiver and a mitigation algorithm was used to assess the acquisition, tracking and position performance. This chapter addresses the test setups and software approaches of the mitigation algorithms studied.

#### 3.1 RF GPS signal with interference generation

##### 3.1.1 GSS STR6560 multi-channel GPS/SBAS simulator

The PLAN group of the University of Calgary possesses two synchronous 12-channel L1-only hardware signal simulation units (GSS STR 6560) associated to a control computer made by Spirent Communications Inc. which is capable of providing comprehensive facilities for development and product testing of satellite navigation equipment and integration studies. The simulator can also reproduce

the environment of a navigation receiver installed on a dynamic platform, exhibiting the effects of high-dynamic host vehicle motion, navigation satellite motion and ionospheric and tropospheric effects. The simulator may be considered as a pseudorange-to-RF converter. Each channel represents a satellite signal at a single carrier frequency. The simulator's capabilities include the following [Spirent, 2003a]:

- Control of the signal power for each channel
- Complex simulated vehicle trajectories
- Multipath simulation
- Satellite constellation definition and modeling
- Atmospheric effects modeling (Ionosphere/Troposphere)
- Vehicle motion modeling for aircraft, cars, and spacecraft
- User-supplied motion trajectories
- Antenna gain pattern manipulation
- Pseudorange error ramping
- Terrain obscuration modeling
- ASCII format scenario files (sharable between scenarios)
- Real time data display, and
- Post-mission truth data output

### **3.1.2 Interference generation combined with GPS signal**

The narrow-band interference simulated in the test (continuous wave (CW),

amplitude modulation (AM) and frequency modulation (FM)) was generated by an ESG E4431B signal generator. It can provide a maximum specified frequency of 2 GHz, at a maximum specified power of 10 dBm which is sufficient to jam GPS signals. The GPS and interference signals were combined in a GSS 4766 interference combiner unit which facilitates the use of commercial-off-the-shelf (COTS) signal generators as fully integrated interference sources with Spirent Satellite Navigation Simulators, such as the GSS 6560. The COTS signal generators are controlled through an IEEE-488-compliant (GPIB) bus, via *SimGEN* for *Windows*, hosted on the control PC. The interference signal is defined along with all the other scenario parameters from within *SimGEN*'s normal user GUI environment. The RF outputs are combined with the satellite signal generators (SSG) in the GSS 4766 interference combiner unit (ICU). The system hardware configurations are shown in Figure 3.1.

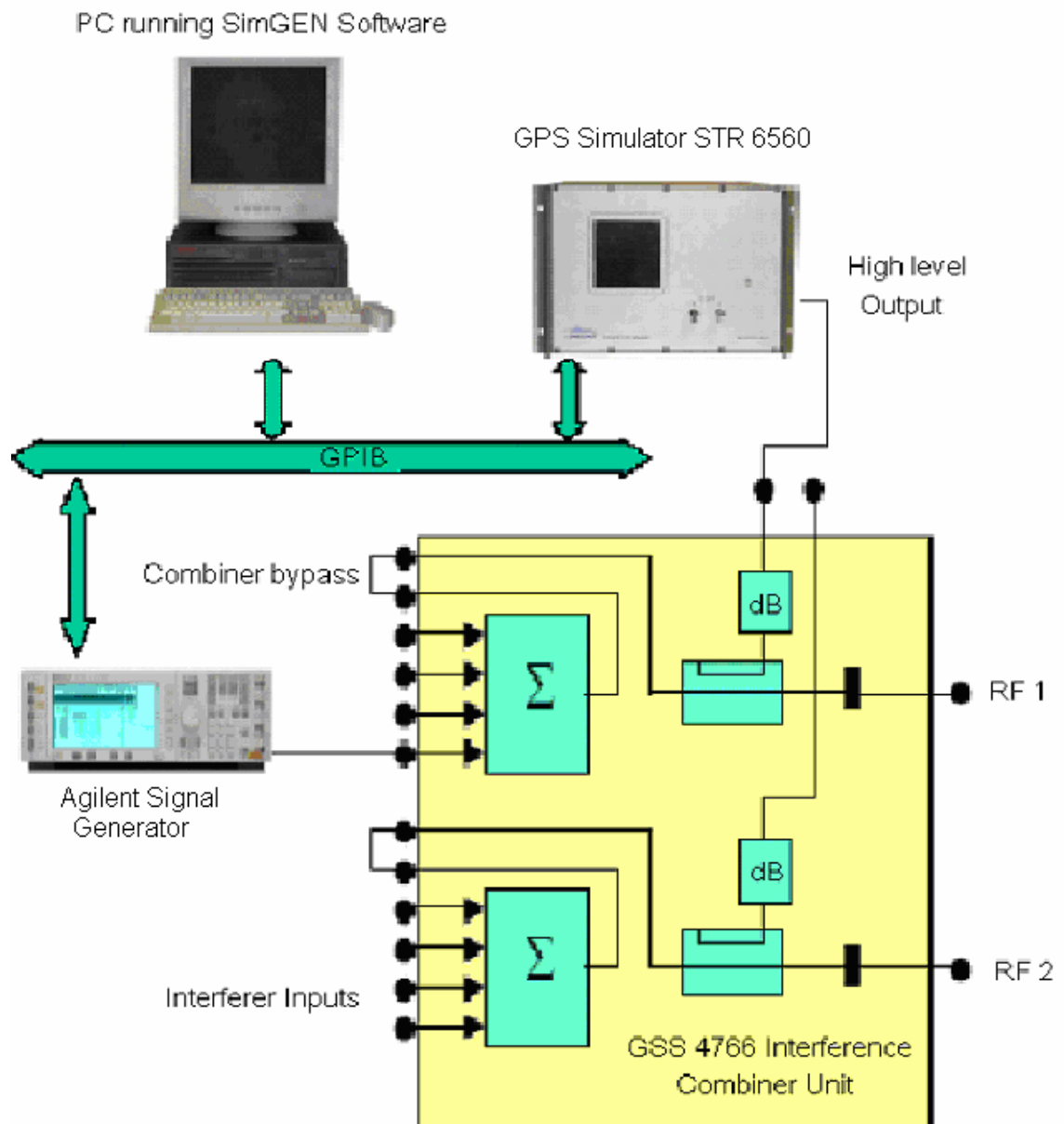


Figure 3.1: System hardware configuration

### **3.2 Intermediate frequency signal generation, sampling and quantization**

A hardware front-end, *GPS Signal Tap* (Figure 3.2), made by Accord Software & Systems Private Limited was used to collect the digitized IF signal. Only after down-converting, sampling and quantizing can the GPS data be processed by the software receiver. Accord's *GPS Signal Tap* is an L1 frequency GPS receiver front end, which serves as a programmable real time source of digitized GPS signals for a variety of desktop research and development tasks related to signal processing. The *Signal Tap* consists of a two-stage RF down-converter whose second IF can be sampled and stored for analysis by the user at a programmable frequency [Accord, 2003]. The RF down-converter obtains the input GPS satellite signal from an antenna-cable assembly. It uses mixers, local oscillators and band pass filters to down-convert the carrier to a low IF. The IF is then sampled by a chosen sampling frequency to generate the digitized IF signal of the satellites.



Figure 3.2: Hardware front-end “GPS Signal Tap”

The IF bandwidth of the *Signal Tap* is 2 MHz. A signal with 15.42 MHz IF was sampled at sampling rates of 4.75 MHz and 7 MHz in the test, resulting in a base-band signal centred at 1.17 MHz and 1.42 MHz, based on one-bit quantization. The collected data consists of a 1 and 0 sequence which is stored in a binary file. For processing convenience, it was then converted to a 1 and -1 sequence with binary format and sent to the software GPS receiver. Due to the limited capacity of the on-board RAM of *Signal Tap*, only 80 seconds of data could be collected.

### 3.3 Metrics definition

In order to define the performance characteristics of the mitigation algorithm, the following metrics were used:

(1)  $C/N_0$ : Carrier-to-Noise Density Ratio (dB). It is one of the most important measurement values used to define the quality of a signal. The nominal noise floor has a spectral density of approximately -204 dBW/Hz. The minimum guaranteed GPS signal power for L1 C/A-code is -160 dBW, which implies a  $C/N_0$  equal to  $C - N_0 = 44$  dBW-Hz. Receivers incorporating different correlation processes will have differences in  $C/N_0$ ; the short term variation in the  $C/N_0$  can be used as an estimate of signal degradation caused by interference.

(2) Jamming-to-Signal ratio (J/S).  $J/S = J-S$  (dB), where S and J are the incident signal power and incident jamming power, respectively, at the antenna. This measure, which can be controlled through *SimGEN* software, characterizes the relative interference power compared with the GPS signal strength.

(3) Estimated pseudorange errors: these errors are calculated by using  $C^3\text{NavG}^{2\text{TM}}$ , a software package developed by University of Calgary's PLAN Group.  $C^3\text{NavG}^{2\text{TM}}$  is a C-language program that processes pseudoranges and Doppler data in both static and kinematic modes to determine position and velocity in either single point or differential mode. An epoch-by-epoch least-squares solution is used, which is highly suitable for the type of sensitivity analysis required herein. This software allows the measurement of the degradation due to the interference on the pseudorange measurements.

(4) Position domain: With knowledge of the true position and velocity of the receiver from the output of the simulator, position and velocity errors can be computed. Hence, navigation performance in the presence of interference mitigation effects can be investigated.

Errors due to multipath and atmospheric effects have been removed from all of the tests in this thesis in order to isolate the errors of interest. Only interference and random noise will have an influence on the results.

In order to keep exactly the same conditions for all tests, all simulations were processed within the same period and satellite constellation: November 17, 2003, from 13:30:26 to 13:31:46. Only the sky view at the beginning of the simulation was provided in Figures 3.3, because the constellation changes very little in 80 seconds.

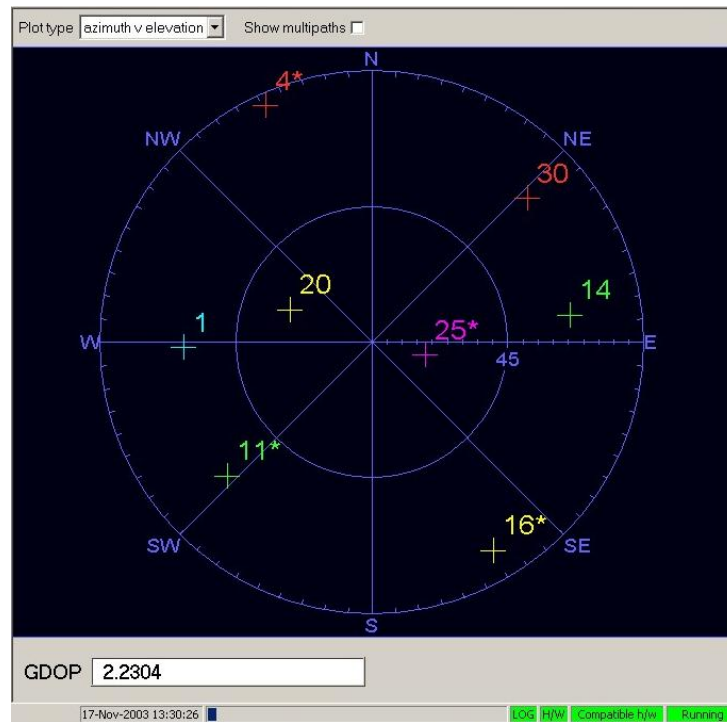


Figure 3.3: Sky view at the beginning of the simulation

### 3.4 Software approach of FFT-based mitigation algorithm

Prior to de-spreading, the GPS signal has noise-like characteristics over the system bandwidth. Therefore, any narrow-band RFI has strong correlations between samples in which the GPS signals are uncorrelated. Therefore, the spectral peaks of interference can be discriminated and suppressed from the GPS signal and the thermal noise (Gaussian distribution) through an adaptive threshold power level and an adaptive notch filter.

### 3.4.1 Interference detection

The first stage of an FFT-based interference mitigation algorithm is interference detection. Three methods are normally used for independent on-board interference monitoring:

#### 1) Correlator power Output

The correlator power output indicates the average post-correlation SNR which is computed from the following equation:

$$SNR_{pc} = \frac{I^2 + Q^2}{Expected\_Noise\_Floor} \quad (3.1)$$

where I and Q are the 1 ms In-phase and Quadra-phase prompt correlator signals, respectively. The level and variance of  $SNR_{pc}$  are a function of noise and interference in the signal, and therefore are candidates for interference detection.

#### 2) Carrier Phase Vacillation

Carrier phase vacillation provides a measure of the variance or jitters in carrier phase measurements from one measurement epoch to the next, and is defined as [Ndili and Enge, 1997]:

$$CPV = \frac{|CP_i - CP_{i-1}|}{T} \quad (3.2)$$

where  $CPV$  = Carrier phase Vacillation

$CP$  = Carrier phase

$T$  = Time duration of epoch

$i$  = Epoch index

$T$  is the time duration of epoch and  $i$  is the epoch index

The carrier phase referenced above is computed from the arctangent of the In-phase and Quadra-phase measurements. Phase swings of 180 degrees, due to data bit changes, are taken into account and do not affect the detection results. Receiver clock noise as well as interference contributes to vacillations in the carrier phase measurements. Interference contributes most, so carrier phase vacillation is therefore a candidate for interference detection. The limitation of this method is that it is only effective for a medium level interference. When the interference level is high, no carrier phase can be tracked, thus carrier phase vacillation cannot be calculated.

### 3) Automatic gain control (AGC) gains

The control loop of the AGC, located on the signal down-conversion/digitization path, acts by adjusting the threshold levels of the adaptive analog-to-digital converter (ADC) to maintain a specified ratio of digitized signal output levels. The quantizer threshold level is therefore associated with the interference level and can be used as an indication of the occurrence of interference.

Table 3.1 shows the summarized decision statistic results with CW interference, with percentages of incidence of false alarm (FA), missed detection (MD), normal operation (NO) and normal detection (ND) [Ndili and Enge, 1997]. Normal operation means the decision statistic result falls in the region of correct detection, while normal detection means the result falls in the region of correct non-detection as shown in Figure 4.5.

Table 3.1: Decision statistic results summary

	MD	FA	NO	ND
Correlator	0.0%	3.0%	56.7%	40.3%
Power output				
Carrier Phase	0.0%	10.4%	49.3%	40.3%
Vacillation				
AGC Gain	0.0%	1.5%	58.2%	40.3%

Because the control of the AGC in the *Signal Tap* cannot be accessed, the AGC gain method was not taken into account. Due to the relative large false alarm rate of the carrier phase vacillation method, the correlator power output method was viewed as a better method for use in this thesis.

### 3.4.2 Interference mitigation

The basic principle of an FFT-based mitigation algorithm is to determine the statistical properties of non-Gaussian distributed interference and to improve the

SNR by eliminating all interference. The mitigation process will certainly cause signal loss. So, if the interference has been successfully detected, the mitigation algorithm is applied to the input data; if, not, the normal acquisition and tracking procedure is applied directly.

This algorithm first transforms the incoming IF signal into the frequency domain using the FFT. In order to remove the bias in the frequency domain due to the bandwidth and the non-linear property of the *Signal Tap*, the signal is averaged over small intervals and the resulting mean is subtracted from the spectrum over the corresponding interval.

Figures 3.4 and 3.5 compare the 1 ms FFT results with and without CW interference (no unit for power spectrum).

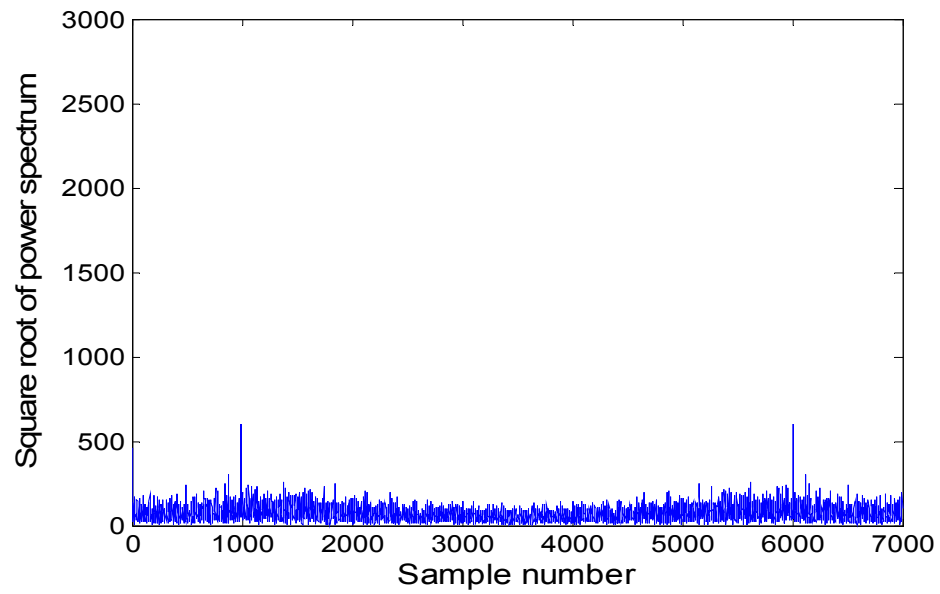


Figure 3.4: 1 ms FFT without CW interference

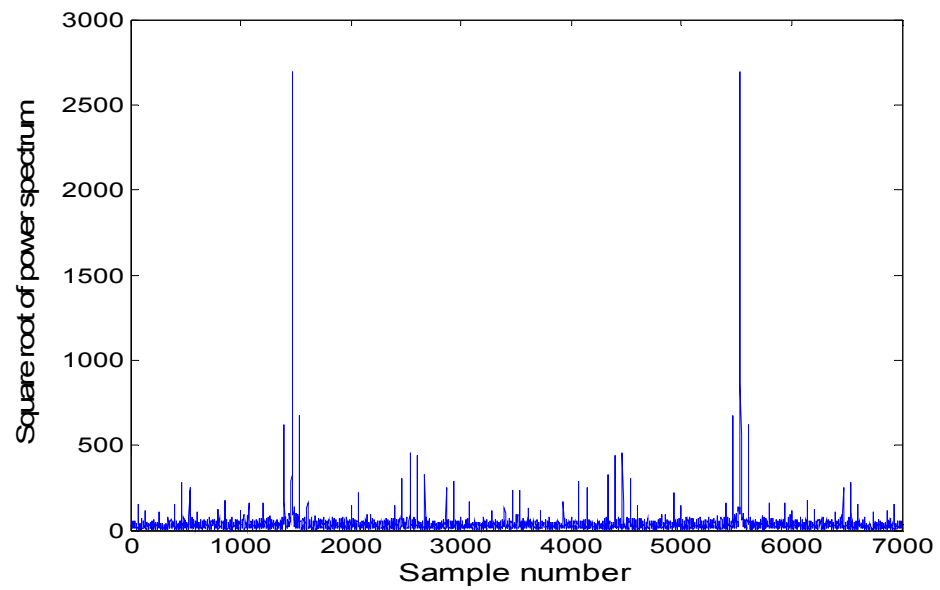


Figure 3.5: 1 ms FFT with CW interference ( $J/S = 30$  dB)

The 1 ms FFT analysis period is from  $-\pi$  to  $\pi$  and, so, the spectrum is symmetrical. The natural frequency  $\omega_0$  lies in the middle of the sample number axis (X axis). It can be seen from Figure 3.6 that, even with one pure tone CW interference, the influence of CW interference in the frequency domain is not a single line. Interference spreads out through the whole spectrum due to the finite FFT analysis period which causes spectral leakage (a detailed analysis of the mitigation of spectral leakage effects will be given in Chapter 7). So simply removing one frequency component with the largest power spectrum line is not sufficient. In implementation, further analysis is needed to decide which frequency component must be removed. The judging criterion is based on the statistical analysis of the input signal. Traditionally, the standard deviation of the resulting normalized spectrum is multiplied by a fixed value to set a detection threshold for determining the presence of RFI [Cutright et al., 2003]. The optimal estimate of this fixed value is determined empirically. However, for high-level interference, a fixed detection threshold is not good enough. Since the post-correlation SNR is a good indicator of interference level, it is reasonable to associate the detection threshold with the post-correlation SNR. In this thesis, an adaptive interference detection threshold determination method that is a function of the standard deviation of the normalized spectrum and the post-correlation SNR is used. The test results show that better performance can be achieved through this adaptive detection threshold. After the detection threshold is determined, the normalized spectrum is then compared against the threshold and bins exceeding the

detection level are identified. The bins containing RFI, along with a variable number of surrounding bins, are then set to zero in the original frequency domain spectrum. The effect of removing the frequency bins is equal to applying band-pass filters in the time domain. The Inverse Fast Fourier Transform (IFFT) of this spectrum is taken which yields a new time domain signal without RFI.

Figure 3.6 shows the flowchart of the frequency excision algorithm. In summary, in order to obtain the optimal anti-jamming performance, three parameters have to be carefully chosen:

- 1) the average interval to remove bias
- 2) detection threshold, and
- 3) the number of samples to be removed near the bin containing the RFI

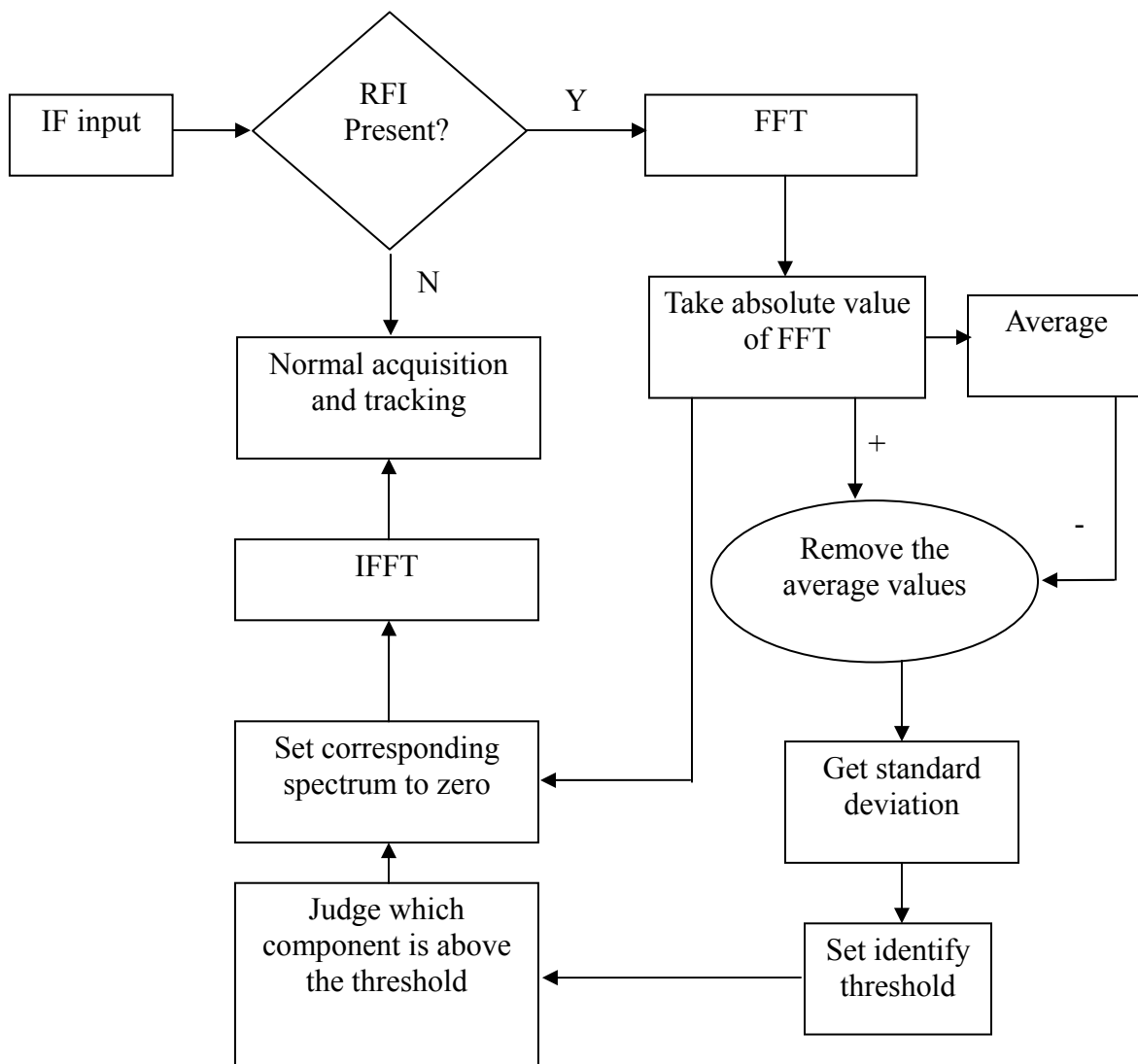


Figure 3.6: Flowchart of frequency excision algorithm

## CHAPTER 4

# Mitigation Analysis in Acquisition

### 4.1 CW Interference frequency determination

The GPS C/A-code is a Gold code with a short 1 ms period. Because of this, the C/A-code does not have a continuous power spectrum. Instead, it has a line spectrum whose components are separated by 1 KHz [Ward, 1996]. Figure 4.1 illustrates a typical Gold code spectrum from the GPS constellation.

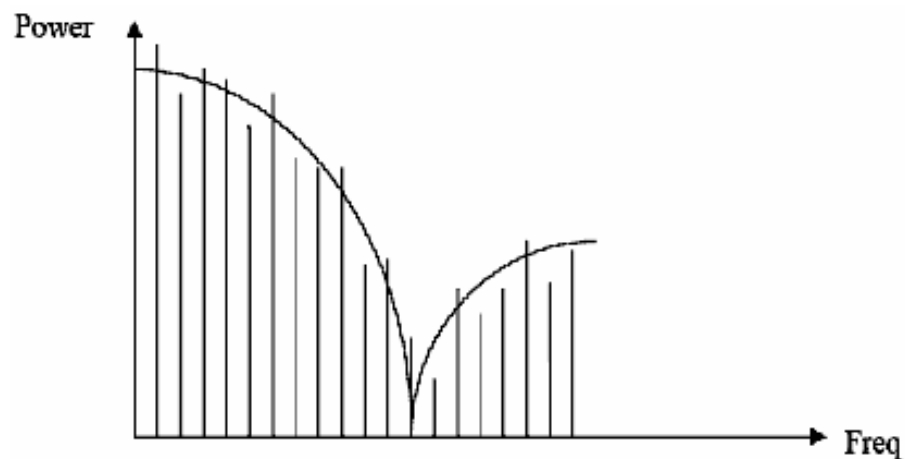


Figure 4.1: Spectrum of Gold code [from Heppe, 2002]

While the envelope of the spectrum approximates an ideal Sinc function, a clear line spectrum can be observed, with some components above and some below the ideal envelope. A narrow-band RFI signal could accidentally coincide with a strong spectral line of the Gold code and leak through the correlator, leading to a stronger than expected residual line into the PLL. Thus, narrow-band interference can be potentially more damaging than expected due to the line spectrum of the Gold codes used for ranging.

Although it is typical for each line in the C/A-code power spectrum to be 24 dB or more lower than the total power [Ward, 1996], there are usually some lines in every C/A-code that are stronger. These phenomena cause more of a problem during C/A-code acquisition than in tracking. Table 4.1 summarizes the worst line frequencies and the worst line (strongest) amplitudes for every Pseudorandom Noise (PRN) code used in GPS [Ward, 1996].

Table 4.1: Worst C/A line for each of the 37 codes

C/A-code PRN Number	Worst line Frequency (kHz)	Worst Line Amplitude (dB)	C/A-code PRN Number	Worst line Frequency (kHz)	Worst Line Amplitude (dB)
1	42	-22.71	20	30	-22.78
2	263	-23.12	21	55	-23.51
3	108	-22.04	22	12	-22.12
4	122	-22.98	23	127	-23.08
5	23	-21.53	24	123	-21.26
6	227	-21.29	25	151	-23.78
7	78	-23.27	26	102	-23.06
8	66	-21.50	27	132	-21.68
9	173	-22.09	28	203	-21.73
10	16	-22.45	29	176	-22.22
11	123	-22.64	30	63	-22.14
12	199	-22.08	31	72	-23.13
13	214	-23.52	32	74	-23.58
14	120	-22.01	33	82	-21.82
15	69	-21.90	34	55	-24.13
16	154	-22.58	35	43	-21.71
17	138	-22.50	36	23	-22.23
18	183	-21.40	37	55	-24.13
19	211	-21.77			

In this thesis, the CW interference frequency was set at 1575.462 MHz, offset by 42 KHz from the central frequency of L1. From Table 4.1, it is clear that this is the worst line frequency of PRN 1. This interference frequency is chosen to obtain the strongest interference for PRN 1. The following analysis in acquisition and

tracking is based on PRN 1. Thus, the mitigation performance achieved is under the worst conditions for this code.

## 4.2 Impact of CW interference on correlation function

### 4.2.1 CW frequency effect on correlation function

In this test, the C/A-code signal was mixed with CW interference with a power level of 10 dB higher than the code signal and a frequency that varied from the central frequency of L1 by 2.8 kHz to 500 kHz. Figure 4.2 depicts the correlation result, where the delta frequency is the code spectral line on which the CW interference is superimposed.

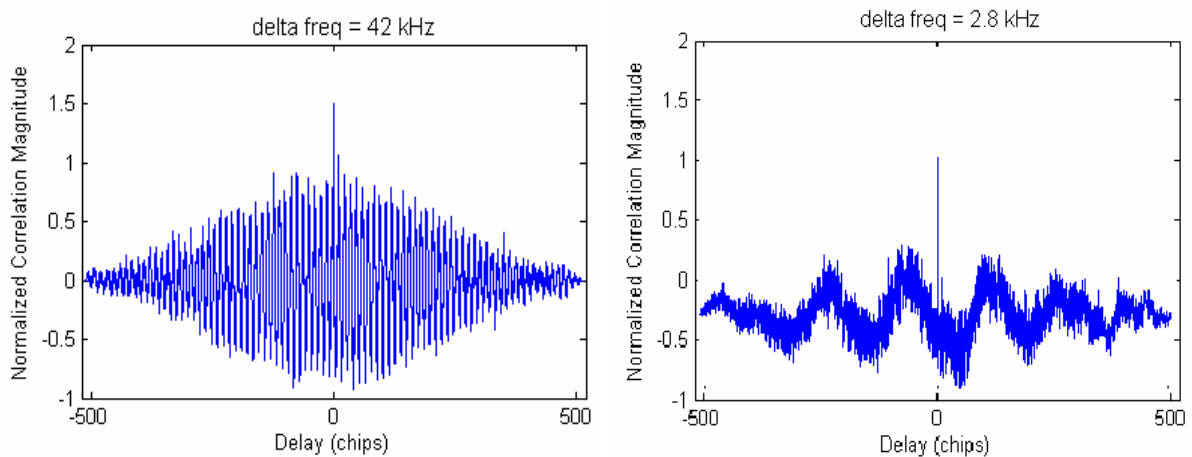


Figure 4.2: Correlations for different spectral lines

It can be seen that both the correlation functions have actually a sinusoidal function whose oscillation frequency depends on the CW interference frequency. So interference occurring at different frequencies will have totally different effects

on GPS signal acquisition or tracking. For  $\Delta f = 42$  kHz, the generated correlation is worse because the autocorrelation peak is difficult to identify, which implies that some acquisition concerns may appear. On the contrary, for  $\Delta f = 2.8$  kHz, the peak stands out against the rest of the plot which means that the added CW interference may imply no interference in acquisition or tracking.

#### **4.2.2 CW power effect on correlation function**

The test was performed under the condition of a C/A-code signal facing CW interference with different powers (0 dB, 10 dB, 15 dB and 20 dB higher than the code), but at the same frequency ( $\Delta f = 42$  kHz). The global aspect of the correlation function resulting from such interference phenomenon is shown in Figure 4.3.

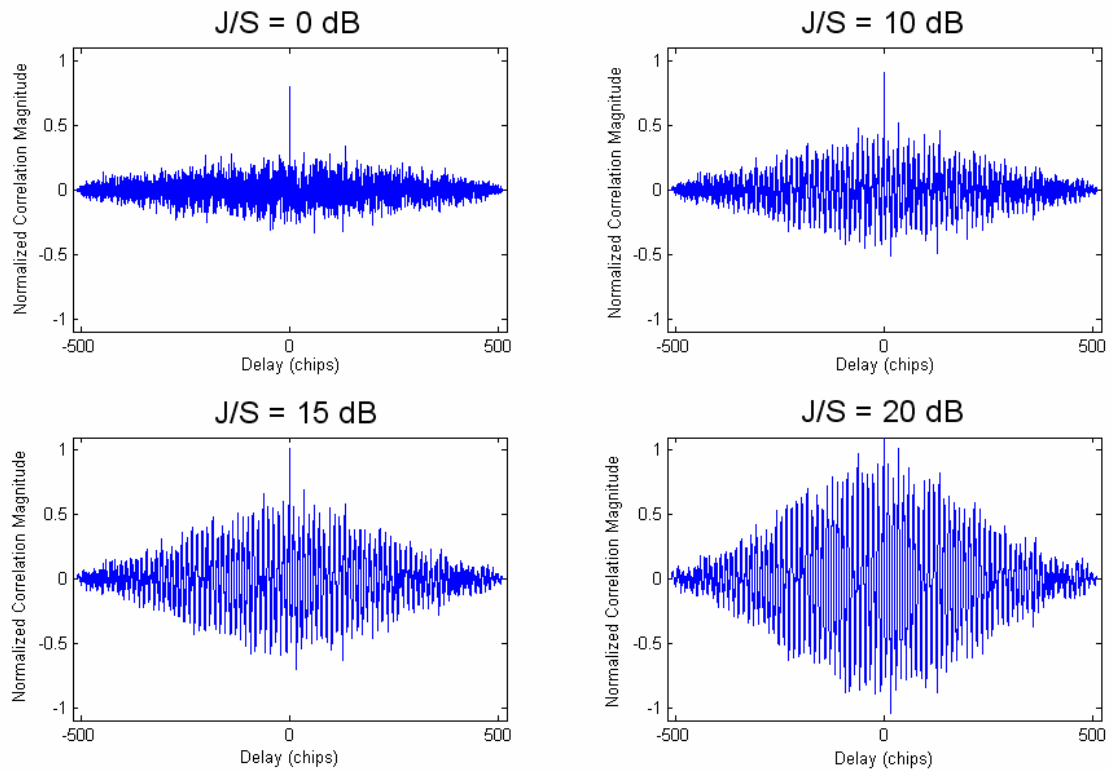


Figure 4.3: Correlation for CW interference of different power levels

The correlation functions have a sinusoidal modulation. The amplitude of oscillations increases with the CW interference power. Higher  $J/S$  buries the correlation peak into the oscillations. When the  $J/S$  is more than 20 dB, the oscillations mask the peak. So when  $J/S$  equals 15 dB, it can still acquire a signal without any mitigation methods. When  $J/S$  continues to increase, the correlation peak is buried into the oscillations and the signal cannot be acquired without mitigation methods. These results will be confirmed in the following acquisition test.

### 4.3 Mitigation result using a 4.75 MHz sampling rate

In this scenario, the intermediate frequency was sampled at 4.75 MHz and 1 bit quantization was used. If the signal is sent directly to the software receiver without any mitigation, the acquisition results are as shown in Figure 4.4:

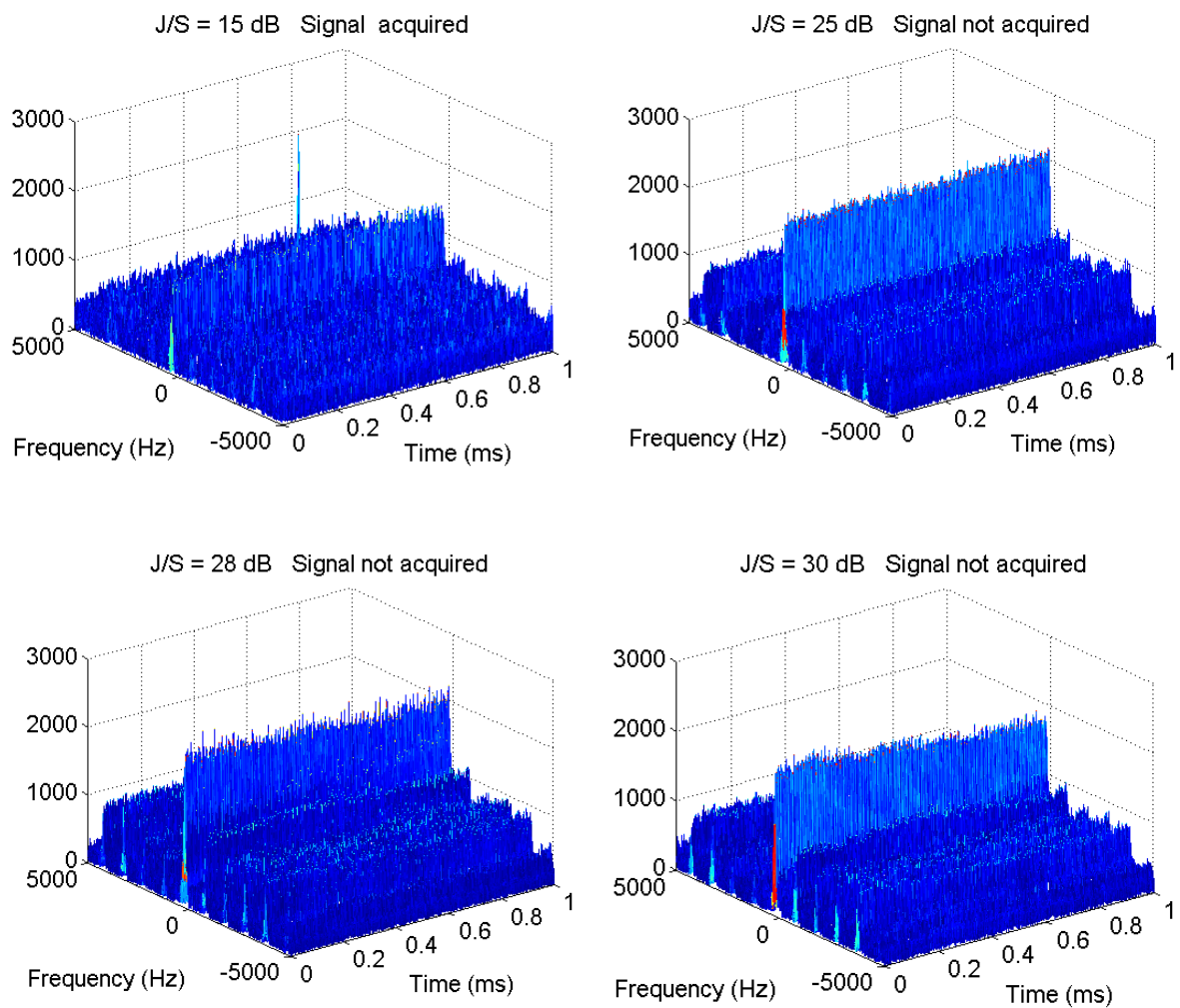


Figure 4.4: Acquisition results without mitigation

The results clearly show a sinusoidal trend of the correlation value due to the sinusoidal waveform of interference which constitutes most of the noise component of the correlation output. The correlation gain is fixed, but the noise floor is increased with the interference power level. So when the J/S increases to a certain value, the correlation peak is totally buried into the oscillations and causes acquisition failure.

Signal acquisition depends on the correlation peak and the detection threshold. The detection threshold should be carefully chosen to avoid false detection and missed detection. The relation between false detection probability, noise power and detection threshold is as follows [Kaplan, 1996]:

$$\text{PDF of noise without signal: } P_n(x) = \frac{x}{\sigma_n^2} e^{-\left(\frac{x^2}{2\sigma_n^2}\right)} \quad (4.1)$$

$$\text{PDF of false alarm: } P_{fa} = \int_{S_T}^{\infty} P_n(x) dx \quad (4.2)$$

The result of integrating equation 4.2 using the PDF of equation 4.1 is:

$$P_{fa} = e^{-\left(\frac{S_T^2}{2\sigma_n^2}\right)} \quad (4.3)$$

where  $S_T$  is the detection threshold,

$\sigma_n$  is the noise power, and

$P_{fa}$  is the PDF of false alarm.

Rearranging Equation 4.3, yields the threshold in terms of the desired single trial probability of false alarm and the measured 1-sigma noise power:

$$S_T = \sigma_n \sqrt{-2 \ln(p_{fa})} \quad (4.4)$$

The correlation noise is assumed to be Gaussian and the detection threshold is computed using the envelopes shown in Figure 4.5.

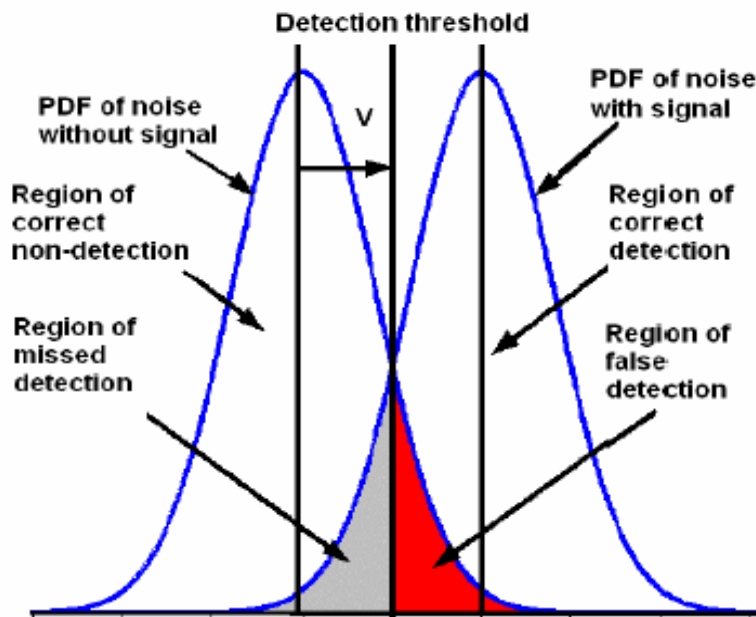


Figure 4.5: PDF of noise and signal used in computation of noise power [after Kaplan, 1996]:

The noise probability density function (PDF) is determined by the mean and standard deviation of all correlation values. Ninety-seven percent of the

correlation value is taken as the noise power [Deshpande and Cannon, 2004]. The false detection probability is then used to determine the detection threshold. A standard value of 10% for false detection probability is used in the analysis throughout this thesis.

By using these acquisition parameters, when J/S is no more than 15 dB, the GPS receiver can use the inherent anti-jamming ability of the spread spectrum system to successfully acquire the signal as shown in Figure 4.4. When J/S increases, the amplitude of the sinusoidal modulation of the correlation value will exceed the correlation gain, the correlation peak will be totally buried in the noise, and no GPS signal can be acquired. If the frequency domain excision algorithm is applied before correlation, the acquisition result will be improved as shown in Figure 4.6:

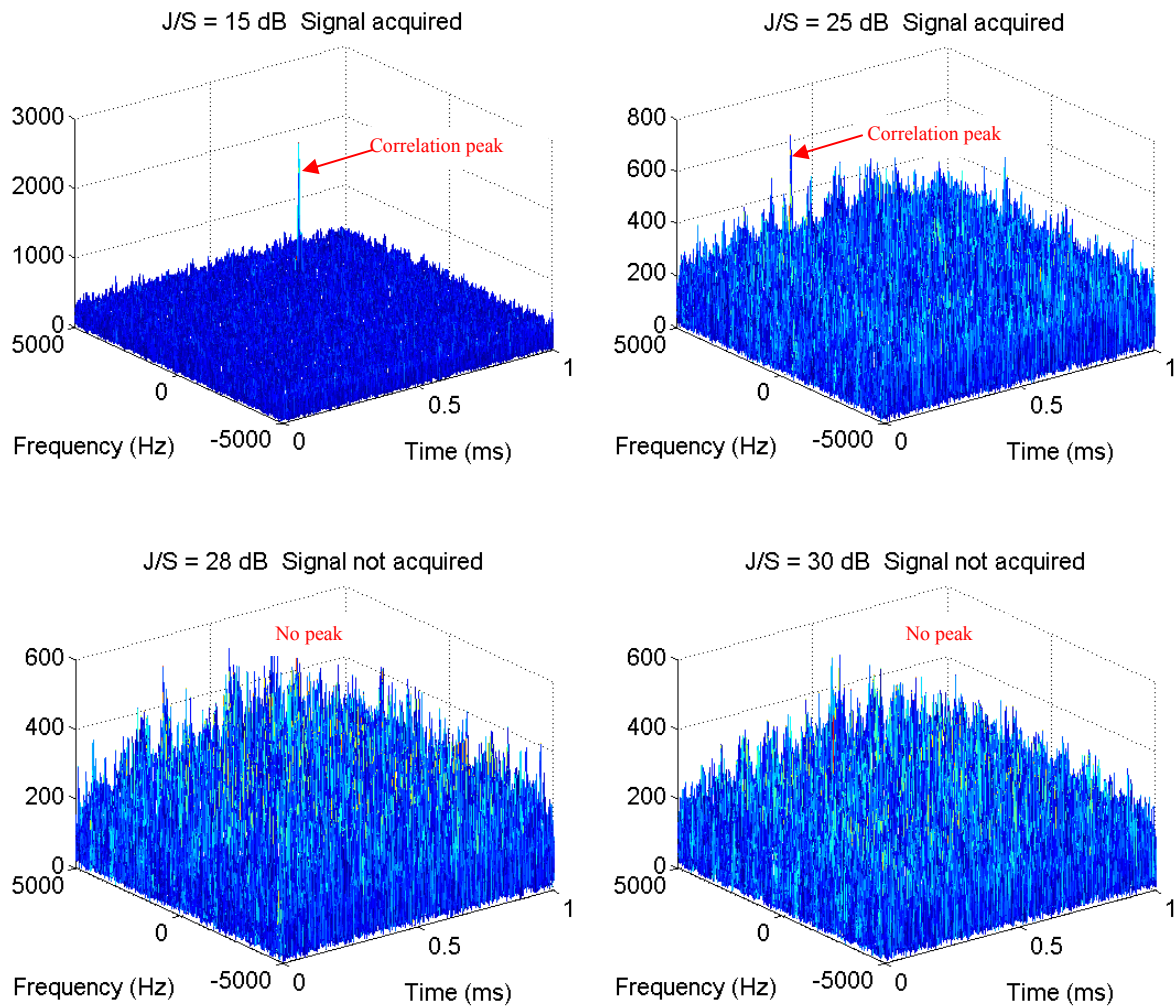


Figure 4.6: Acquisition results with mitigation at a 4.75 MHz sampling rate

These four tests were conducted under the same conditions. The only difference is the interference power. Because the *Signal Tap* cannot be synchronized with the hardware simulator, the acquisition cannot start at the same point each time. Therefore, the correlation peak does not occur at the same point with different values of  $J/S$ , the code phase being a function of the starting point. When  $J/S$  is low, i.e.,  $J/S$  equals to 15 dB, the impact of this mitigation algorithm is not obvious.

Although the mitigation algorithm can remove the sinusoidal oscillation of the correlation value, the acquisition result is the same compared with no mitigation. In both cases, the correlation peak stands out well against the noise. When the J/S reaches 25 dB, the correlation peak is buried into the oscillation without mitigation. On the contrary, this algorithm can effectively remove the oscillation and correctly ascertain the correlation peak.

Table 4.2 shows the peak value versus noise floor and SNR under different interference power conditions.

Table 4.2: Peak value versus noise floor and SNR

J/S (dB)	Peak value	Noise floor	SNR (ratio)
15	2205.9	166.1	13.3
25	735.3	103.4	7.1
28	598.8	82.4	7.2
30	552.7	79.8	6.9
No interference	2723.7	200.3	13.6

Note: no units for peak value and noise floor

With the use of the frequency excision algorithm, the interference frequency component was removed but, at the same time, parts of the signal component and noise component have been removed as well. Thus, it can be seen from Table 4.2 that the peak values and noise floors were reduced when this mitigation algorithm was applied. The higher the value of J/S, the more interference is associated with the signal. When J/S increases to a certain level, the frequency property of the interference will not be distinguished from the signal by this

mitigation algorithm. As  $J/S$  continues to increase to 28 dB, the correlation peak cannot be found even if this algorithm is applied. The mitigation ability of this algorithm therefore is limited to scenarios where  $J/S$  is no more than 25 dB.

#### **4.4 Mitigation result using a 7 MHz sampling rate**

In this scenario, an intermediate frequency was sampled at 7 MHz with the use of 1 bit quantization. The other parameters are the same as in the 4.75 MHz sampling scenario. The acquisition result with mitigation is shown in Figure 4.7:

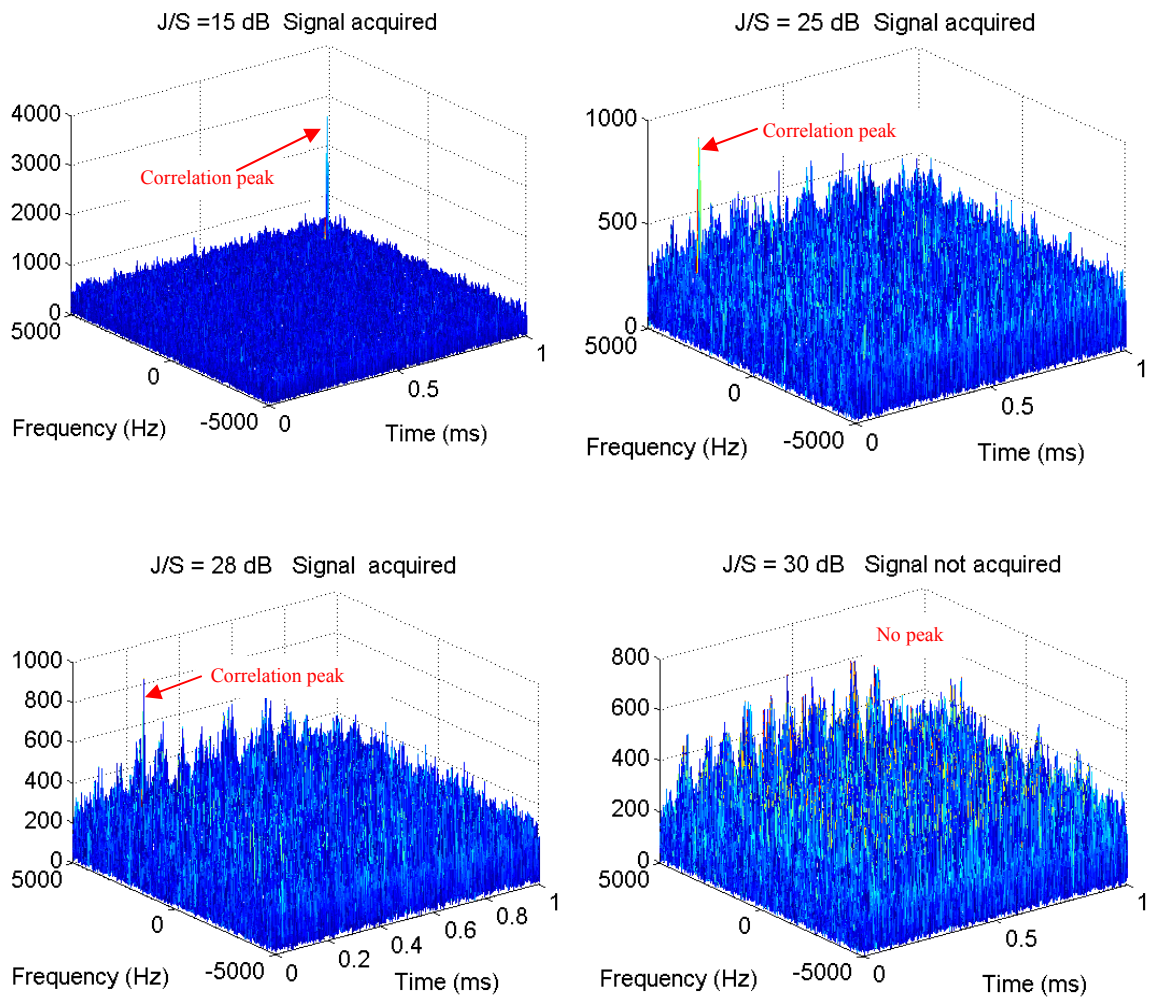


Figure 4.7: Acquisition results with mitigation at a 7 MHz sampling rate

From the plots in Figure 4.7, it can be seen that when  $J/S$  increases to 28 dB, signal acquisition is still possible. It is obvious that there is a 3 dB anti-jamming improvement with a 7 MHz sampling rate compared with the 4.75 MHz sampling rate. The cause of this phenomenon will be discussed in next section.

## 4.5 Nyquist's law and analysis of sampling rate on acquisition

### 4.5.1 Nyquist's law

If the highest frequency contained in an analog signal  $X_{a(t)}$  is  $F_{max} = W$  and the signal is sampled at a rate  $F_s > 2F_{max} = 2W$ , then  $X_{a(t)}$  can be exactly recovered from its sample values. When the sampling of  $X_{a(t)}$  is performed at the minimum sampling rate  $F_s = 2W$ , the reconstruction formula is as follows [Proakis, 1996]:

$$x_a(t) = \sum_{n=-\infty}^{\infty} x_a\left(\frac{n}{2W}\right) \frac{\sin 2\pi W(t - n/2W)}{2\pi W(t - n/2W)} \quad (4.5)$$

The sampling rate of  $F_s = 2W$  is called the Nyquist's rate.

From the Fourier theory aspect, the ideal sampling function is:

$$\sum_{m=-\infty}^{\infty} \delta(t - mT_s) \Leftrightarrow f_s \sum_{n=-\infty}^{\infty} \delta(f - nf_s) \quad (4.6)$$

Equation 4.4 states that the Fourier transform of a periodic train of delta functions, spaced  $T_s$  seconds apart, consists of another set of delta functions weighted by the factor  $f_s = 1/T_s$  and regularly spaced  $f_s$  Hz apart along the frequency axis. Sampling is equivalent to multiplying a signal by a train of delta functions

separated by a sampling interval. In the frequency domain, this can be interpreted as a convolution with delta functions separated by the sampling frequency.

This result implies that the frequency domain representation of the sampled signal contains multiple replicas of the original spectrum shifted in frequency and added. It also illustrates the necessity of proper selection of the sampling frequency  $f_s$  to avoid overlap of the shifted spectra and thus avoidance of aliasing. Figure 4.8, provides an example of the aliasing phenomenon.

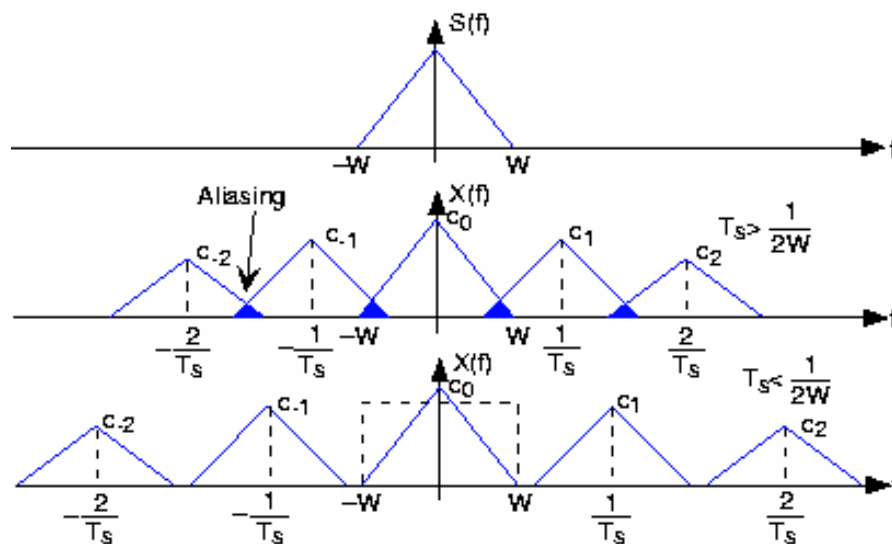


Figure 4.8: Spectrum aliasing

The spectrum of an arbitrary band-limited (to  $W$  Hz) signal is shown in the upper plot. If the sampling interval  $T_s$  is chosen too large relative to the bandwidth  $W$ , aliasing will occur. In the lower plot, the sampling interval is chosen sufficiently

small to avoid aliasing. Note that, if the signal were not band-limited, the component spectra would always overlap.

From Figure 4.8, it is clear that the bandwidth of the signal plays an important role in correctly choosing the sampling frequency. Here attention should be paid that it is the bandwidth of the signal and not the signal's frequency that plays this important role in choosing sampling frequency.

#### **4.5.2 Analysis of sampling rate on acquisition**

A 2 MHz filter is used in the second down-conversion stage of the *Signal Tap*, resulting in an IF spectrum between 14.42 MHz and 16.42 MHz. According to the sampling theory mentioned in the previous section, if the IF bandwidth is 2 MHz, then a 4.75 MHz sampling rate is suitable. However, in reality, the filters in the *Signal Tap* are composed of tuned circuits and sudden transitions from infinite to zero attenuation are not possible. The sharper the required cutoff, the more expensive and the more bulky the filter becomes. Also, realistic filter components have a finite thermal coefficient such that the passband of the filter must be widened to allow for this thermal variation. Hence it is difficult to meet the ideal characteristics that are required to provide a very fine separation between the replica spectra.

Based on the analysis above, it can be concluded that aliasing is irreversible and

can be prevented only by attenuating high frequency content before the sampling process. To prevent aliasing completely, a perfect filter that passes all energy from DC to the highest frequency of interest and rejects all energy at and above the Nyquist frequency is needed. Unfortunately, perfect filters are not physically realizable in analog or digital form. Physically realizable filters must have variations in the passband, a smooth transition from the passband to the stopband, and finite attenuation in the stopband. Note that finite attenuation means that one cannot eliminate aliasing, but only reduce it. If the sampling rate is increased, the requirement for the filter will be lower. Therefore, the variation and dispersion of the filter will have less impact on the performance of ADC. That is the reason why the high sampling rate provides better performance in this application.

#### **4.6 Influence of coherent integration time on interference mitigation**

Coherent integration is also called pre-detection integration [Ray, 2003]. Pre-detection is the phase of signal processing that occurs after the IF signal has been converted to base band by the carrier- and code-stripping processes, but prior to being passed through a signal discriminator, i.e. prior to the nonlinear signal detection process.

Coherent integration time determines the shape of the frequency response of the

correlation triangle. The span of the correlation triangle is between  $-T$  to  $+T$ , where  $T$  is the code chip width and the span of the main lobe of the Sinc curve is between  $-f_c$  and  $+f_c$  where [Kaplan, 1996]

$$f_c = \frac{1}{\text{Pre detection\_Period}} \quad (4.7)$$

For example, for a prediction period of 4 ms, the first null point of the Sinc curve is at  $\pm 250$  Hz. Thus, the coherent correlation time must be as long as possible to operate under weak or RFI signal conditions, in order to obtain a higher correlation gain. It must be as short as possible to operate under high-dynamic stress signal conditions. Thus the pre-detection integration time is a compromise design. However, during initial acquisition period, the receiver does not know where the navigation data bit transition boundaries are located. So another limit of coherent integration time is that it cannot exceed 20 ms, which is the 50 Hz navigation message data period. The plots in Figure 4.9 show the different acquisition results under different coherent integration times where a 7 MHz sampling rate is used.

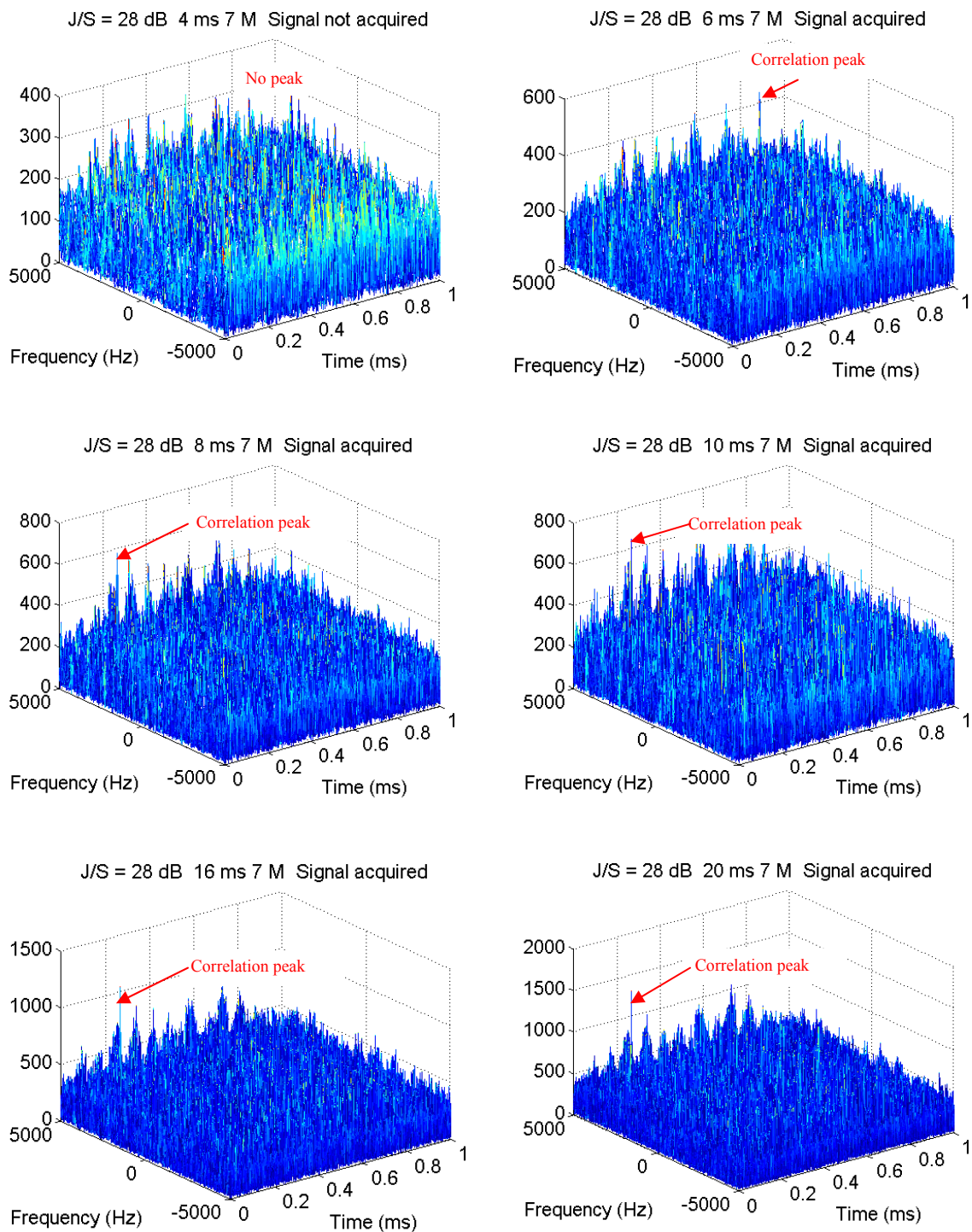


Figure 4.9: Impact of coherent time on mitigation results

In this scenario,  $J/S$  is set to 28 dB, which is relatively high, in order to show the impact of coherent time on mitigation results. As can be seen from the plots in Figure 4.9, no correlation peak appears if the integration time equals 4 ms. When coherent integration time reaches 6 ms, the algorithm reports that the signal has been acquired. But the acquired Doppler and code delay is apparently not correct; the acquisition results should be same, since these results were from the same data set. At least an 8 ms integration time is needed to correctly acquire the signal. With a high level of interference, the longer the coherent integration time, the better the mitigation results on acquisition. It is not surprising to see that the best mitigation result can be achieved when coherent integration time reaches 20 ms.

## 4.7 Conclusion

For low level interference (i.e.,  $J/S$  less than 15 dB), a GPS receiver can use its inherent anti-jamming property of spread spectrum to acquire the signal. For high level interference, spectrum analysis is a useful tool to mitigate interference. The maximum tolerance of effectively mitigating CW interference in acquisition when using this algorithm can reach 28 dB of  $J/S$  if a high sampling rate and a long coherent integration time are employed.

## CHAPTER 5

# Mitigation Analysis in Tracking and Position

### 5.1 CW interference mitigation results in tracking

In this scenario, 10 seconds of data was collected and interference was applied after 4 seconds from the starting point. The In-phase prompt (IP) component, Doppler accuracy and estimated  $C/N_0$  were compared. There are two reasons why interference was applied after 4 seconds:

- 1) To ensure that the acquisition is processed under a clean environment so that the tracking error is isolated.
- 2) To ensure convergence of the tracking process before commencing the performance comparison. Thus, the impact of interference is only on tracking.

#### 5.1.1 IP component mitigation results

The plots in Figure 5.1 show the IP component from the correlator output with a sampling rate of 4.75 MHz.

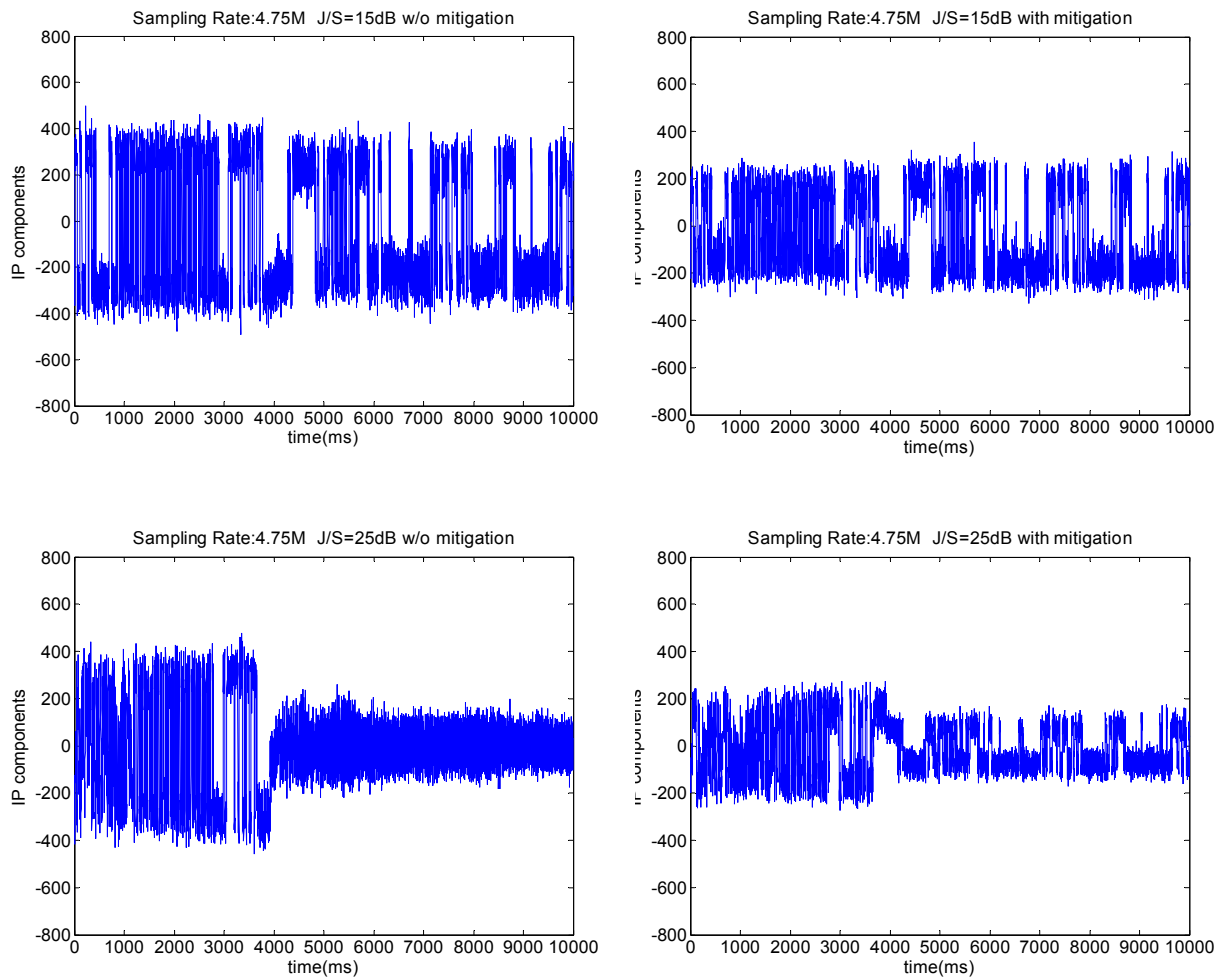


Figure 5.1: IP component comparison

In Figure 5.1, results without mitigation are shown on the left hand side plots, while the right hand side plots depict the results with mitigation. For low J/S (i.e., J/S equals 15 dB) CW interference has no influence on the output of the IP component and the mitigation algorithm provides no improvement to the tracking results. Besides that, the correlation output reduces significantly due to loss of the

signal component as a consequence of application of the frequency excision algorithm.

When interference power is high (i.e., J/S equals 25 dB) the improvement with use of the mitigation algorithm is apparent. The data bit transition is clear and the navigation data can be decoded thereafter compared with the noise only output without mitigation. The improvement is limited to 30 dB of J/S; if greater than that, the correlator output consists only of noise, even if the mitigation algorithm is applied.

The sampling rate still plays an important role in tracking. When the sampling rate is increased from 4.75 MHz to 7 MHz, the maximum J/S is 35 dB for this algorithm to take effect in tracking. There is a 5 dB improvement, as compared with a 4.75 MHz sampling rate.

The IP component is only a coarse descriptor of the GPS data. Here the maximum tolerance for the mitigation algorithm means that the software receiver can obtain the data bit, but this cannot be guaranteed to be 100 percent correct. Whether it can pass through bit synchronization and preamble checking is investigated in Chapter 6.

### 5.1.2 Doppler mitigation results

Figures 5.2 and 5.3 show the Doppler tracking results at 4.75 MHz and 7 MHz sampling rates.

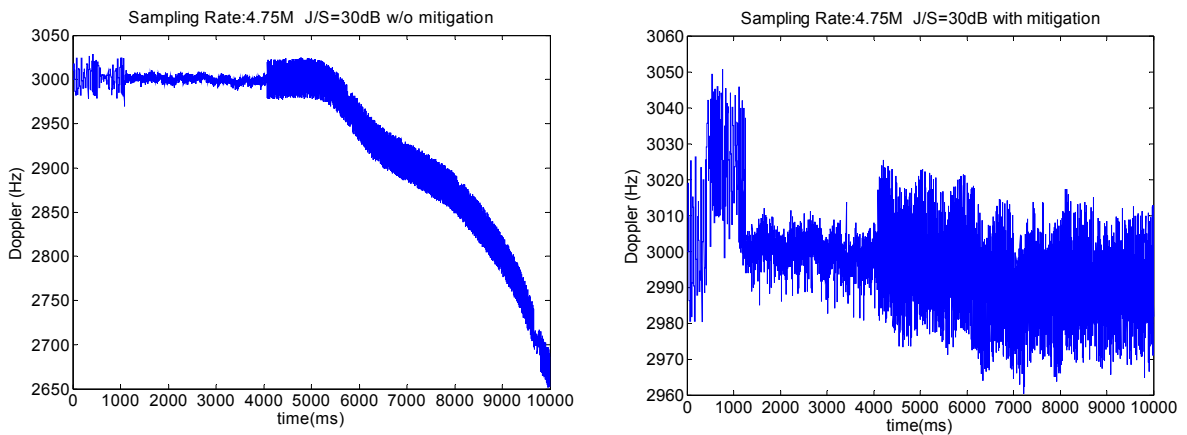


Figure 5.2: Comparison of Doppler with 4.75 MHz sampling rate

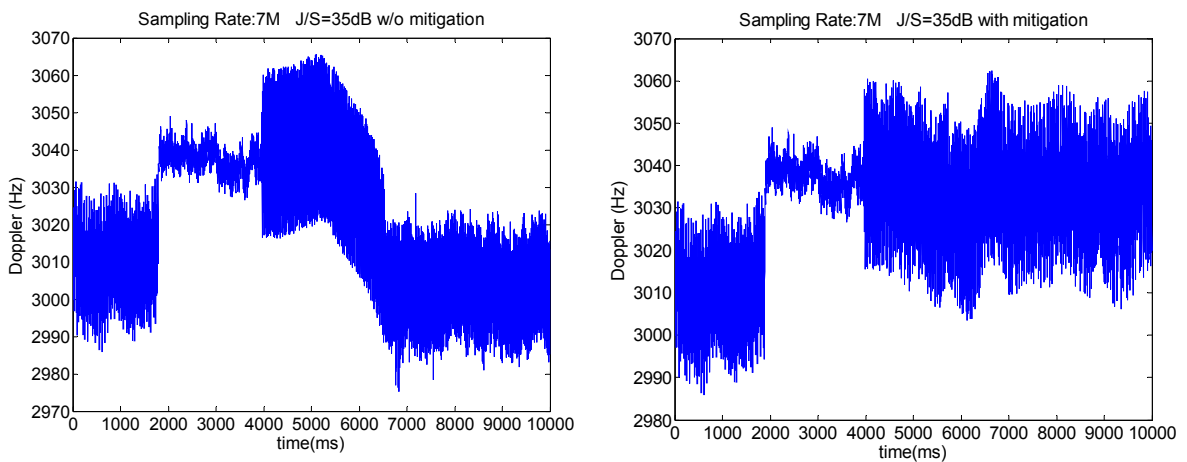


Figure 5.3: Comparison of Doppler with 7 MHz sampling rate

Figures 5.2 and 5.3 show the maximum tolerance of the mitigation algorithm in Doppler tracking. The left hand side of the plot is the result without mitigation and the right hand side is the result with mitigation.

When a high level interference ( $J/S$  greater than 15 dB) is applied, the phase lock loop is unlocked, causing the Doppler tracking result to drift greatly. With the application of the mitigation algorithm, although the standard deviation of the Doppler output is increased due to SNR loss of this algorithm, the effect of interference on the phase lock loop is eliminated. The maximum tolerance of  $J/S$  is 30 dB for a 4.75 MHz sampling and 35 dB for a 7 MHz sampling rate.

With the mitigation algorithm, the Doppler output can be kept in the right track. However, the accuracy of the result needs further analysis. The true Doppler value at any time can be found in the output file of the simulator, because the GPS signal is produced in the hardware simulator. Thus, it is possible to calculate the Doppler tracking error. Figure 5.4 shows the root mean square values of the Doppler error for different values of  $J/S$  from 15 dB to 35 dB in relation to different sampling rates.

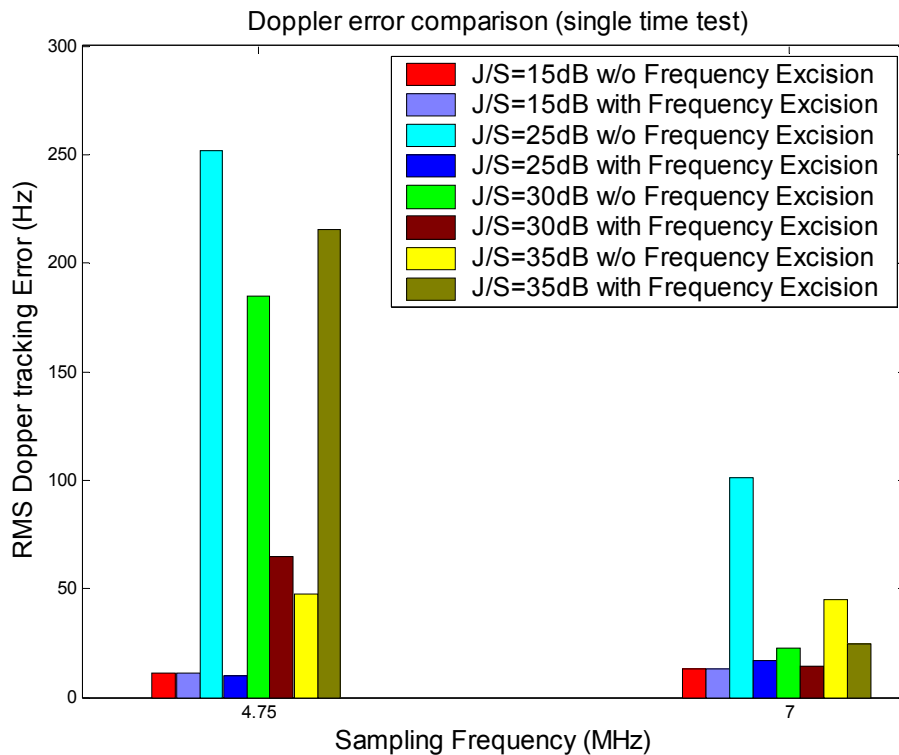


Figure 5.4: Doppler error comparison (5 seconds of data)

Figure 5.4 shows the RMS error of the tracking Doppler compared with the true Doppler from the simulator. It is obvious that a high sampling rate produces a lower RMS error. When the interference level is lower, i.e.,  $J/S$  equals to 15 dB or less, there is no obvious improvement with mitigation due to the inherent anti-jamming property of the spread spectrum system. If  $J/S$  is greater than 15 dB, in most of the cases, the improvement with mitigation is apparent except for the instance where  $J/S = 35$  dB at a 4.75 MHz sampling rate where an unexpected result occurs. The RMS error is much smaller than for  $J/S$  below 35 dB, and the RMS error becomes bigger when the mitigation algorithm is applied. This

phenomenon is due to the short data analysis period. In this test scenario, only 5 seconds of data was analyzed in order to save processing time; in the process, random factors have apparently dominated the result. So In order to remove the effects of random factors, a longer analysis period and a stochastic repeatability test are needed.

Figure 5.5 shows the result of the average of six tests with different J/S values. Each time, the tracking process lasts for 30 seconds.

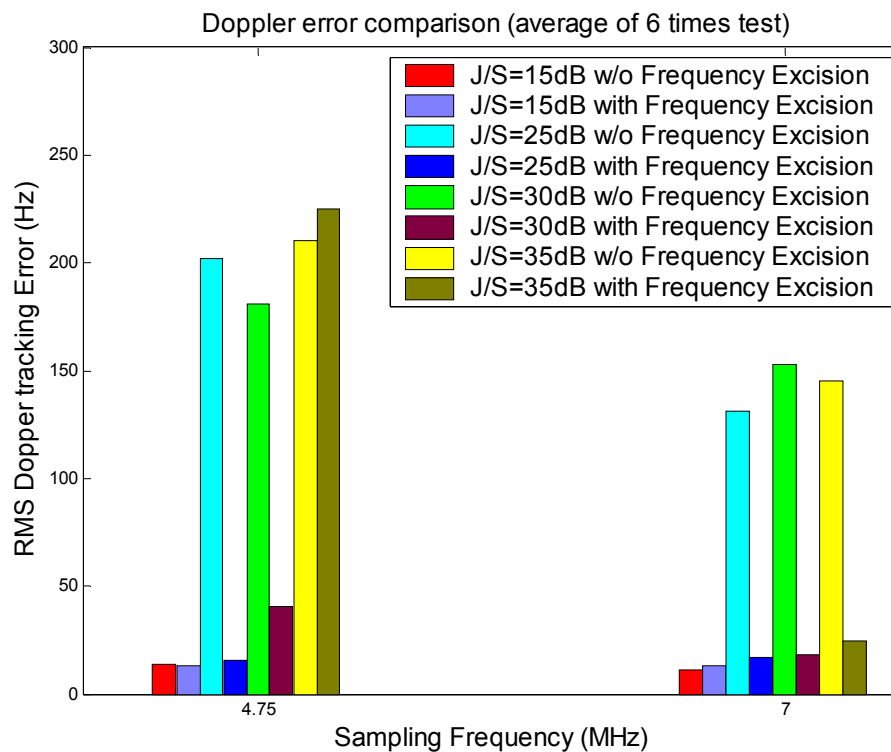


Figure 5.5: Doppler error comparison (30 seconds of data)

These results are more reasonable than the single test results shown in Figure

5.4. Without mitigation, the Doppler error is not proportional to the interference level. Under this condition, the tracking loop is divergent and the GPS receiver loses lock on the Doppler.

With mitigation, the Doppler error is much smaller than the results observed without mitigation and this error is proportional to the interference level. The only exception is where the J/S equals 35 dB with a 4.75 MHz sampling rate. The RMS error is greater than without mitigation. In this case, the interference level actually exceeds the maximum tolerance of the mitigation algorithm with a 4.75 MHz sampling rate. The mitigation algorithm is not reliable under this condition, thereby requiring use of a high sampling rate. For a J/S of 35 dB with a 7 MHz sampling rate, the mitigation algorithm is still effective in tracking. The Doppler error is restricted to a reasonable level and the overall RMS error of 7 MHz sampling is smaller than with for 4.75 MHz sampling. These results are from the average of six tests and can be said to be statistically repeatable.

### **5.1.3 Estimated $C/N_0$**

In practice, the ratio of total carrier power to the noise density  $C/N_0$  in dB-Hz is the most generic representation of signal power as it is independent of the implementation of the receiver front-end bandwidth.  $C/N_0$  can also be used as the lock detector to indicate a loss of lock of the DLL. In a software receiver, the  $C/N_0$  measurement can be estimated as [Parkinson and Spilker, 1996]:

$$\frac{\hat{C}}{N_0} = 10 \log_{10} \left[ \frac{1}{T} \frac{\hat{\mu}_{NP} - 1}{M - \hat{\mu}_{NP}} \right] \quad (5.1)$$

where

$$\hat{\mu}_{NP} = \frac{1}{K} \sum_{K-1}^K NP_K \quad (5.2)$$

$$NP_k = \frac{\left( \sum_{i=0}^M I_i \right)_k^2 + \left( \sum_{i=0}^M Q_i \right)_k^2}{\left( \sum_{i=1}^M (I_i^2 + Q_i^2) \right)_k} \quad (5.3)$$

M is the sample number.

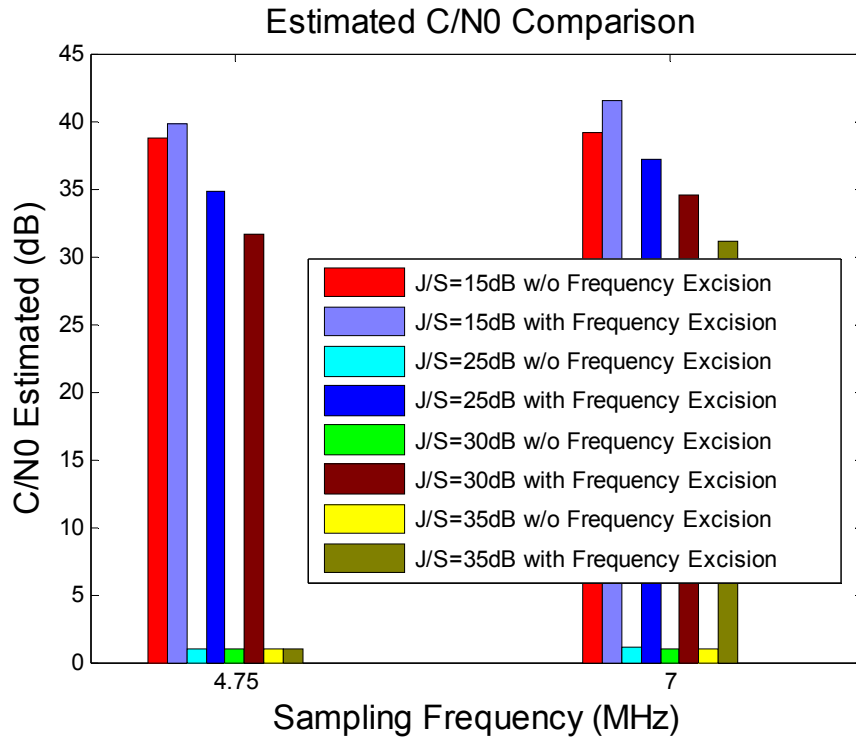


Figure 5.6: C/N<sub>0</sub> comparison

Figure 5.6 shows the improvement in C/N<sub>0</sub> with mitigation. The mitigation result follows the same trend as the Doppler results. For lower values of J/S, the improvement is very small. Much improvement occurs for medium level interference. For J/S greater than 15 dB, the C/N<sub>0</sub> tends to be zero without mitigation due to the loss of lock on DLL while, with mitigation, the estimated C/N<sub>0</sub> is high enough to keep code and carrier locked. The higher the sampling rate, the better the C/N<sub>0</sub> estimation is. In the interference level of 35 dB of J/S, a 7 MHz sample provides a good C/N<sub>0</sub> estimation while a 4.75 MHz sample produces total loss of lock.

## 5.2 CW Interference mitigation results in position domain

### 5.2.1 Benchmarks for performance analysis in the position domain

In the position domain test, all error sources have been turned off except noise. The impact of non-removable random noise in the hardware simulator and *Signal Tap* will be discussed in this section. The position error level under the noise-only error source condition will be used as benchmark for interference mitigation performance comparisons in the position domain. Figure 5.7 shows the horizontal and vertical position errors under noise-only conditions.

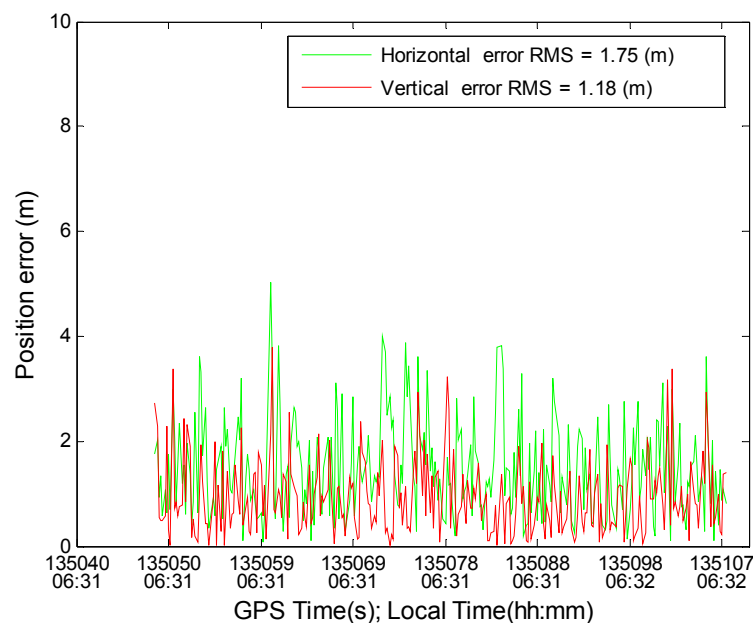


Figure 5.7: Position errors under noise-only conditions

Due to the randomness of noise, a one-time test result is not enough. In order to

measure repeatability, the test was carried out six times under the same conditions. Figure 5.8 shows the results of the six consecutive tests.

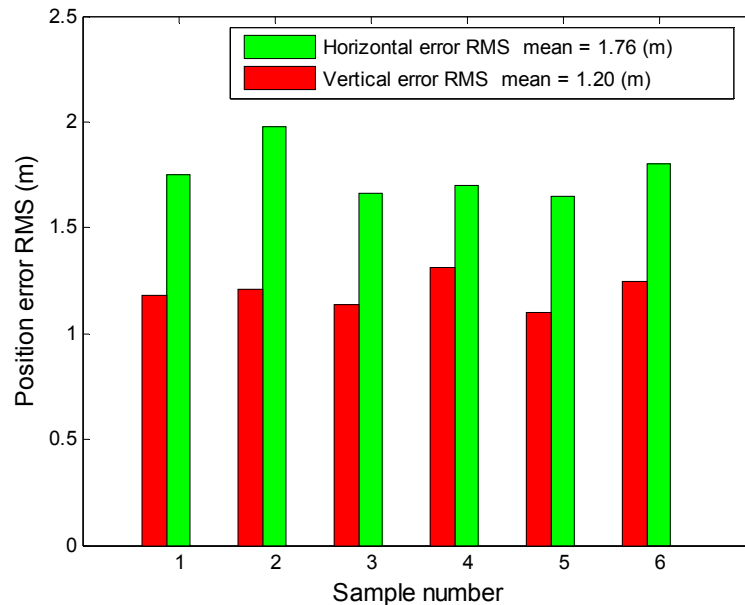


Figure 5.8: Position error comparison of 6 tests under noise-only conditions

It can be seen from Figure 5.8 that, when all the other error sources have been removed except noise, the expected horizontal position RMS error is around 1.8 metres and the vertical RMS error around 1.2 metres (the PDOP is 1.9 and is essentially constant over the scenario). When the mitigation algorithm is applied, some of the signal frequency components will be removed, causing the distortion in the correlation peak. So the expected position RMS error will increase. If the RMS error can be kept below a reasonable level, the mitigation process is successful. Otherwise, it will be declared a failure.

### 5.2.2 Warm and cold start

The mitigation performance in the position domain was analyzed under two conditions: warm start and cold start. The definition of warm start in this thesis is to start acquisition in a “clean” environment without any interference. Interference is then applied after the convergence of signal tracking. By comparison, cold start means that acquisition is started after the interference is applied. The reason of setting these two scenarios lies in the fact that the required  $C/N_0$  differs for acquisition and tracking.

The effects of RFI on code correlation and loop filtering are to reduce the  $C/N_0$  of all of the GPS signals. If the  $C/N_0$  is reduced below the tracking threshold, the receiver will lose its ability to obtain measurements from the satellites. As the line of sight range to the source of RFI increases, the  $C/N_0$  increases. A good rule of thumb for the acquisition threshold  $C/N_0$  for a GPS receiver is about 6 dB higher than the tracking threshold [Kaplan, 1996]. If the receiver is jammed out of tracking the GPS signals, the distance from the interference source must be increased such that the effective  $C/N_0$  increases by about 6 dB before the GPS receiver can reacquire again. This also means that, when the GPS signal is acquired, even if the interference level increases, the receiver is still able to track the signal. Stated another way, the impact on the position solution is not as serious as that when the same level of interference occurs during the acquisition period.

In warm start conditions, only the tracking procedure is under the interference environment. The required  $C/N_0$  is lower than in cold start. The tolerance for interference is thus higher, so the mitigation results should be different.

### **5.2.3 CW interference mitigation in the position domain**

Due to the limited memory capacity of the *Signal Tap*, only 80 seconds of data could be collected. The GPS position can be fixed only after the receiver collects the required ephemeris. The first three sub-frames that last 18 seconds have to be decoded in order to get the required ephemeris, so 60 seconds of position data can be provided for analysis.

The software GPS receiver is nonlinear, especially near its tracking threshold. It is very difficult to predict the tracking threshold for a given dynamic scenario. Only a Monte Carlo simulation can assist in studying this phenomenon. Heuristic techniques are usually used to predict the signal tracking threshold. For a second-order loop with an 18 Hz noise bandwidth and a 20 ms pre-detection integration time, the rule of thumb tracking threshold is 28 dB-Hz [Kaplan, 1996], and this was the value used in this test. If the estimated  $C/N_0$  is below this threshold, the receiver decides that the tracking process failed and the receiver attempts to reacquire again.

Figure 5.9 compares the mitigation results in cold and warm start conditions. A

second order loop filter with 18 Hz noise bandwidth and a 20 ms pre-detection integration time was used.

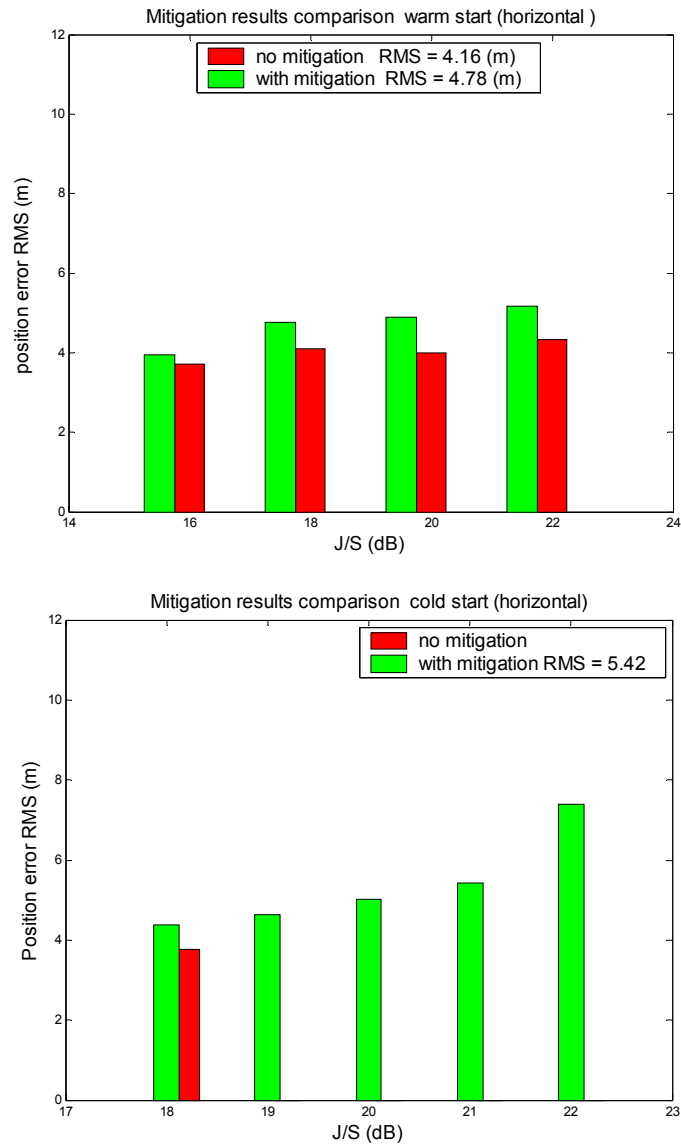


Figure 5.9: Comparison of mitigation results with CW interference

It can be seen from Figure 5.9, when interference is applied, the position error

RMS increases. This is the expected result, because the mitigation algorithm also removes part of the signal energy when the interference frequency component is removed, causing distortion in the correlation peak. This increased position error is caused by small pseudorange errors on all satellites.

In a warm start environment, no improvement in the position domain is observed when the mitigation algorithm is applied. On the contrary, the horizontal root mean square error is worse with mitigation. This is because when the interference frequency component is excised, and some of the signal component has been removed as well. At any interference level, the signal frequency component will always mix with the interference frequency to a certain degree. If the interference power level is not high, the inherent anti-jamming property of the spread spectrum system can mitigate the interference without any extra processing. With mitigation, due to the signal loss upon frequency excision, the resulting position solution is slightly degraded.

Under cold start conditions, acquisition is performed in an interference environment. As discussed before, acquisition requires  $C/N_0$  6 dB higher than tracking. At the same level of interference, the inherent anti-jamming ability may not be enough to enable acquisition. Unlike tracking, this level of interference may cause acquisition problems. Incorrect acquisition results may cause divergence of the tracking loop, making position fixing impossible or producing very a large position error. Thus, in a cold start condition, the mitigation algorithm is essential.

From Figure 5.9, it can be seen that no GPS solution is found for J/S greater than 22 dB. The maximum tolerance for CW interference is 22 dB in cold start with mitigation. Without mitigation, the maximum tolerance in cold start is 18 dB while, with mitigation, the improvement is 4 dB. Figure 5.10 shows the effect of the sampling rate on the mitigation algorithm on position.

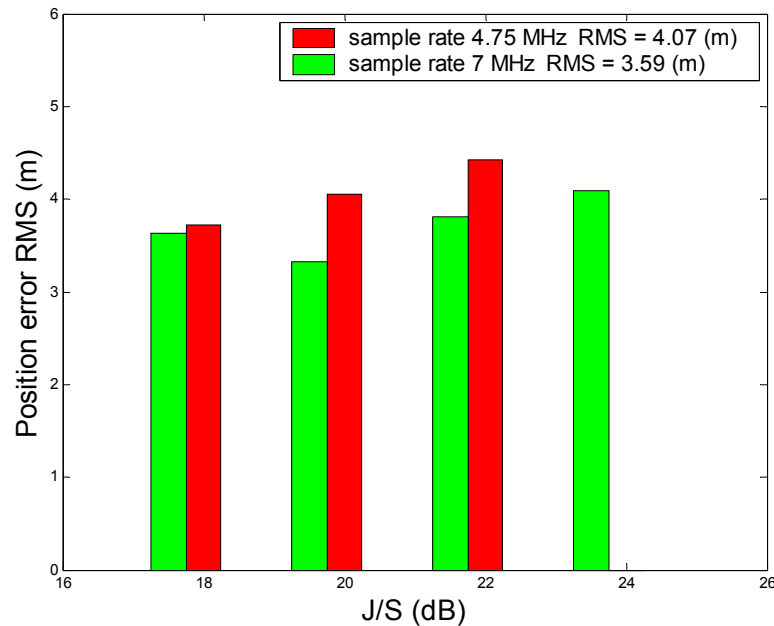


Figure 5.10: Comparison of the effect of the sampling rate on position

A higher sampling rate is associated with a slightly smaller RMS error in position. Furthermore, the anti-jamming capability increases by 2 dB if the sampling rate increases from 4.75 MHz to 7 MHz.

#### 5.2.4 Stochastic repeatability test

All the results in Section 5.2.3 were observed under a one-time test. Because of the characteristics of interference, random factors such as noise originating in the *Signal Tap* play an important role in the performance of the interference mitigation algorithm. For the study of the effects of interference, statistical analysis is an essential tool. In order to measure the repeatability of the test, the latter was carried out six times under the same conditions. Based on the use of the software GPS receiver, the only difference between tests is the random noise. The plot in Figure 5.11 shows results of the six repeated tests. The J/S was set to 21 dB with a cold start, using 10 ms and 20 ms coherent integration times in each of the six tests.

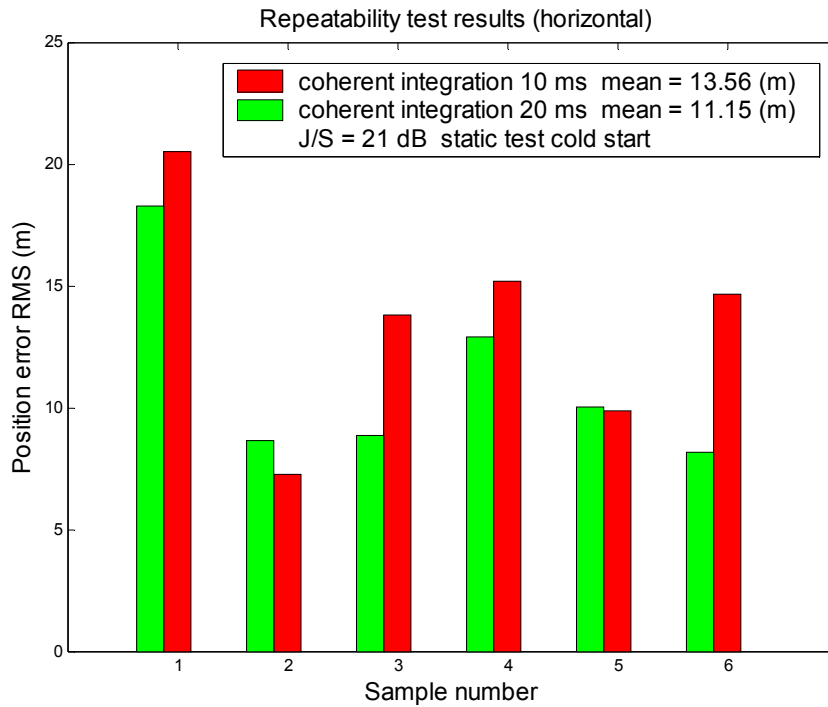


Figure 5.11: Comparison of coherent integration time on position

As can be seen from Figure 5.11, the mitigation algorithm is repeatable when  $J/S$  equals 21 dB in a cold start condition, because the position solution is reasonable in all six of the tests.

In five of six trials, the result based on a 20-ms coherent integration time was better than the result with 10 ms coherent integration time, on which basis it can be said that the 20 ms coherent integration time has better performance statistically. The only time that the 10 ms coherent integration time has better performance is in test 2; that result is due to the bit transition which may occur based on a 20 ms integration time interval while it does not occur with a 10 ms

interval. During the acquisition period, no prior knowledge about the data bit boundary is provided. Even the pre-detection integration time is limited to within 20 ms; there is still a chance that a data bit transition may occur.

For test 1, the error is larger than that of the other 5 samples due to the presence of random noise. In test 1, the noise happens to be slightly larger than in other tests and the mitigation algorithm amplifies it. This result occurs because higher random noise mixes the interference spectrum more with the signal and makes the mitigation algorithm excise more signal energy, thus causing more distortion in the correlation peak and introducing a greater pseudorange error.

Figure 5.12 shows the rate of success in obtaining position solutions under different interference levels when the mitigation algorithm is applied. If no position can be calculated, or if the position error exceeds 50 metres (meaning that the error is well above the normal value and the result is not reliable), the algorithm declares a failure. A series of six tests were carried out at each interference level.

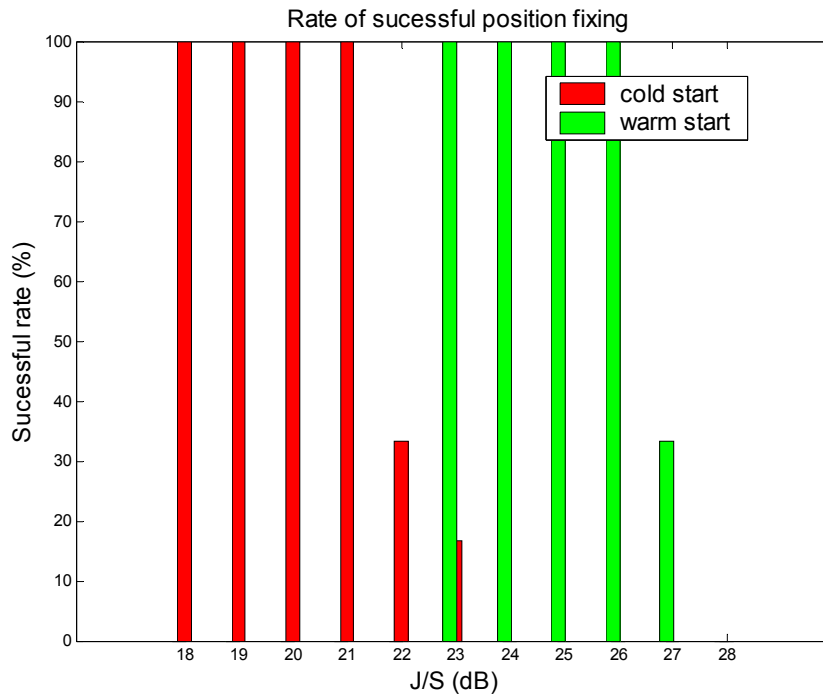


Figure 5.12: Rate of successful position fixing

Under cold start conditions, when the  $J/S$  is no greater than 21 dB, the success rate in obtaining a position solution is 100 percent. If the  $J/S$  increases to 22 dB or 23 dB, the success rate is reduced to 33.3 percent or 16.7 percent, respectively. If the  $J/S$  continues to increase, no solution can be obtained. The mitigation algorithm is statistically stable when the  $J/S$  is no greater than 21 dB in a cold start condition.

In warm start conditions, when the  $J/S$  is no greater than 26 dB, a 100 percent success rate in obtaining a solution can be achieved. If the  $J/S$  increases to 27 dB, the success rate is reduced to 33.3 percent. If the  $J/S$  continues to increase, it is

not possible to obtain a solution. The mitigation algorithm is statistically stable when the J/S is no greater than 26 dB under warm start conditions.

### 5.3 AM interference mitigation results in the position domain

Amplitude modulation (AM) is a method of impressing data onto an alternating-current (AC) carrier waveform. The highest frequency of the modulating data is normally less than 10 percent of the carrier frequency [Proakis, 1996a]. The instantaneous amplitude (overall signal power) varies depending on the instantaneous amplitude of the modulating data.

Considering the modulating waveform is a sine function, the amplitude modulation of a signal can be expressed as:

$$\alpha[1 + K_m \cos \omega_m t] \sin \omega_c t \quad (5.4)$$

where

$\omega_c$  = the angular frequency of the carrier

$\omega_m$  = angular frequency of the signal to be modulated

$K_m$  = modulation index

$\alpha$  = scalar notation for amplitude of the carrier

From Equation 5.4, it can be seen that an AM signal is determined by five parameters:

- Signal level
- Centre frequency
- Wave form
- Frequency of the signal to be modulated, and
- Modulation depth

An Agilent ESG E4431B signal generator was used in this thesis to generate an AM signal and a frequency modulation (FM) signal. In this signal generator, the modulating waveform can be selected from sine, square, ramp or triangle forms. The frequency of the modulating signal must be in the range of 0.0001 to 50 kHz. The modulation depth is specified as a percentage, ranging from 0 to 100% [Spirent, 2003b].

The AM signal frequency is fixed, while only the amplitude changes. In the frequency domain, the impact of AM interference on the GPS signal spectrum is similar to CW interference. Only the amplitude of the interference frequency component is changing with the AM parameter, which means that the frequency excision algorithm can be used to remove the AM interference.

However, the impact of different AM parameters on the effectiveness of the

mitigation algorithm is different. The plots in Figure 5.13 illustrate the impact of the modulating signal frequency on mitigation results.



Figure 5.13: Impact of modulating signal frequency of AM interference on mitigation results

The mitigation result is similar when the frequency of the modulating signal is changed from 10 Hz to 100 Hz. The modulating signal frequency is relatively low compared with the centre frequency. In the analysis period, the change in the AM interference amplitude is very small, so that the modulating signal frequency does not have much influence on the mitigation results of the GPS position solution.

Figure 5.14 shows the influence of the modulation depth of AM interference on position.

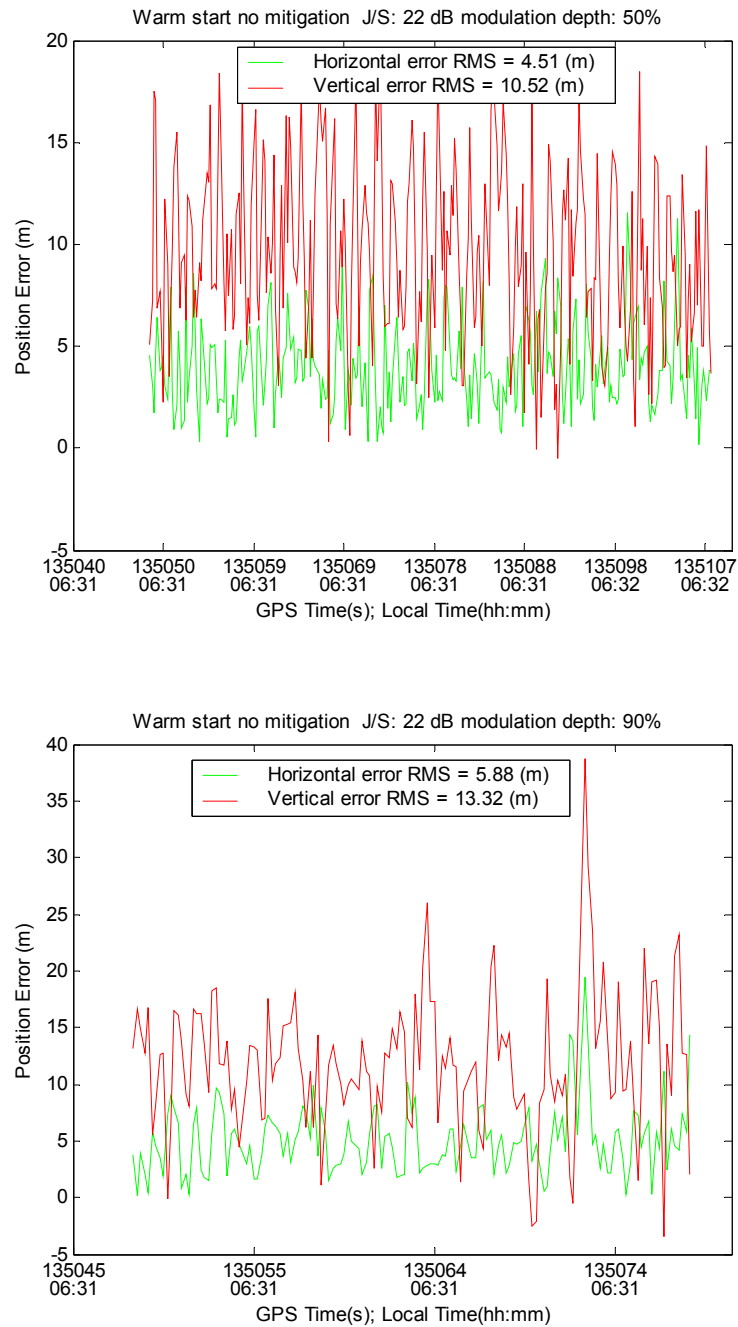


Figure 5.14: Influence of modulation depth of AM interference on mitigation results

The modulation depth determines the amplitude of the AM signal. From Equation 5.3, it can be seen that, when the modulation depth is 100 percent, the peak value of the AM signal will double. The increase of modulation depth is somehow like the increase of AM interference power. When modulation depth increases from 50 percent to 90 percent, the RMS position error increases by 30 percent. In the case of a modulation depth of 90 percent, it can be seen from the plot above that no GPS solution can be fixed after a GPS time of 135078 seconds. This implies that modulation depth plays an important role in the influence of AM interference, perhaps even causing the loss of tracking in the tracking loop.

Figure 5.15 compares the mitigation results with AM interference under cold start conditions.

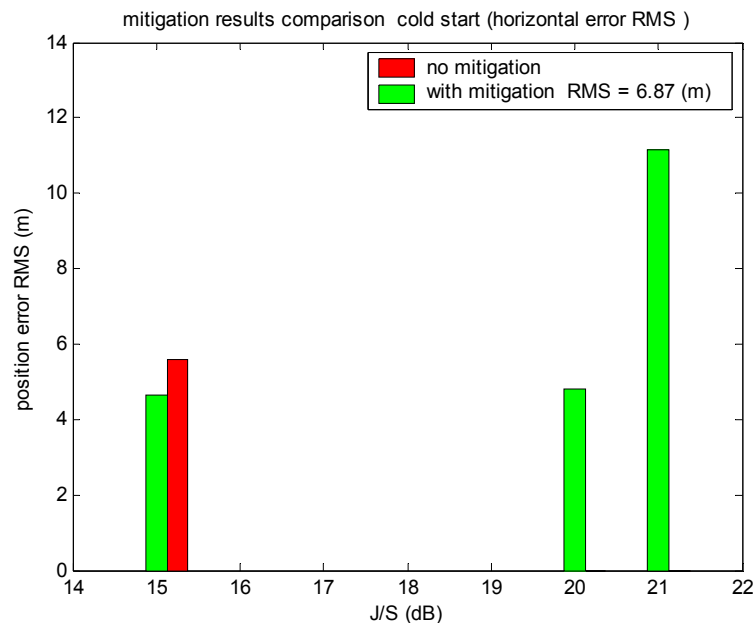


Figure 5.15: Mitigation results comparison with AM interference

From the plot in Figure 5.15, it can be seen that no solution is achieved with a J/S greater than 15 dB without the mitigation algorithm. The tests with mitigation have not been carried out due to concerns over managing the workload for J/S = 16, 17, 18, and 19 dB. The maximum tolerance for AM interference is 15 dB without mitigation under cold start conditions.

Using the mitigation algorithm, the maximum tolerance for AM interference is 21 dB. No solution can be obtained when the J/S is greater than 21 dB which represents a 6 dB improvement achieved with the mitigation algorithm, as compared with no mitigation. The mitigation algorithm is generally effective in mitigating AM interference in cold start conditions.

#### **5.4 FM interference mitigation results in the position domain**

FM is a modulation in which the instantaneous frequency of a sine wave carrier is caused to depart from the centre frequency by an amount proportional to the instantaneous value of the modulating signal. In FM, the carrier frequency is called the centre frequency. FM is a form of angle modulation. The mathematical expression of an FM signal is as follows. If the instantaneous frequency varies linearly with the modulating signal, the FM signal can be expressed as:

$$\alpha \sin((\omega_c + kf(t))t) \quad (5.5)$$

In the case of phase modulation, the phase of the carrier varies with the modulation signal and, in the case of FM, the phase of the carrier varies with the integral of the modulating signal. Thus, there is no essential difference between phase and frequency modulation. The term FM is generally used to include both modulation types. If the modulating waveform is assumed to be a sinusoidal signal at a frequency  $f_m$ , the frequency modulation of a signal can be expressed as:

$$\alpha \sin((\omega_c + k \cos(\omega_m(t)))t) \quad (5.6)$$

where

$\omega_c$  = the angular frequency of the carrier

$\omega_m$  = angular frequency of the signal to be modulated

$k$  = maximum frequency deviation of the carrier, and

$\alpha$  = scalar notation for amplitude of the carrier

An FM signal is determined by five parameters as in the equation above:

- Signal level
- Centre frequency of the carrier
- Wave form
- Frequency of the signal to be modulated

- Frequency deviation

The deviation of the modulating signal is dependent upon the centre frequency of the main signal. Table 5.1 shows the frequency limits versus three centre frequency values [Spirent, 2003b].

Table 5.1: Frequency limits versus centre frequency

Centre Frequency (MHz)	Lower Limit (kHz)	Upper Limit (kHz)
500	0.05	5000
>500 to 1000	0.1	10000
>1000 to 2000	0.2	20000

The FM signal frequency is changing. In the frequency domain, the impact of FM interference on the GPS signal spectrum is similar to that of swept CW interference. The sweeping rate depends on the frequency of the signal to be modulated and the frequency deviation. In the FFT analysis period, more frequency components will exist compared with CW interference. Although the frequency excision algorithm is still effective in removing the FM interference, the performance will degrade. More signal energy will be cut off, causing a decrease in the estimated  $C/N_0$ . The extent of the degradation is proportional to the frequency of the signal to be modulated and the frequency deviation, because the number of interference components in the FFT analysis period is proportional to the frequency of the signal to be modulated and the frequency deviation.

Table 5.2 shows the frequency of the signal to be modulated with respect to FM interference on position. The central frequency of the FM interference is on the carrier frequency of L1 with an associated frequency deviation of 100 KHz.

Table 5.2: Comparison of FM frequency on GPS position

Frequency to be Modulated (Hz)	1	5	50	500	1000
Horizontal error RMS (m)	4.65	4.45	4.66	4.74	No solution
Vertical error RMS (m)	10.36	10.68	10.60	14.00	No solution

When the FM frequency is lower, the number of interference frequency lines in the FFT analysis period will be lower. As shown in Table 5.2, there is no large difference in the solution for different FM frequency values from 1 Hz to 50 Hz. When the frequency increases to a few hundred Hz, the position error increases rapidly and, eventually, the receiver will lose lock.

Figure 5.16 illustrates the influence of frequency deviation of FM interference on the solution. The central frequency of the FM interference is on the carrier frequency of L1 and the frequency to be modulated is 50 Hz.

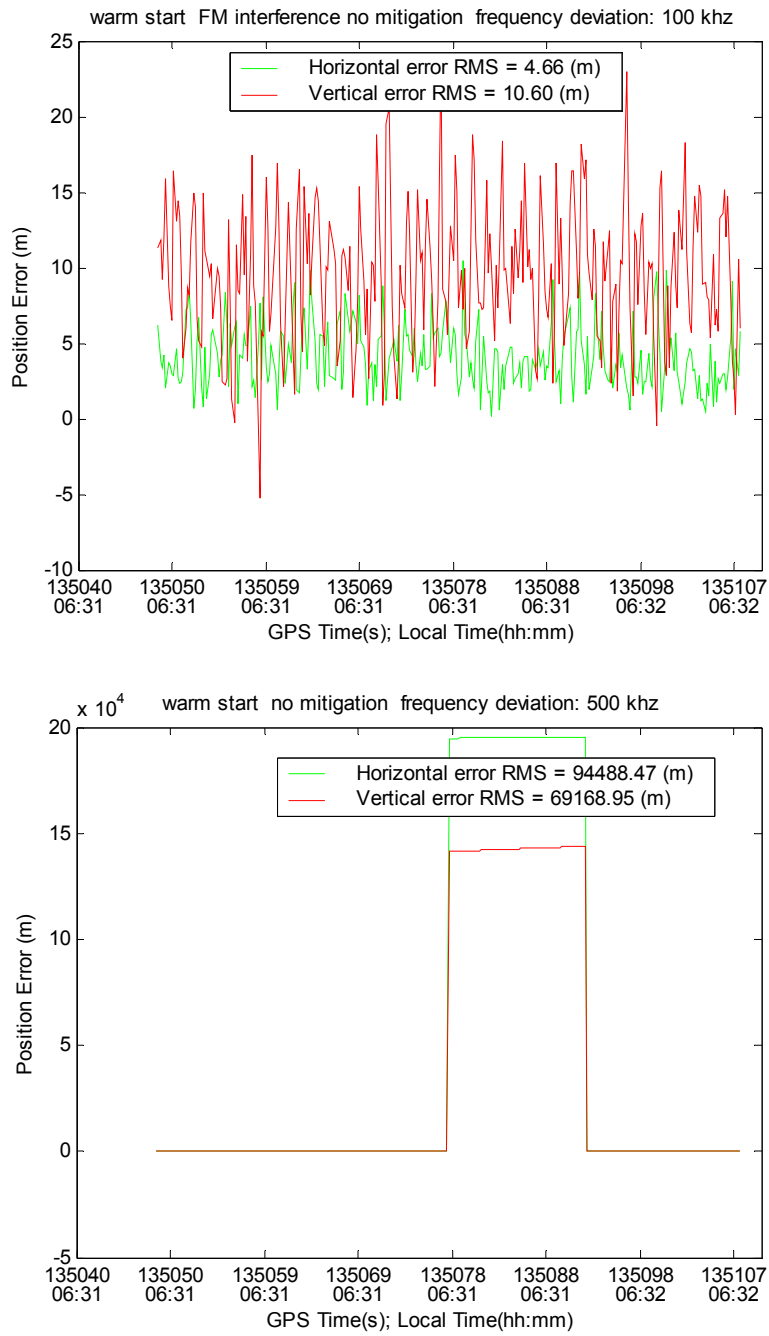


Figure 5.16: Influence of frequency deviation of FM interference on position

When the frequency deviation is small, for example, the narrow-band FM interference with a frequency deviation within 100 KHz, the frequency deviation has very little influence on position. The RMS error stands at the same level as that for the CW interference with the same interference power. If the bandwidth of FM interference becomes wide, for example, when the frequency deviation is set to 500 KHz, the position error becomes extremely large. The frequency deviation plays an important role on the influence of FM interference on GPS position solution.

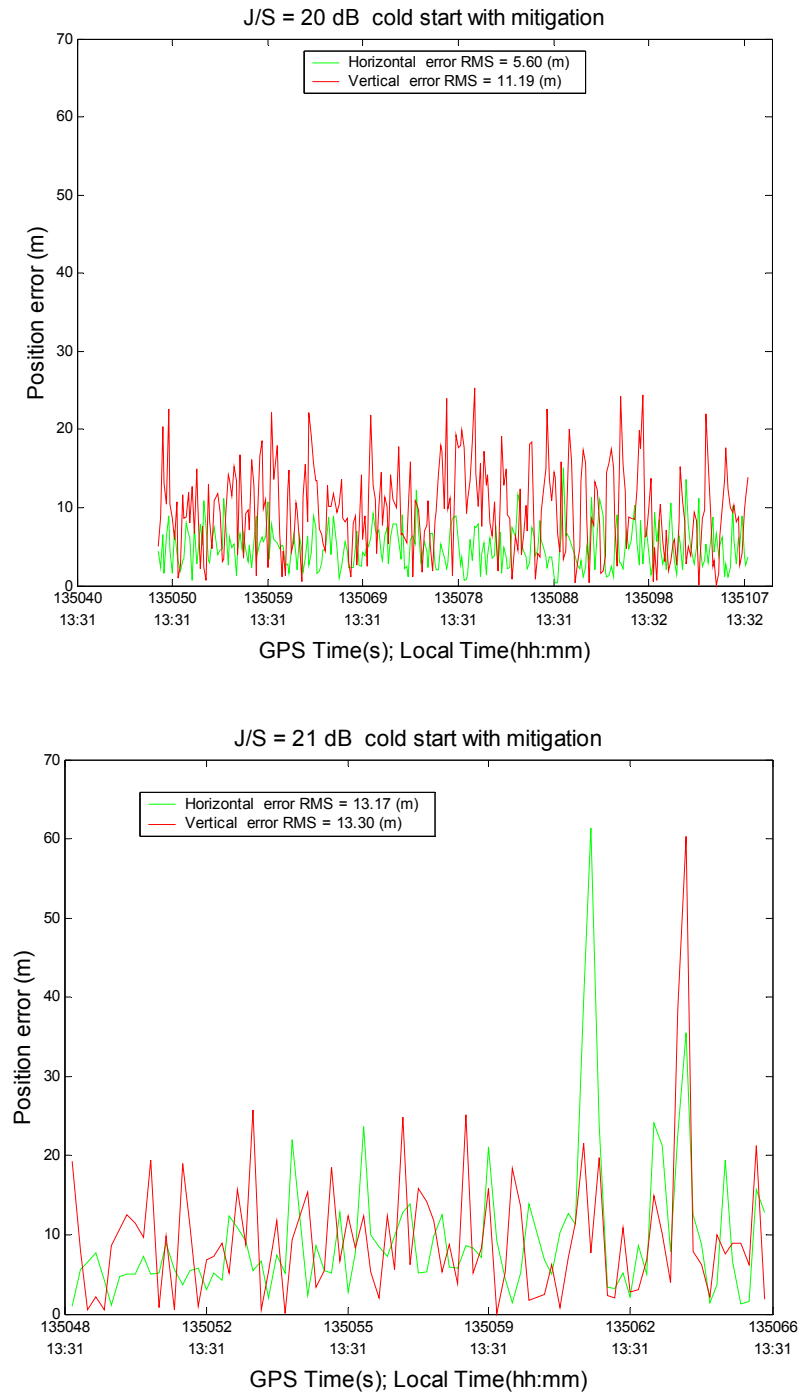


Figure 5.17: Mitigation results with FM interference

Figure 5.17 illustrates the mitigation results with FM interference. The parameters of FM interference are established for test purposes as follows:

- centre frequency: GPS L1
- frequency deviation: 100 KHz, and
- modulate frequency: 5 Hz

Under this FM configuration, when the  $J/S$  equals 20 dB, the position error is stable and restricted to a reasonable level. When  $J/S$  increases to 21 dB, the position error increases rapidly and, after GPS time of 135066 seconds, no position can be obtained. This implies that the receiver loses lock in the tracking loops.

The maximum tolerance for this mitigation algorithm to take effect for FM interference is defined by a  $J/S$  of 20 dB for 100 kHz while, without use of the mitigation algorithm, the maximum tolerance of the software receiver is a  $J/S$  of 15 dB. Thus, the tolerance increases by 5 dB with the use of the mitigation algorithm under cold start conditions.

If the modulation frequency or frequency deviation increases, the maximum tolerance will also decrease, because a greater amount of signal energy will be excised by the mitigation algorithm, causing FM interference to be more of a problem than AM interference on the GPS receiver. At the medium modulation

level, the maximum tolerance of this mitigation algorithm for FM interference is one dB lower than for AM interference.

## CHAPTER 6

# Kinematic Tests

### 6.1 Test setup

The kinematic mode was simulated using a combination of the hardware simulator and *SimGEN* software. A simple motion model was used that allows the user to specify constant speed motion in a perfect circle about a fixed point. The vehicle describes a perfectly flat circle in the local geographic plane and, as the earth is curved this will produce slight variations in height above the ellipsoid as the vehicle traverses the circle. This effect will increase with circle radius. In this test, the circle radius was set to 1000 m, so that the variation in height is very low.

### 6.2 Results and analysis

To investigate the impact of integration time in the loop filters on the solution in dynamic and under interference conditions, the test was set to constant velocity at 80 m/s which simulates the high dynamic experienced in land vehicles, with a J/S of 21 dB. Integration times of 1 ms, 2 ms, 4 ms and 6 ms were tested, with the results shown in Table 6.1:

Table 6.1: Impact of integration time in loop filters on position errors

Integration time (ms)	1 ms	2 ms	4 ms	6 ms
Horizontal RMS error (m)	1066097.1	216309.5	278293.4	15.5
Vertical RMS error (m)	222133.3	50233.7	888585.7	6.0
Satellites been tracked	1,14,16,25	1,14,16,20, 25,30	11,14,20, 25,30	14,16,25, 30

As shown in Table 6.1, 6 ms of integration time can successfully mitigate the influence of interference and yield a reasonable solution. But only four satellites can be tracked, constituting a low availability. In this case, a long integration time causes a low dynamic capability. If the integration time is reduced to 2 ms or 4 ms, dynamic capability has been improved and six satellites can be tracked. But a large position error exists due to the impact of interference. Under interference conditions, the signal is weak and longer integration time is needed. If the problem of large position error can be solved, both high accuracy and an acceptable level of availability can be achieved.

The large position error is caused by the tracking of one or more satellites that

may have sizeable range errors. Figure 6.1 shows the pseudorange errors of different satellites using 2 ms integration time.

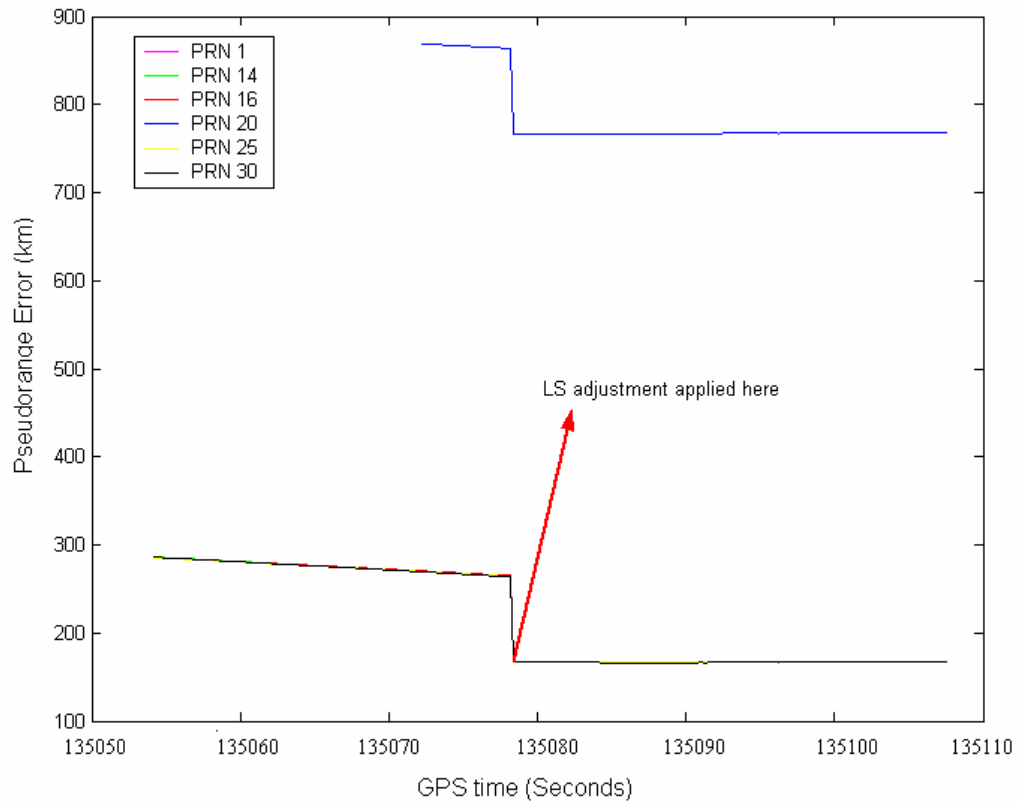


Figure 6.1: Pseudorange errors compared with true value

In this situation, an integration time of 2 ms allows the tracking of six satellites. However, the pseudoranges cannot converge to their true values after a least squares (LS) adjustment. One large pseudorange error exists and this measurement carries the same weight (due to the limitation of the current version of software receiver) in the least squares solutions, causing divergence of the

estimation results. This error however could be removed using a fault detection and exclusion algorithm if sufficient measurement redundancy is available.

Before the least squares adjustment, the pseudorange error is due to the clock error. This error should be in the same scale for different satellites because they use the same simulated inner clock. From Figure 6.1, it is obvious that satellite 20 is abnormal. PRN 20 is offset from the others by about 600 km which represents a 2 ms transmission time error. This error is an integer millisecond error caused by the bit synchronization error, because one bit synchronization error produces a one millisecond error in a pseudorange measurement. If the bit synchronization result has a two bit offset from the true value, this error will exist throughout the succeeding pseudorange calculation process. That is to say, if the signal is not re-acquired again, this error will continue to persist. In order to eliminate this error, further investigation into the bit synchronization process is needed.

The histogram approach is used to perform bit synchronization in the software GPS receiver. This approach breaks a data bit period (20 ms) into 20 C/A-code 1 ms epoch periods and senses sign changes between successive epochs. For each sensed sign change, a corresponding histogram cell count is incremented until a count in one specific cell exceeds the other 19 bins by a pre-specified amount.

The detection procedure can be described as follows [Parkinson and Spilker, 1996]:

- 1) A cell counter  $K_{cell}$  is arbitrarily set and runs from 0 to 19.
- 2) Each sensed sign change is recorded by adding 1 to the histogram cell corresponding to  $K_{cell}$
- 3) The process continues until one of the following occurs:
  - (a) Two cell counts exceed threshold  $T_2$
  - (b) Loss of lock
  - (c) One cell count exceeds threshold  $T_1$
- 4) If (a) occurs, the bit synchronization fails and is reinitialized. If (b) occurs, one tries to reestablish lock. If (c) occurs, bit synchronization is successful, and the C/A-code epoch count is reset to the correct value.

Figure 6.2 shows one such histogram of successful bit synchronization along with count thresholds.

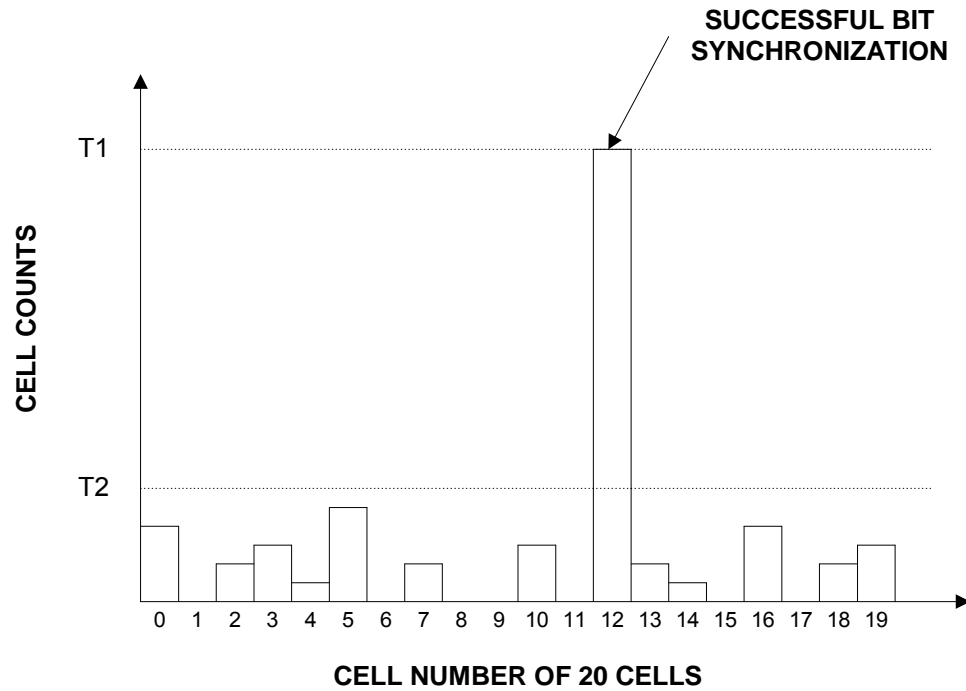


Figure 6.2: A histogram showing successful bit synchronization

The thresholds  $T_1$  and  $T_2$  are determined as follows [Parkinson and Spilker, 1996]:

$$T_1 = 25 \times T_{bs} \quad (6.1)$$

$$25T_{bs} - 3\sqrt{50T_{bs}P_{esc}(1-P_{esc})} \geq T_2 \geq 50T_{bs}P_{esc} \quad (6.2)$$

where,  $T_1$  — Threshold 1

$T_2$  — Threshold 2

$T_{bs}$  — Bit synchronization duration

$P_{esc}$  — Probability of making an error in determining a sign change at  
a desired  $C/N_0$

From the above discussion it is clear that, under interference conditions, there exists the possibility that one bin may exceed the threshold 1 while the true bin is still under threshold 2 due to the interference effect, causing the data bit to be synchronized at the wrong bin. Figure 6.3 shows the bit synchronization result for PRN 20.

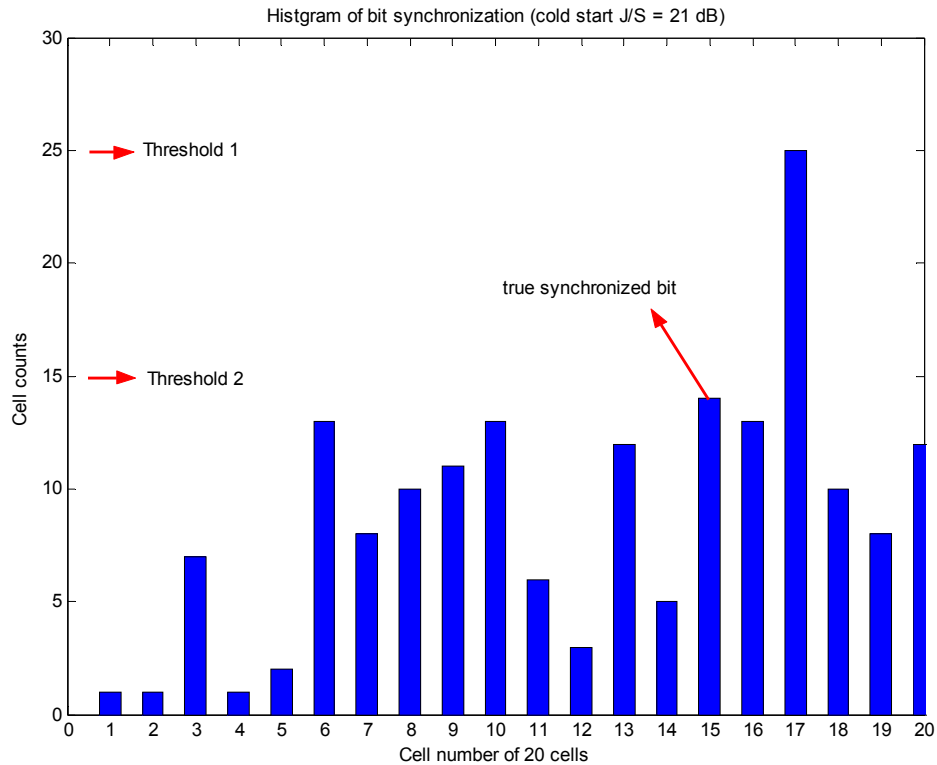


Figure 6.3: Bit synchronization result for PRN 20

It can be seen that only cell 17 exceeds threshold 2, and it is the only cell to reach threshold 1. Through a detection procedure, the bit synchronization process is declared to be successful and the data bit transition point is assumed to be at cell 17 which is 2 bins away from the true value of cell 15.

The true bit synchronization point can be found from the warm start tracking results. This is because the warm start and cold start are from the same data set and only a few points are skipped for cold start processing. The data bit transition point should be the same. However, the bit synchronization result from a warm

start is as shown in Figure 6.4.

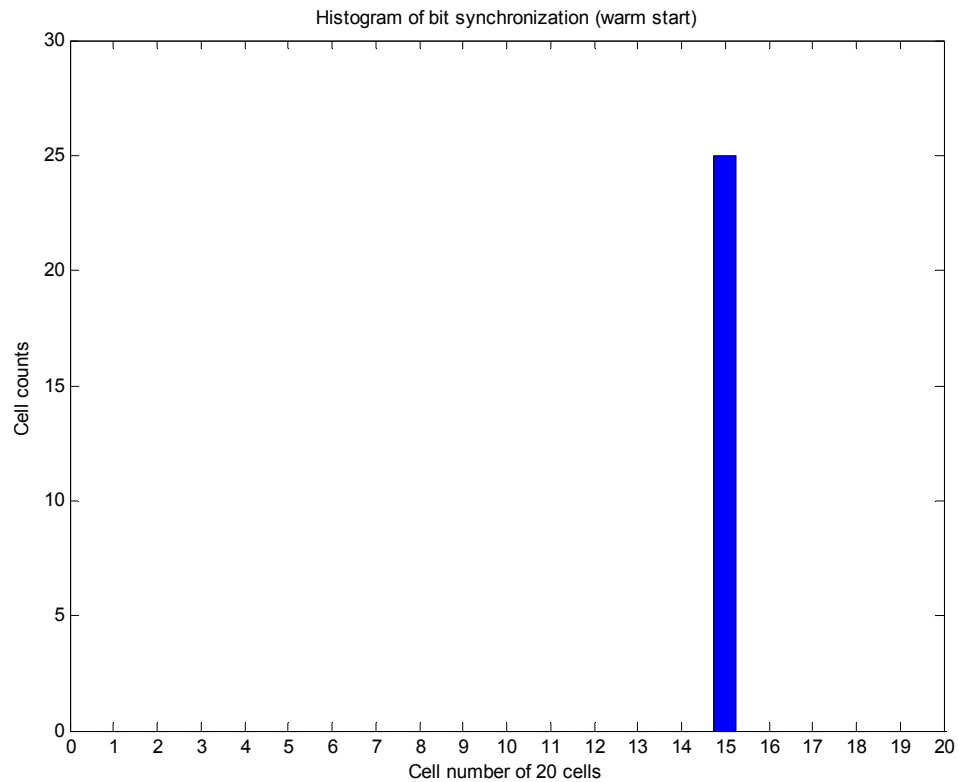


Figure 6.4: Histogram of bit synchronization in warm start

The synchronization result has 2 cells offset from the true point. To improve bit synchronization performance, the following two methods can be used:

- 1) Use a soft threshold for threshold 2. This threshold is associated with the noise floor. If the noise level is high, the threshold will be lower. There will be a high possibility of two cells exceeding threshold 2 before one cell exceeds threshold 1. The bit synchronization will restart again instead of a

bit being synchronized at an incorrect point.

- 2) If 2 cells exceed threshold 2, go back to acquisition instead of starting bit synchronization again, because the required acquisition  $C/N_0$  is about 6 dB higher than tracking. The bit synchronization error is most probably caused by an inaccurate acquisition result. If acquisition is re-started, the acquisition detection threshold can be adjusted through the newly calculated noise floor. The acquisition result will be more precise and there is a high possibility that the bit synchronization result will be true.

Figure 6.5 shows the bit synchronization result with the improved procedure.

The synchronized bit transition point is at the correct place.

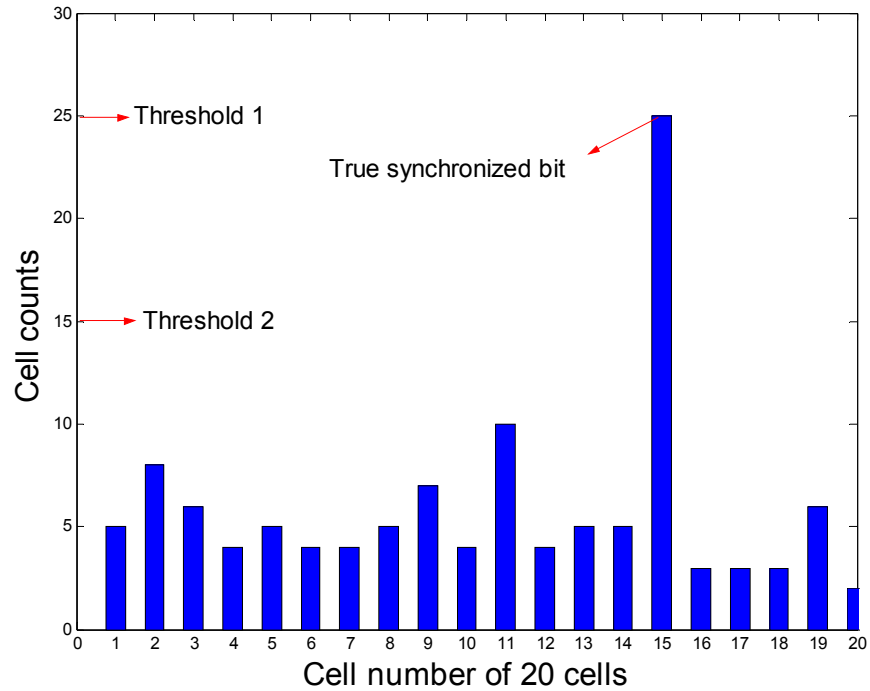


Figure 6.5: Histogram of bit synchronization using the improved procedure

Figure 6.6 shows the pseudorange measurement error when using the improved bit synchronization procedure. After the least squares adjustment, the errors of all the satellites converge to their true values.

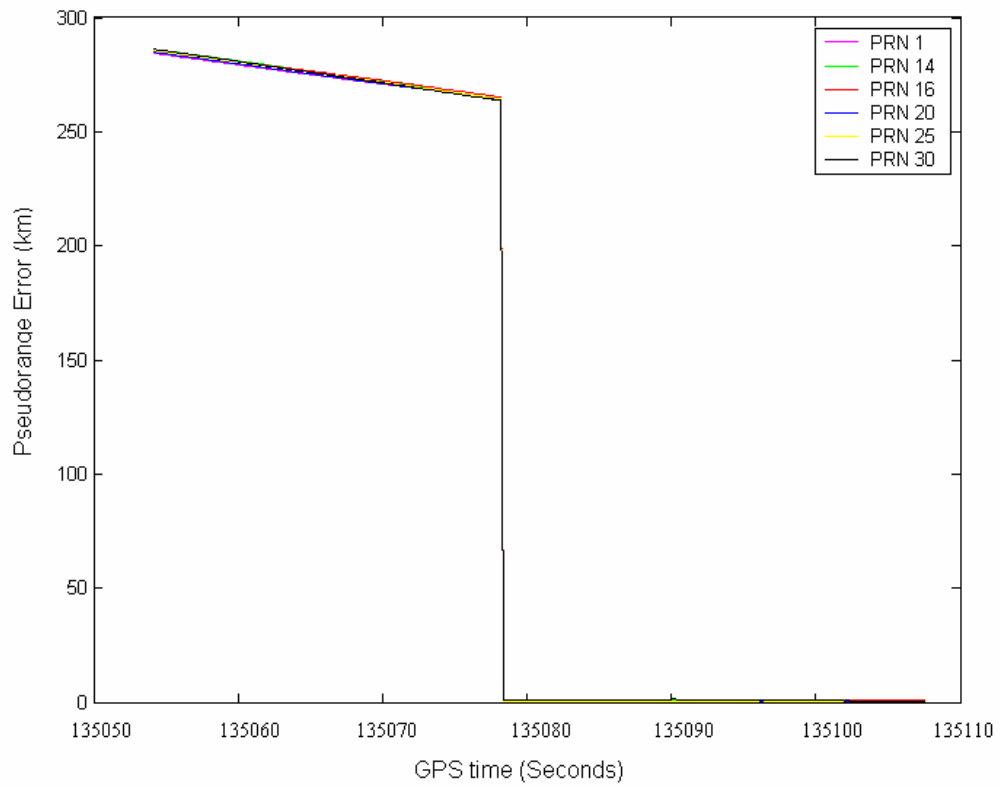


Figure 6.6: Pseudorange error using improved bit synchronization procedure

Figure 6.7 below shows the stochastic repeatability test results under kinematic mode with frequency excision mitigation algorithm and improved bit synchronization procedure (J/S 21 dB, velocity 80 m/s, and cold start).

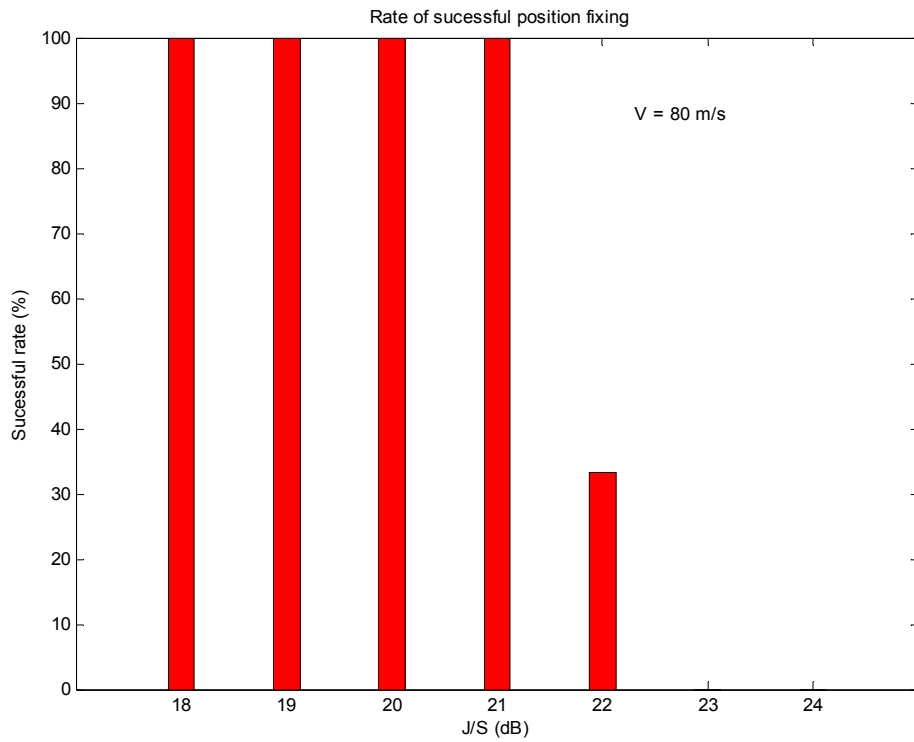
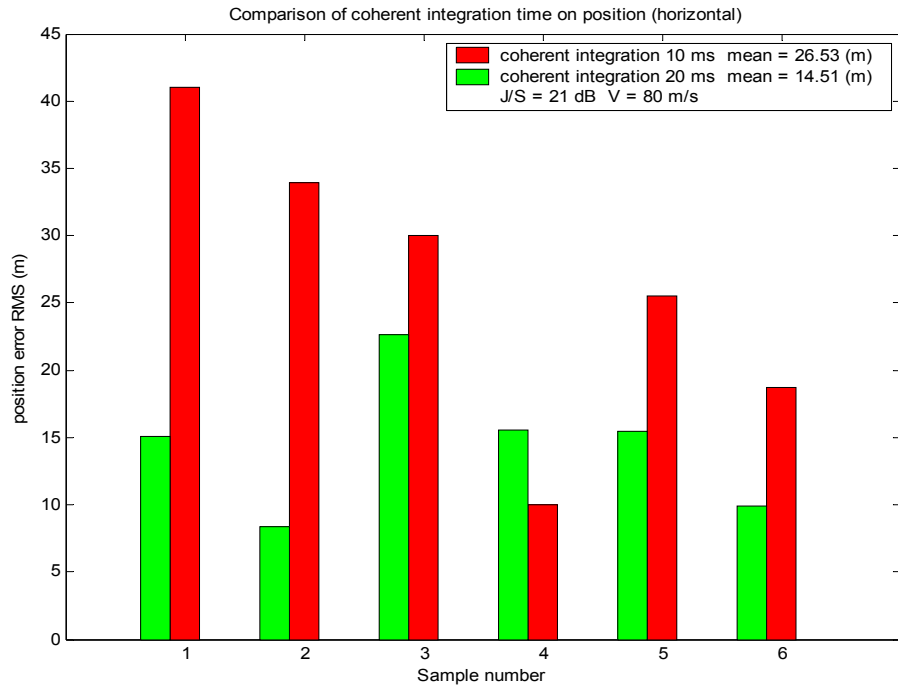


Figure 6.7: Stochastic repeatability test results under kinematic mode

The results show that, when J/S is below 21 dB, the position error is stable and restricted to within 10 metres. The success rate of obtaining position is 100 percent.

When the J/S increases to 21 dB, the position error varies but can still be restricted to within 25 metres; the success rate of obtaining a correct position is also 100 percent. When J/S increases to 22 dB, the success rate of obtaining a correct position is reduced to 33.3 percent. If J/S is greater than 22 dB, a position cannot be obtained. A 20 ms coherent integration time has better performance statistically. The frequency excision algorithm with improved acquisition based on bit synchronization result is statistically stable when the J/S is no greater than 21 dB under high dynamic conditions.

## CHAPTER 7

# Application of Data Window in FFT-based Mitigation Algorithm

### 7.1 The advantage of using a data window

In the previous chapters, the traditional FFT-based frequency excision interference mitigation algorithm has been discussed. This method can remove most of the interference energy in the frequency domain. The drawback is that it can suppress energy only in the main-lobe spectral bins which is not adequate due to the residual interference distributed throughout the spectrum by these side-lobes, especially when interference power level is high.

FFT operations assume a periodic extension of a finite sequence that is to be transformed. For each block of  $N_p$  samples of the input sequence which is used to do FFT analysis, if the  $N_p$  samples are not periodic in the FFT's window of observation, a discontinuity occurs at the FFT's block boundary. So the FFT of a signal often exhibits high spectral side-lobes due to the finite aperture processing interval. The behavior of these side-lobes is much like a broad band interference

source in terms of contributing energy to all FFT spectral bins. Because of that, no threshold can be selected that will allow the removal of the interference energy without also removing excessive signal spectrum. This phenomenon is called spectral leakage.

Spectral leakage that survives the frequency domain filtering operation may severely degrade the performance of the mitigation algorithm. To mitigate the effect of spectral leakage, a data window is applied prior to computing the FFT. Windowing smoothes the discontinuities at the block boundary and therefore lessens the effect of spectral leakage. The windowed FFT can be expressed as:

$$X(k) = \sum_{n=0}^{N_p-1} w(n)x(n)e^{\frac{-j2\pi kn}{N_p}}, \quad k = 0, 1, \dots, N_p - 1 \quad (7.1)$$

The window function  $w(n)$  determines the amount of spectral leakage in the DFT output:

$$w(n) = 1 \quad n = 0, 1, \dots, N_p - 1 \quad (7.2)$$

If  $w(n)$  is set to identity as in Equation 7.2, then Equation 7.1 reverts to non-windowed processing which is the same as the traditional FFT output. In this situation, it is equivalent to using a rectangular window. The Fourier transform of

the rectangular window is a Sinc function with the first side-lobe reduced by 13 dB relative to the main lobe.

When the frequency of a signal is not exactly one of the DFT frequencies, the signal energy will be spread across the spectrum proportional to the width of the main lobe and the height of the side lobes of the window [Capozza, et al., 2000]. In the traditional FFT, which is equivalent to a rectangle windowed FFT, the first side lobe attenuation is only -13 dB. The interference frequency is much easier to mix with the signal frequency, causing degradation of the mitigation performance. So selecting a window with lower side lobes will reduce the amount of spectral leakage. However, a lower side lobe usually results in a wider main lobe, causing reduced spectral resolution.

## **7.2 Window selection**

The objective of using a data window in an interference mitigation algorithm is to minimize the spectrum spreading of the interference frequency component in order to minimize the number of frequency bins that will be excised. At the same time, the degradation of the GPS signal will also be minimized when no interference is presented. Thus, window selection requires a trade-off between the reduction in SNR due to the signal attenuation caused by introducing window operation and the effectiveness of the spectral containment for interference.

The windowing helps by reducing the inherent frequency broadening of each

interferer caused by the finite duration of the FFT. This reduction in the number of frequency samples occupied by a narrow-band interferer results in a reduction in the amount of signal energy removed by the excision process. Unfortunately, windowing also degrades the  $C/N_0$  of the correlator by the following factor [Capozza, et al., 1999]:

$$\frac{\left[ \sum_{k=0}^{N-1} w(k) \right]^2}{N \sum_{k=0}^{N-1} w^2(k)} \quad (7.3)$$

Degradation can be as high as 3 dB for the more powerful window functions. Similarly, frequency containment is proportional to a window's lowest side lobe level. In the window selection process, SNR loss and side lobe attenuation must be balanced. Three commonly used windows, the Blackman-Harris, Hamming, and Gaussian windows are compared in the following sections.

### 7.2.1 Blackman-Harris window

The equation for computing the coefficients of a minimum 4-term Blackman-Harris window is as follows [Harris, 1978]:

$$w[k+1] = \alpha_1 - \alpha_2 \cos\left(2\pi \frac{k}{n-1}\right) + \alpha_3 \cos\left(4\pi \frac{k}{n-1}\right) - \alpha_4 \cos\left(6\pi \frac{k}{n-1}\right) \quad (7.4)$$

where  $0 \leq k \leq (n-1)$

$$\alpha_1 = 0.35875$$

$$\alpha_2 = 0.48829$$

$$\alpha_3 = 0.14128$$

$$\alpha_4 = 0.01168$$

This window function can be plotted as shown in Figure 7.1.

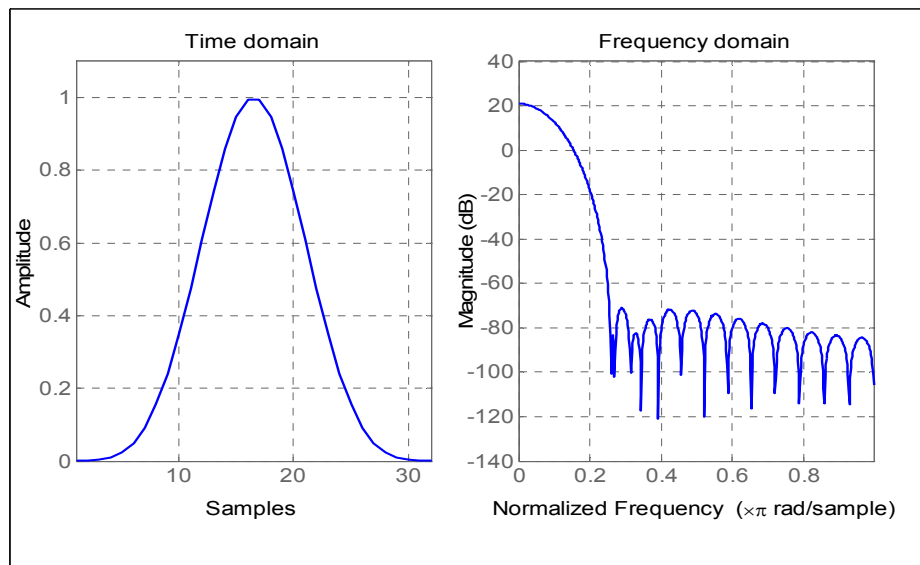


Figure 7.1: Plot of 4-term Blackman-Harris window

A 4-term Blackman-Harris window has a -92 dB side lobe. The performance of frequency containment for the interference component is excellent. The low side lobe levels essentially restrict the spectral leakage. However, high signal

attenuation at the FFT block transitions results in a 3 dB SNR loss.

### 7.2.2 Hamming window

The coefficients of a Hamming window are computed from the following equation [Oppenheim and Schaffer, 1989]:

$$w[k + 1] = 0.54 - 0.46 \cos\left(2\pi \frac{k}{n-1}\right) \quad (7.5)$$

where  $0 \leq k \leq (n-1)$

This window function can be plotted as shown in Figure 7.2

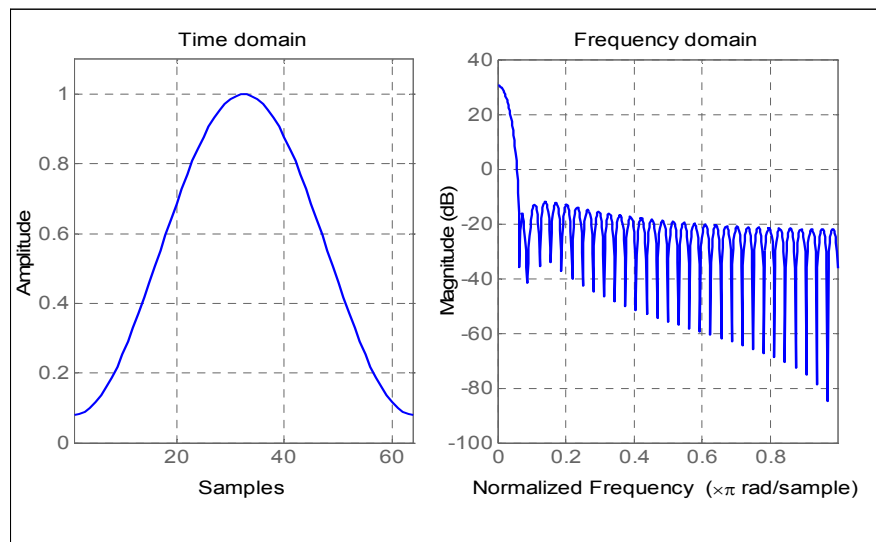


Figure 7.2: Plot of Hamming window

A Hamming window has a -40 dB side lobe level, and provides intermediate frequency containment capability. The SNR degradation resulting from a

Hamming window is less than 1.36 dB.

### 7.2.3 Gaussian window

The coefficients of a Gaussian window are computed from the following equation [Harris, 1978]:

$$w[k+1] = e^{-\frac{1}{2} \left[ \alpha \frac{k-N}{N/2} \right]^2} \quad (7.6)$$

where  $0 \leq k \leq (n-1)$  and  $\alpha \geq 2$

and  $\alpha$  is the reciprocal of the standard deviation. The width of the window is inversely related to the value of  $\alpha$ . A larger value of  $\alpha$  produces a narrower window. This window function can be plotted as shown in Figure 7.3 where  $\alpha$  was set to 2.5:

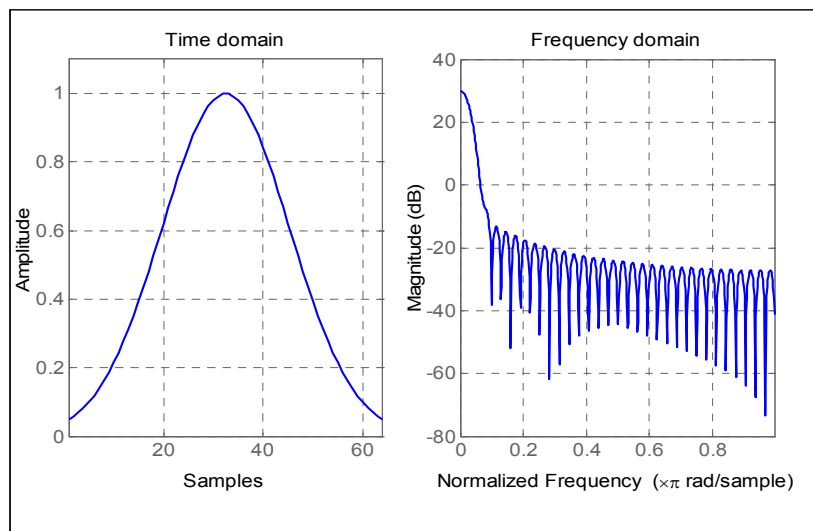


Figure 7.3: Plot of Gaussian window

A Gaussian window has a -43.4 dB side lobe level, providing intermediate frequency containment capability. The SNR degradation resulting from Gaussian window is less than 1.36 dB which is similar to a Hamming window.

In GPS applications, the interference level is normally well above the -13 dB side lobes of the rectangular window. The spectrum herein exhibits significant spectral leakage. The windowing operation reduces the amount of the spectrum that must be excised, thus preserving more of the desired signal spectrum.

To minimize the degradation of the SNR due to the window while maintaining frequency content, the overlapped processing technique was used. The overlapped processing allows the tails of the window to be eliminated, thereby substantially reducing the output SNR loss. With 50 percent overlapped processing, the SNR loss can be reduced to as low as 0.6 dB [Capozza, 1999]. In GPS receiver design, these losses may be included as part of the receiver noise figure budget, since they represent degradation of the output  $C/N_0$ . In the interference mitigation algorithm developed in this thesis, an optimal design strategy was used which includes an interference detection algorithm. This algorithm enables interference suppression only when it is needed. It would also reduce insertion loss.

A Blackman-Harris window was used in the test, because it provided the lowest

side-lobe among the available windowing methods. A relatively high level of SNR loss was compensated by overlapped processing.

### **7.3 Implementation of overlapped processing**

The advantage of the overlapped processing lies in two aspects:

- Reduces the effect of the signal attenuation from the windowing operation on the output SNR, and
- Mitigates the effects of data rejection near the boundaries of the data collection interval.

The disadvantage of the overlapped processing is obvious. It doubles the processing load since it requires a second processing path which includes a window, forward FFT, excision operation, and inverse FFT.

A level of either 50 or 75 percent overlapped processing is normally used. Use of 75 percent overlapping requires four times the usual processing time, which presents a great computational burden for a software receiver. A 50 percent overlapping figure is used in this thesis. The block diagram of 50 percent overlap processing is shown in Figure 7.4 [Capozza, 2000]:

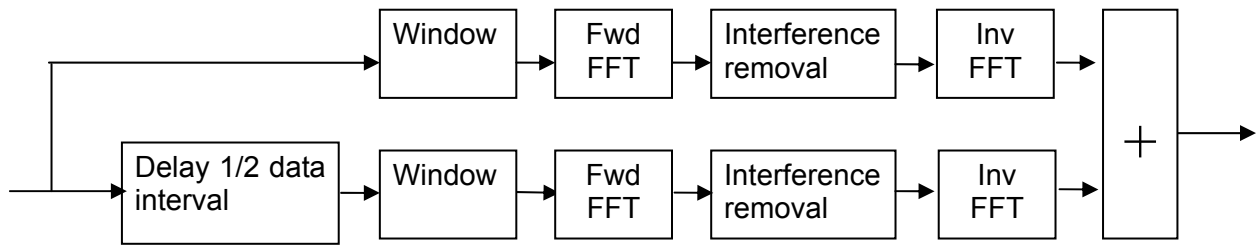


Figure 7.4: Block diagram of 50 percent overlap processing

In a software receiver, block processing is used instead of an epoch-by-epoch approach. The interference mitigation process also uses the block processing approach. The intervals selected for processing can be long or short. The selection criterion is a function of the stability of the interference signal. Shorter processing intervals offer a smaller number of wide-bandwidth spectral filters, while long intervals offer a large number of narrow-bandwidth filters to the excision process. In this case, 4 ms was selected as processing interval. No obvious improvement can be obtained for longer intervals, but FFT processing time increases rapidly as the interval increases.

Each path in the processing chain produces one half of the usable output sequence as shown in Figure 7.4. The input signal is broken down into two paths offset by one half of the processing interval. The 1/4 samples at the beginning and end of each inverse FFT block are discarded, leaving the middle 1/2 samples, which are appended to 1/2 samples from the second inverse FFT. The samples from each path are then combined to form the final samples for the entire

processing interval and the resulting time series are assembled on the timelines. These overlapped intervals are merged by simple addition and are presented to subsequent Doppler removal and Gold code compression. Here, the time synchronization of each path has not been taken into account which will cause some frequency selectivity. This is an artifact which is not desired. If a delay is added in the first path after the inverse FFT and filters are added in both paths on the timelines, more optimal results may be achieved.

## **7.4 Results and analysis**

Figure 7.5 presents an enlarged section of spectra obtained by the 4 ms FFT processing of the non-windowed and windowed data, respectively.

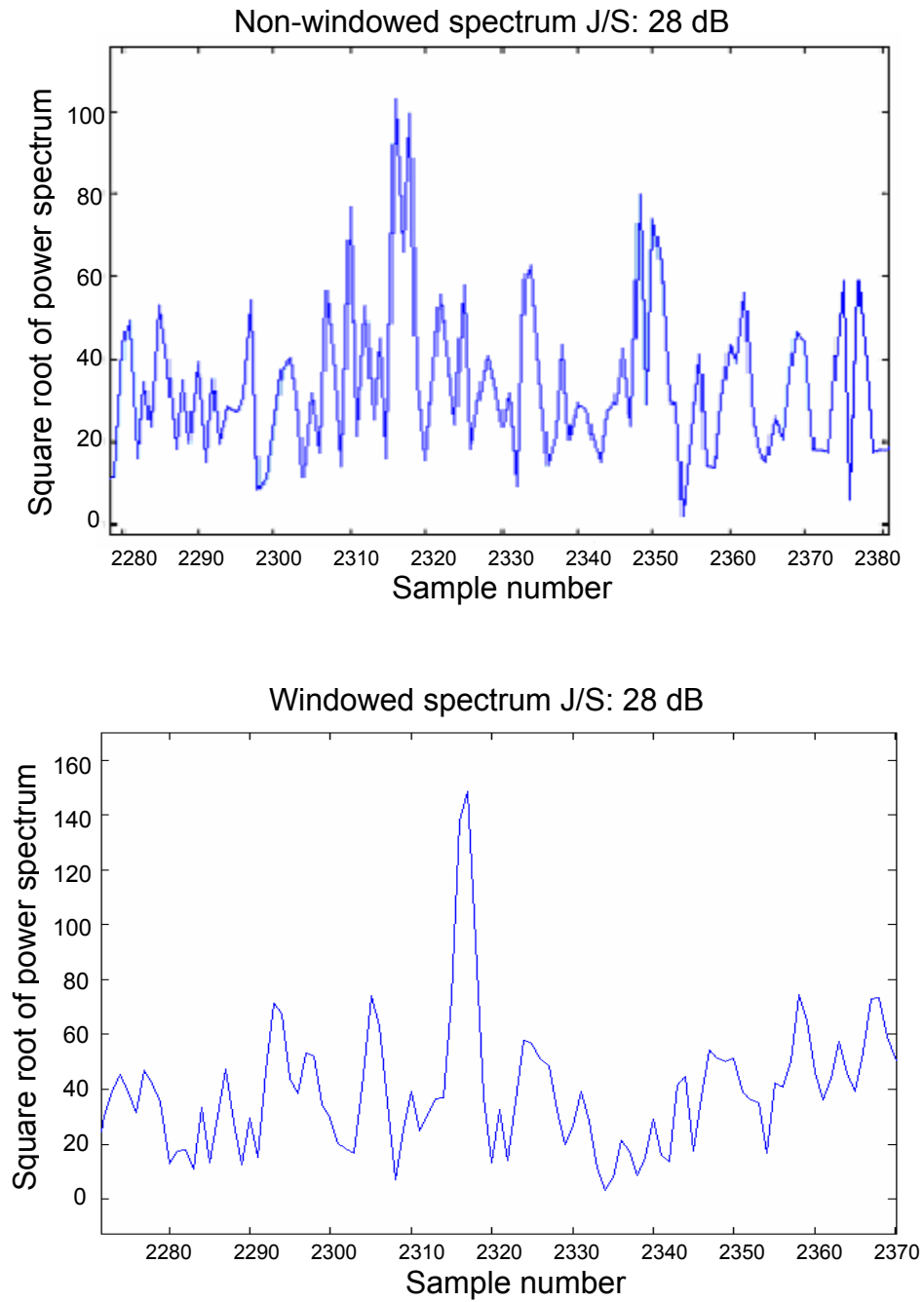


Figure 7.5: Enlarged spectra of windowed and non-windowed data

As can be seen from the plots in Figure 7.5, the windowing operation increases

the concentration of the interference frequency and reduces the number of frequency bins that need to be excised. Windowing reduces the amount of spectrum that must be excised, thus preserving more of the desired signal spectrum. As a result, less signal energy loss and less distortion in the correlation peak improve the accuracy of the position estimation and increase the maximum tolerance of the interference mitigation algorithm. The plots in Figure 7.6 show the effect of windowing on position estimation.

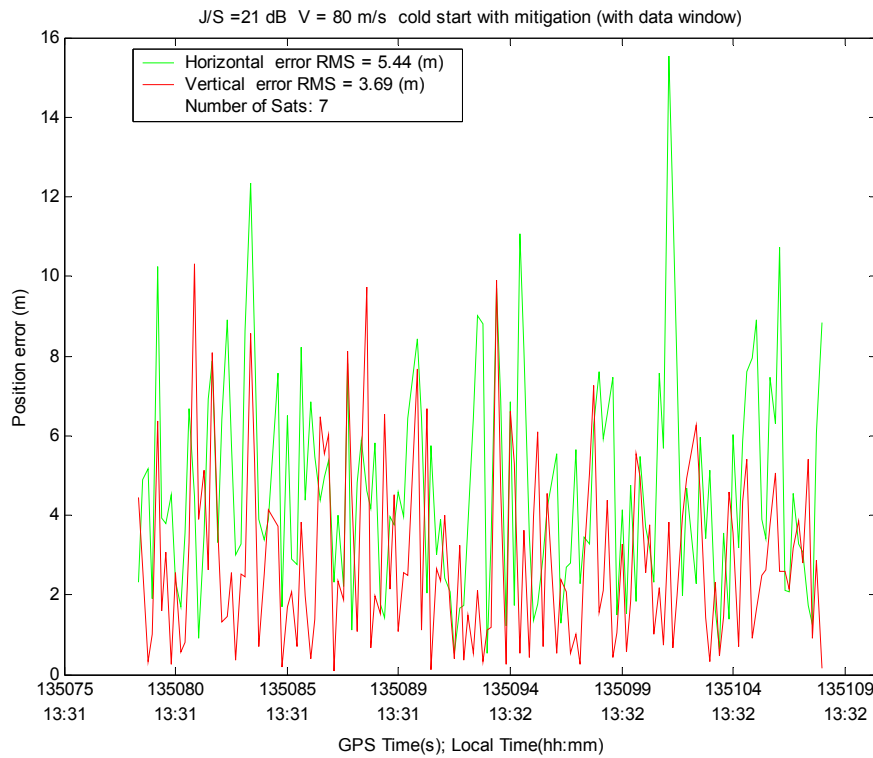
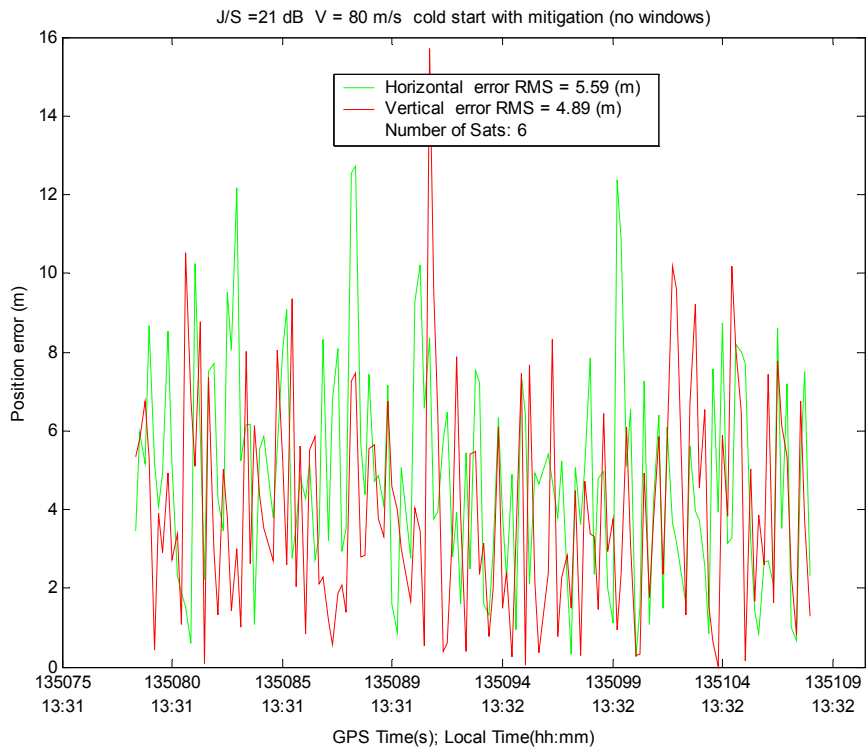


Figure 7.6: Effect of windowing on GPS position estimation.

The test was carried out in kinematic mode. The speed of the vehicle was set to 80 m/s under a J/S of 21 dB and in a cold start environment. From the GPS position results, using a windowing operation, the position error root mean square shows a slight improvement. Vertical error RMS decreased from 4.9 m to 3.7 m and the horizontal RMS error decreased slightly from 5.6 m to 5.4 m. The number of satellites that can be tracked increased from six to seven, which means that employing a windowing operation allows all of the simulated satellites to be tracked.

The addition of tracked satellites may not entail a commensurate improvement of reliability because, if the pseudorange of the additional satellite has a large error and it is used in least squares estimation, this satellite may deteriorate the estimation result. In order to analyze the performance of the additional satellite, the pseudorange errors of all the satellites are given in Figure 7.7. From this figure, the reliability of the satellites can be analyzed.

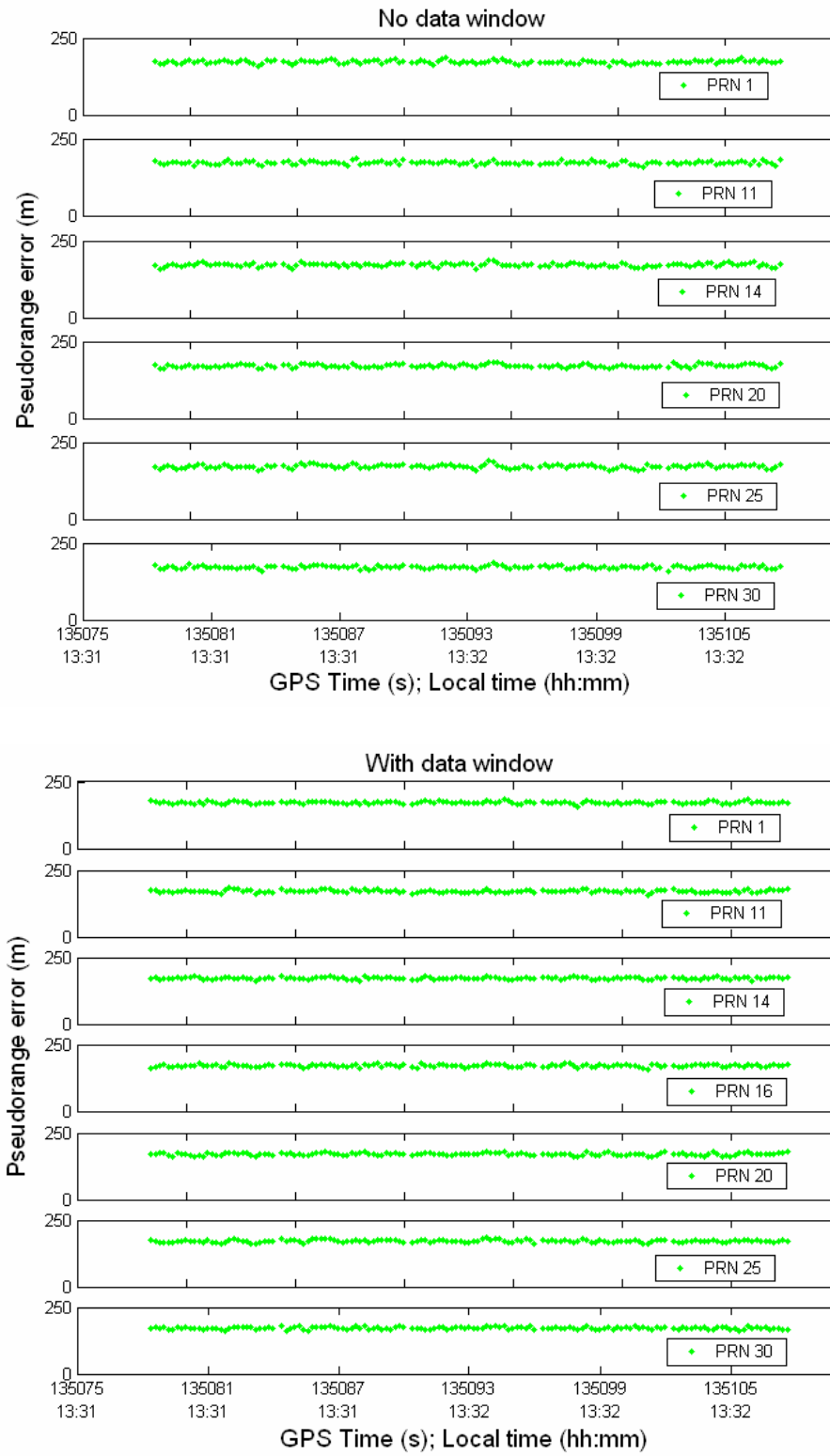


Figure 7.7: Pseudorange error comparison between “with window” and “without window”

Only with the use of a windowing operation can satellite 16 be tracked. As it can be seen in Figure 7.7, the pseudorange error of PRN 16 is at the same scale as other satellites, which means that the measurement of this additional satellite is reliable. By employing windowing, a greater number of satellites can be effectively tracked and higher sensitivity can be achieved.

The above result came from a one-time test. In order to guarantee the stability of this result, the test was carried out six times to produce a stochastically reliable result. Under each J/S condition, the test was repeated six times. The results are shown in Figure 7.8 and 7.9.

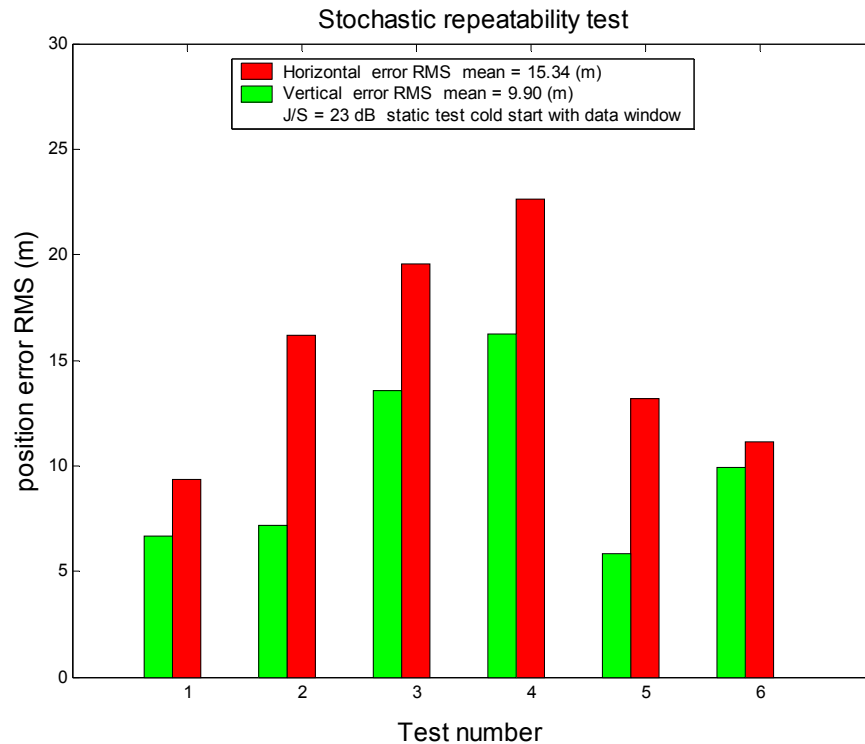


Figure 7.8: Position errors of stochastic repeatability test with windowing

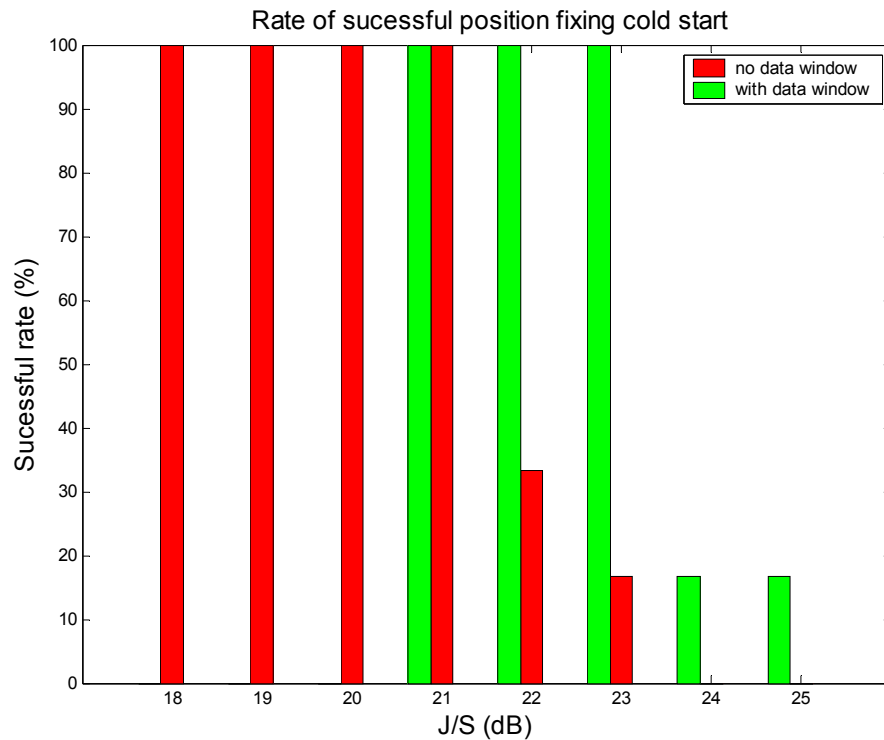


Figure 7.9: Success rate of stochastic repeatability test with windowing

When  $J/S$  is below 23 dB, the position error is within 10 metres in all of the six tests. If  $J/S$  increases to 23 dB, the position error increases also. The position error varies for different samples due to the random noise. In some test samples, the RMS error can reach 20 metres; however, the success rate in terms of obtaining reasonable position solutions is still 100 percent with the window operation. Thus, the interference mitigation algorithm of the data window, combined with frequency excision, is statistically stable when  $J/S$  no greater than 23 dB.

When J/S increases to 24 and 25 dB, even with a windowing operation, the successful rate of obtaining satisfactory position solutions is reduced to 16.7 percent, which means that only one out of 6 tests can achieve a solution. Under this circumstance, the mitigation result is not stochastically repeatable. The maximum tolerance of this mitigation algorithm with a data window is 23 dB under cold start conditions. If the J/S is greater than 25 dB, a position cannot be obtained.

From the above analysis of test results, the advantage of using a data window before FFT transform is apparent. Although the improvement in position accuracy is slight, the sensitivity has been improved, since more satellites can be effectively tracked. Use of a data window, combined with the frequency excision algorithm, can successfully mitigate interference of J/S values no greater than 23 dB under cold start conditions. The maximum tolerance increases by 2 dB, as compared to a traditional frequency excision algorithm, thus improving the sensitivity.

## CHAPTER 8

# Conclusions and Recommendations for Future Work

### 8.1 Conclusions

A RFI mitigation algorithm based on spectral analysis has been developed in this thesis. The strategies of using an adaptive threshold for interference detection and bit synchronization and using improved acquisition based on earlier information were used to improve the mitigation results. The effectiveness of this algorithm for CW, AM and FM interference has been investigated in acquisition, tracking and position domain with the help of a software GPS receiver, a hardware simulator and a signal generator. The influence of coherent integration time, tracking loop bandwidth and integration time in the loop filter on the mitigation results has also been investigated. The advantages of using windowing and overlap processing before FFT are discussed and implemented in the mitigation algorithm. Different sampling rates were used during the data collection and the results of using different sampling rates have been compared and analyzed.

Based on the results and findings obtained from the above results, the following specific conclusions can be drawn:

1. The frequency excision algorithm is effective in mitigating a certain power level of narrow-band RFI. An adaptive detection threshold that is a function of the standard deviation of the normalized spectrum and the correlator power output has better mitigation performance than the fixed detection threshold which is suggested in the literature. The scalar factor in this function is determined empirically and changes with different kinds of interference.
2. To obtain optimal mitigation results, this mitigation algorithm should combine with some degree of control on software receiver parameters. For example, adaptive selection of the following parameters may prove useful: coherent integration time; tracking loop bandwidth; and integration time in the loop filter for different interference levels and receiver dynamics.
3. The maximum tolerance of this algorithm in acquisition is a J/S of 28 dB with a 7 MHz sampling rate and a 20 ms coherent integration time. It produces a 3 dB increase compared with a 4.75 MHz sampling rate whereas, in tracking, the maximum tolerance entails a J/S of 30 dB at a 4.75 MHz sampling rate and 35 dB at a 7 MHz sampling rate.

4. In the position domain, for CW interference, no improvement was observed with use of the mitigation algorithm in a warm start environment. In a cold start environment, a stochastic repeatability test shows that the maximum J/S is 21 dB to achieve a 100 percent success rate in position fixing with use of the mitigation algorithm. Without the mitigation algorithm, due to the inherent anti-jamming property of the spread spectrum system, the J/S can reach a maximum level of 18 dB.
  
5. In high dynamic mode (with a velocity of 80 m/s), by employing a soft threshold in bit synchronization and improved acquisition based on a combination of earlier information and a carefully chosen value for integration time in the loop filter, the maximum mitigation ability for position fixing can reach 21 dB in a cold start environment, the same level as in static mode.
  
6. This mitigation algorithm also effectively deals with AM and FM interference, but the maximum tolerance is less than that found in the case of CW interference. Also, FM interference causes more of a problem than AM interference on this mitigation algorithm. In medium level modulation and cold start conditions, the maximum tolerance for AM interference with mitigation was observed at a J/S of 21 dB, which represents a 6 dB improvement as compared to no mitigation algorithm. Whereas, for FM interference, the maximum tolerance is 20 dB, a 5 dB improvement was observed as compared

to no mitigation algorithm.

7. Windowing and overlap processing before FFT transform has proven to be an effective strategy to improve the performance of the frequency excision algorithm. Although the improvement in position accuracy is slight, a larger number of satellites can be effectively tracked. Thus, sensitivity is improved. A data window combined with a frequency excision algorithm can successfully mitigate interference of J/S values no greater than 23 dB in cold start conditions, a 2 dB improvement as compared to a conventional frequency excision algorithm.

## **8.2 Recommendations for future work**

All of the tests conducted in this thesis are based on 1-bit analog-to-digital (A/D) conversion. The 1-bit A/D converter is widely used in commercial GPS receivers. However, in applications where RF interference may become a problem, a 1-bit A/D converter is highly vulnerable to being captured by a CW jammer. For RFI mitigation, the amount of narrow-band RF interference suppression is related to the number of effective bits of A/D conversion precision that can be achieved at IF.

Based on the above analysis, it is recommended, firstly, that future research be undertaken to investigate the impact of the quantization bit on the mitigation

algorithm and the selection of the appropriate bit of quantization. There exists the trade-off between computational burden and anti-jamming performance. Due to the limited control provided by the *Signal Tap*, the software Global Navigation Satellite System (GNSS) simulator developed by the University of Calgary's PLAN group may be a useful tool for this research.

The interference data set used in this thesis is simulated; thus, the interference type is known before the mitigation algorithm is applied. However, in practical applications, no prior knowledge is known about the interference. The second recommendation for future research is to develop an algorithm to distinguish the interference types and to develop a strategy for applying the various interference detection thresholds.

## References

- Accord Software & Systems Private Limited (2003). *GPS Signal Tap Users Guide version 1.1*. Bangalore, India. pp. 1-1.
- Badke, B. and Spanias, A.S. (2002). *Partial band interference excision for GPS using frequency-domain exponents*. Acoustics, Speech, and Signal Processing, 2002. Proceedings (ICASSP '02). IEEE International Conference on, Volume: 4, 13-17 May 2002, Pages: 3936 – 3939.
- Capozza, P.T., Holland, B. J., Li, C., Moulin, D., Pacheco, P., Rifkin, R. (1999), *Measured effects of a narrowband interference suppressor on GPS receivers*, In Proceedings of 55<sup>th</sup> annual meeting of the Institute of Navigation, June 1999, Cambridge, MA, Pages: 645 – 651.
- Capozza, P.T., Holland, B. J., Hopkinson, T. M., Landrau, R. L.(2000), *A single-chip narrow-band frequency-domain excisor for the global positioning system (GPS) receiver*, Solid-State Circuits, IEEE Journal of , Volume: 35 , Issue: 3 , March 2000, Pages: 401 – 411.
- Cooley, J.W. and Tukey, J.W. (1965) *An algorithm for the machine calculation of complex Fourier series*, *Math. Comput.* 19, Pages: 297–301.
- Cutright, C., Burns, J. R., Braasch, M. (2003). *Characterization of Narrow-band interference mitigation performance versus quantization error in software radios*. In Proceedings of 59<sup>th</sup> annual meeting of the Institute of Navigation, June 2003, Pages: 323–332.
- Deshpande, S., Cannon, M.E. (2004). *Interference Effects on the GPS Signal Acquisition*, National Technical Meeting, Institute of Navigation, 26-28 January, 2004, Pages: 1026 – 1037.
- Dipietro, R.C (1989). *An FFT-based Technique for Suppressing Narrow-Band Interference*, in PN Spread Spectrum Communications Systems. Acoustics, Speech, and Signal Processing, 1989. ICASSP-89., 1989 International Conference on, 23-26 May 1989, Pages:1360 - 1363 vol.2
- Dong, L. (2003), *IF GPS Signal Simulator Development and Verification*, MSc. thesis, UCGE reports 20184, the University of Calgary

Harris, F. J.(1978) *On the Use of Windows for Harmonic Analysis with the Discrete Fourier Transform*. Proceedings of the IEEE. Vol. 66, January 1978, pp. 51-84.

Heppe, S. (2002). *GPS and GNSS RFI & Jamming Concerns I*. ION GPS-2002 Tutorial, Portland, Oregon, pp. 45

Kaplan, E. (1996). *GPS Satellite Signal Characteristics, Understanding GPS Signal Characteristics*. Artech House, Inc., 685 Canton Street, Norwood, MA 0206.

Krumvieda, K., Madhani, P., Cloman, C., Olson, E., Thomas, J., Axelrad, P., Kober, W. (2001), *A complete IF Software GPS Receiver: A tutorial about the Details*, ION GPS 2001, 11-14 September, 2001, Salt Lake City, UT, Pages: 789 – 811.

Li, L. and Milstein, L. (1982), *Adaptive Algorithms for Estimating and Suppressing Narrow-Band Interference in PN Spread-Spectrum Systems*, Communications, IEEE Transactions on [legacy, pre - 1988], Volume: 30, Issue: 5, May 1982, Pages: 913 – 924.

Lin, D.M., Tsui, J. (2000), *Comparison of acquisition methods for software GPS receiver*, Proceeding of ION GPS 2000, 19-22 September, 2000, Salt Lake City, UT, Pages: 2385 – 2390.

Ma, C., G. Lachapelle, and M.E. Cannon (2004) *Implementation of a Software GPS Receiver*. Proceedings of GNSS 2004, Institute of Navigation, Long Beach, CA. September 21-24.

MacGougan, G.D. (2003), *High Sensitivity GPS Performance Analysis in Degraded Signal Environments*, M.sc. thesis, UCGE reports 20176, the University of Calgary

Ndili and Per Enge (1997). *Receiver autonomous interference detection*. In Proceedings of 53<sup>rd</sup> annual meeting of the Institute of Navigation, June 1997 Albuquerque, New Mexico, Pages: 79 – 88.

Oppenheim, A.V., and Schafer, R.W. (1989). *Discrete-Time Signal Processing*. Prentice-Hall, 1989, pp. 447-448.

Parkinson, B. and Spilker, J. J. (1996). *Global Positioning System: Theory And Applications Volume 1*. American Institute of Aeronautics and Astronautics, Inc.,

Peterson, B., Hartnett, J., Fiedler, R., Nebrich, A. (1996). *Frequency Domain Techniques for fast GPS acquisition and interference detection/rejection*. Navigation: Journal of the institute of navigation, Vol.43, No. 3, Fall 1996.

Proakis, J.G and Ketchum, J.W. (1982). Adaptive Algorithms for Estimating and Suppressing Narrow-Band Interference in PN Spread-Spectrum Systems COM-30 (May 1982), IEEE Trans. Communications, Volume: 30, Issue: 5, Pages:913 – 924.

Proakis, J.G. (1996a). *Digital signal processing: principles, algorithms, and applications*. Prentice-Hall, Inc., Upper Saddle River, New Jersey 07458, pp. 243.

Proakis, J.G. (1996b). *Interference suppression in spread spectrum systems*. Spread Spectrum Techniques and Applications Proceedings, 1996, IEEE 4th International Symposium on, Volume: 1, 22-25 Sept. 1996, pp.259 – 266.

Przyjemski, J., E. Balboni, and J. Dowdle. (1993). *GPS anti-jam enhancement techniques*. Proc. ION 49<sup>th</sup> annual meeting, Cambridge, MA, June 1993, pp. 41-50.

Raquet, J.F. (2004), *ENGO 699.10 Lecture note: GPS receiver design*, Department of Geomatics Engineering, The University of Calgary.

Rash, G. D. (1997). *GPS Jamming In A Laboratory Environment*. In Proceedings of the Institute of Navigation ION GPS-97 (September 16-19, 1997, Kansas City, Missouri), pp. 389–398.

Ray, J.K. (2003), *ENGO 699.73 Lecture note: Advanced GPS Receiver Technology*, Department of Geomatics Engineering, The University of Calgary.

Rifkin, R. and Vaccaro, J.J.(2000). *Comparison of narrowband adaptive filter technologies for GPS*. Position Location and Navigation Symposium, IEEE 2000 , 13-16 March 2000. Pages:125 – 131.

Spirent communications limited (2003a). *SimGEN (Including SimLOCATE) user manual*. Software for the Spirent range of satellite navigation simulator products

Spirent communications limited (2003b). *User manual for the GSS 4765 interference simulation system operation with SimGEN for windows*.

Tsui, James B-Y. (2000). *Fundamentals of Global Positioning System Receivers: A Software Approach*, John Wiley & Sons Inc.

Tukey, J. W. and Cooley, J. W. (1966). *An algorithm for the machine calculation of complex Fourier series*, Math. Comput. 19, 297–301 (1965).

Van Nee, R.D.J., COENEN, A.J.R.M. (1991). *New Fast GPS Code-Acquisition Technique using FFT*, Electronic Letters, Vol. 27, pp.158 -160, Jan. 1991.

Wang, C. and Amin, M.G. (1998). *Performance analysis of instantaneous frequency-based interference excision techniques in spread spectrum communications*. Signal Processing, IEEE Transactions on Volume: 46, Issue: 1, Jan. 1998, Pages: 70 – 82.

Ward, P. (1996). *Satellite signal acquisition and tracking, in Understanding GPS: Principles and applications*, Elliott Kaplan (ED.), Artech House.

Ward, P.W. (2002). *GPS and GNSS RFI & Jamming Concerns III*. ION GPS-2002 Tutorial, Portland, Oregon, pp. 8-24.

Young, J. A. and Lehnert, J. S. (1994), *Sensitivity loss of real-time DFT-based frequency excision with direct sequence spread-spectrum communication*, Tactical Communications Conference, 1994. Vol.1. Digital Technology for the Tactical Communicator, Proceedings of the 1994, 10-12 May 1994, Pages: 409 - 420